Migration of actinides in natural clay: Interaction of neptunium and plutonium with natural clay

S. Amayri, J. Drebert, D. R. Fröhlich, U. Kaplan
J. V. Kratz, T. Reich, N. Stöbener, N. Trautmann, T. Wunderlich

Institut für Kernchemie, Universität Mainz

Final Report

Support Contract Number
02 E 10166

Institut für Kernchemie
Johannes Gutenberg-Universität Mainz
Fritz-Straßmann-Weg 2
55128 Mainz
Germany

Content

Abstract 4
1 Introduction 5
2 Materials and methods 7
2.1 Materials 7
2.2 Analytical techniques 10
3 Experimental 13
3.1 Sorption (batch experiments) 13
3.2 Diffusion 15
3.3 Speciation 18
3.3.1 XAS, µ-XAS, µ-XRF, and µ-XRD 18
3.3.2 CE-ICP-MS 20
3.3.3 CE-RIMS 20
4 Results and discussion 21
4.1 Batch experiments 21
4.1.1 Batch experiments with Np(V) 21
4.1.2 Sorption isotherms 21
4.1.3 Influence of pH and pCO_2 24
4.1.4 Influence of humic acid (HA) 29
4.1.5 Influence of temperature 31
4.1.6 Influence of ionic strength and background electrolyte 35
4.1.7 Sorption isotherms of Th, U, Np, Pu, and Am in OPA pore water 37
4.2 Diffusion experiments 40
4.3 Speciation experiments 48
4.3.1 XAS, µ-XAS, µ-XRF, and µ-XRD 48
4.3.2 CE-ICP-MS 75
4.3.3 CE-RIMS 82
5 Summary 89
6 References 91
7 Acknowledgment 98

Abstract

The objective of this project was to investigate the transport and retardation processes of the actinides, mainly neptunium (Np) and plutonium (Pu), from a repository of spent nuclear fuels in an accidental scenario. The interaction of Np and Pu in their relevant oxidation states with natural Opalinus Clay (OPA) from Mont Terri, Switzerland has been studied in detail. Furthermore, experiments with thorium (Th), uranium (U), and americium (Am) were performed for comparison.

The sorption of NpO_2^+, UO_2^{2+}, Pu^{3+}, Am^{3+}, Pu^{4+}, and Th^{4+} on OPA in pore water at pH 7.6 was investigated in batch experiments and distribution coefficients were determined. The results showed that the tri- and tetravalent actinides are strongly sorbed on OPA with K_d values higher than those of the hexa- and pentavalent actinides, which are weakly sorbed.

The sorption of Np(V) on OPA was studied as a function of pH, aerobic/anaerobic conditions, partial pressure of CO_2, presence/absence of humic acid (HA), background electrolyte, ionic strength, and temperature. The results showed a strong influence of these parameters on Np(V) sorption.

Diffusion parameters for Np(V) were determined for the first time from diffusion experiments with intact OPA bore cores as a function of temperature and presence/absence of humic acid using OPA pore water as mobile phase.

The speciation of Np and Pu on the OPA mineral surface after sorption and diffusion processes was investigated by using different X-ray synchrotron radiation techniques (X-ray absorption spectroscopy (XAS), micro XAS (µ-XAS), micro X-ray fluorescence spectroscopy (µ-XRF), and micro X-ray diffraction (µ-XRD)). The results showed that Np(IV) and Pu(IV) are the most dominant species after sorption and diffusion processes. Furthermore, µ-XRD studies confirmed that iron-bearing mineral phases (pyrite and siderite) are the redox-active mineral phases of OPA which determine the speciation of Np and Pu after uptake on OPA.

CE-RIMS and CE-ICP-MS were successfully applied to detect the Np and Pu species at ultratrace concentrations close to environmental conditions.

The results of this study will be used as input parameters for performance assessment of a future repository for high-level nuclear waste to improve the thermodynamic databases for the uptake of actinides by clay rocks.

1 Introduction

The presence of plutonium (Pu) and minor actinides such as neptunium (Np) in nuclear waste is a major concern for the long-term safety of nuclear waste repositories because of their possible migration from the repository to the environment. The toxicity of the actinide elements and the long half-lives of their isotopes are the primary causes for concern [1].

Argillaceous rocks such as Opalinus Clay (OPA) are under consideration in several European countries, for example in Germany, Switzerland, France, and Belgium as potential host rock and as backfill material for a high-level nuclear waste repository [2 - 5].

The mobility of Np, Pu, and other actinides in aquifers is among several processes controlled by the diffusion in materials as well as the sorption on the surfaces. In the clay formations diffusion is considered to be the main transport mechanism for radionuclides released from a repository [6, 7]. For these reasons, a quantitative knowledge of radionuclide diffusion and sorption onto clay minerals is desirable. To predict the radionuclide mobility in the environment, it is also necessary to have fundamental knowledge about their interaction with rock pore water. Because high-level nuclear waste will significantly heat up the near field of the repository, it is also important to study the radionuclide migration at elevated temperatures.

In general, the lighter actinides have a wide variety of oxidation states from III-VII. Np can exist in aqueous solution in the oxidation states III - VII. The pentavalent cation, NpO_2^+, dominates the aqueous speciation under a wide range of environmental conditions and has a low tendency for hydrolysis, precipitation, and sorption on natural minerals [8 - 10].

Pu exhibits a complicated redox chemistry, where four oxidation states (III - VI) can coexist in natural waters [11, 12]. The lower oxidation states III and IV are the most interesting species with respect to their migration in the environment. Pu^{3+} and Pu^{4+} are stabilized by acidic conditions and prevail as solids with low solubility, which leads to high sorption on mineral surfaces. Over a wide Eh/pH range Pu(IV) is predominant and due the possible formation of colloids, PuO_2 is considered to be one of the most important solids for Pu risk assessment [13].

Hydrolysis, solubility, colloid formation, complexation with inorganic (i.e., dissolved inorganic carbon in OPA pore water) or organic ligands (i.e., HA), and sorption on mineral surfaces are chemical processes that govern the migration behavior of actinides (especially Np and Pu) in the environment. Up to now the migration process of Np and Pu in the environment is not completely understood. Therefore, their chemical species in aqueous

systems determined by redox-reaction and complexation during uptake on clay mineral surfaces have to be considered.

In the framework of this project, “Interaction and transport of actinides in natural clay rocks, under consideration of humic substances and clay organic matter”, OPA from the Mont Terri Rock Laboratory, Switzerland, and the corresponding pore water (pH = 7.6, I = 0.4 [14]) have been selected as references to study the sorption of Np and Pu on natural clay. OPA is rather complex with respect to its mineralogical composition. It consists of 66 ± 11 wt% clay minerals (kaolinite, illite, illite/smectite mixed layers, and chlorite), 14 ± 4 wt% quartz, 13 ± 8 wt% calcite, 3 ± 1.8 wt% siderite, 1.1 ± 0.5 wt% pyrite, and 0.8 ± 0.5 wt% organic carbon [3]. Organic compounds, which can be released from OPA under certain conditions, such as fulvic and humic acids, can interact with the actinides released from the nuclear waste in an incident scenario and significantly affect the sorption and migration behavior of them due to their complexation and redox properties and their ability to form stable colloids.

In this project the basic interaction processes of NpO_2^+, Pu^{3+}, Pu^{4+}, Pu^{6+}, and analogous actinides (i.e., UO_2^{2+}, Am^{3+}, Th^{4+}) in aqueous solutions with OPA were studied. The influence of HA on the sorption of Np and Pu onto OPA was also investigated.

Batch and diffusion experiments were completed by synchrotron based X-ray absorption spectroscopy to determine the structural parameters of Np and Pu sorbed on OPA.

Very sensitive methods such CE-ICP-MS or CE-RIMS were further developed and applied to study the behavior of Np and Pu under environmental conditions enabling the speciation of Np and Pu oxidation states in solution at ultratrace concentrations. CE-RIMS delivers a detection limit for Pu which is better by 2 to 3 orders of magnitude than the one obtained with the previously developed CE-ICP-MS (0.5 ppb for Pu).

2 Materials and methods

2.1 Materials

Opalinus Clay (OPA): In this work, various OPA batches from the Mont Terri Rock Laboratory, Switzerland, were used. Aerobic and anaerobic OPA samples, i.e., powders, thin sections or cylinders were prepared from OPA bore cores. An overview of the different OPA batches and their applications are summarized in Tab. 1.

Table 1: OPA (from Mont Terri) batches and their applications.

OPA bore core	Depth / m	Preparation	Type	Experiment
BHE 24/1	3.30 - 3.56	aerobic	powder	batch / XAS
BDR 2	7.31 - 7.60	anaerobic	powder	batch / XAS
BAE 25/10	6.27 - 6.45	aerobic	thin section, bore core	µ-XAS, diffusion
BHE 24/2	3.56 - 3.89	anaerobic	powder	batch / XAS
BLT 14	2.12 - 2.52	aerobic	bore core	batch / diffusion

Aerobic and anaerobic OPA powders were prepared in air and under Ar atmosphere from OPA bore cores (BHE 24/1) and (BDR 2 or BHE 24/2), respectively. The specific surface area of the aerobic powder measured by N_2 BET equals 41.3 ± 0.5 m^2/g, the cation exchange capacity is equal to 10 ± 4 (meq/kg) [15]. The mineral composition and the content of the trace elements of the used aerobic OPA were measured by X-ray fluorescence analysis and published by Fröhlich et al. [16]. More information about the main physicochemical characteristics of Mont Terri OPA such as composition, microstructure, surface area, surface charge, etc. can also be found in [3]. All OPA powders and cylinders were prepared at the Karlsruhe Institute of Technology - Institute for Nuclear Waste Disposal (KIT-INE).

OPA pore water: The synthetic OPA pore water had a pH of 7.6 and an ionic strength of 0.4 M. It consisted mainly of NaCl with minor amounts of $CaCl_2$, $MgCl_2$, KCl, $SrCl_2$, Na_2SO_4, and $NaHCO_3$ [14]. The exact composition of the artificial pore water used in the batch and diffusion experiments is given in Tab. 2.

Table 2: Composition of the synthetic OPA pore water [14] used in the batch and diffusion experiments.

Salt	Concentration / g/L
NaCl	12.38
KCl	0.12
$MgCl_2 \cdot 6H_2O$	3.48
$CaCl_2 \cdot 2H_2O$	3.79
$SrCl_2 \cdot 6H_2O$	0.14
Na_2SO_4	2.00
$NaHCO_3$	0.04

Humic acids (HA): To study the influence of HA on the sorption and diffusion experiments, the synthetic HA type M42 (batch M145) [17] was used. Synthetic HA M42 has an elemental composition similar to natural HA. The carboxyl group content and proton exchange capacity (PEC) of M42 are 3.51 ± 0.07 meq/g and 3.76 ± 0.09 meq/g, respectively. Phenolic/acidic OH groups content is 2.0 ± 0.2 meq/g. The unmarked M42 HA (batch 145) was used in XAS investigations. Sorption and diffusion experiments were performed using ^{14}C-labeled ([^{14}C] M42 batch R2/06). ^{14}C M42 has a specific activity of 5.8 ± 0.6 MBq/g, a proton exchange capacity of 3.11 ± 0.39 meq/g, and a carboxylic acid content of 2.90 ± 0.06 meq/g [18]. The humic acids M42 were provided by Helmholtz-Zentrum Dresden-Rossendorf - Institute of Radiochemistry.

Chemicals: All chemicals were at least analytical grade. Ultrapure deionized water (resistivity 18 MΩ, Synergy™ Millipore water system, Millipore GmbH, Schwalbach, Germany) was used to prepare the solutions. Experiments under anaerobic conditions (absence of CO_2) were carried out in an argon glove box (Unilab, MBraun, Garching, Germany) with < 10 ppm O_2 using boiled Millipore water for preparing all solutions. All background electrolytes (i.e., OPA pore water, 0.1 M $NaClO_4$, $CaCl_2$) and solutions (i.e., NaOH and $HClO_4$) were prepared by dissolution of the related p.a. chemicals from different commercial sources (Merck, Fluka, Alfa Aeser, Roth and Sigma-Aldrich) in Millipore water.

Stock solutions:

Humic acid: Stock solutions of M42 with 2 g/L were prepared for sorption and speciation experiments by weighting of 10 mg of HA, adding 0.4 mL of 0.1 M NaOH, and filling up with saturated $CaCO_3$ or OPA pore water to 5 mL.

Calcite solutions: For sorption experiments with Np under different partial pressures of CO_2 (ambient $pCO_2 = 10^{-3.5}$ and $pCO_2 = 10^{-2.3}$ atm), solutions saturated with respect to $CaCO_3$ (Merck, Germany) at different pH were prepared under aerobic conditions and in a glove box (Unilab, MBraun, Garching, Germany) filled with a gas mixture of 99.5% Ar and 0.5% CO_2 (Westfalen AG, Germany). In a first step, the pH of aliquots of Millipore water was adjusted by adding appropriate amounts of $HClO_4$ and NaOH. To the samples of pH > 8.5 under aerobic and pH > 7.5 under anaerobic conditions, specified amounts of $NaHCO_3$ and Na_2CO_3 calculated with MINTEQ V.2.52 [19] were added to accelerate the equilibration adjustment with the surrounding atmosphere. Then, $CaCO_3$ was added to all solutions until saturation was reached to ensure calcite equilibrium. All solutions were stirred in open polyethylene (PE) tubes up to two weeks until equilibrium indicated by a constant pH was reached. The tubes were sealed and stored until utilization. In the batch experiments, only the supernatant solution after centrifugation for 10 min at 4.030 g (3K30, Sigma, Germany) was used.

Thorium: A 5×10^{-6} M ^{232}Th stock solution was obtained from solid $Th(NO_3)_4 \cdot 5H_2O$ (p.a., Merck) which was dissolved in 0.1 M HCl to avoid any precipitation of Th by hydrolysis. ^{228}Th ($T_{1/2}$ = 1.912 a) was added as tracer (2.5×10^{-11} M) to the solution.

Uranium: The ^{238}U stock solution was obtained by dissolving solid $UO_2(NO_3)_2 \cdot 6H_2O$ (p.a., Merck) in 0.1 M HNO_3. The concentration of the stock solution was 1.0×10^{-1} M.

Neptunium: The procedures for preparing the stock solutions of $^{237}Np(V)$ and $^{239}Np(V)$ were the same as described in detail elsewhere [16]. The oxidation state of ^{237}Np stock solution was verified by UV-vis absorption spectroscopy with the characteristic absorption band of Np(V) at 980.4 nm. The concentrations of ^{237}Np and ^{239}Np were determined by γ-ray spectroscopy. The resulting stock solutions had a pH value of about 1.5 and a concentration of 1×10^{-2} M $^{237}Np(V)$ and 8×10^{-9} M $^{239}Np(V)$. For the sorption experiments, the pH of the Np stock solutions was adjusted to 3 - 4 using 5 M NaOH.

Plutonium: For the experiments carried out with ^{239}Pu, a 3×10^{-3} M ^{239}Pu stock solution in 9 M HCl was used. The Pu solution was evaporated to dryness and the residue was dissolved in 10 M HCl (with some drops of conc. HNO_3 to oxidize to Pu(VI)). The ^{239}Pu solution was purified from its decay products including ^{241}Am using anion exchange chromatography at 55 °C (150 mm × 4 mm glass column filled with Dowex AG 1-X8 from Bio-Rad Laboratories, Hercules, USA). After a washing step with 8 M HCl, Pu was eluted with 0.5 M HCl. The eluate was evaporated to dryness, fumed three times with 1 M $HClO_4$, and dissolved in 1 M $HClO_4$. A well characterized ^{239}Pu(VI) stock solution (1.8 mL) was obtained with this purification procedure. The trivalent, tetravalent, and pentavalent oxidation states of Pu were obtained from the purified Pu(VI) stock solution by potentiostatic electrolysis. The oxidation state purity was verified by UV-vis spectroscopy at the characteristic absorption bands at 600 nm for Pu(III), 470 nm for Pu(IV), 568 nm for Pu(V), and 830 nm for Pu(VI) [20, 21].
The concentration of the ^{239}Pu stock solutions was determined by liquid scintillation counting (LSC). The resulting stock solutions had a concentration of 6×10^{-4} M Pu(III), 6×10^{-4} M Pu(IV), 5×10^{-4} M Pu(V), and 3×10^{-3} M Pu(VI). The same purification procedure was applied to obtain 1×10^{-3} M ^{242}Pu(VI) stock solution, which was used for the preparation of OPA thin sections and diffusion samples for µ-XAS, -XRF, and -XRD investigations.

Americium: A 2.5×10^{-5} M stock solution of ^{241}Am in 0.005 M HCl was prepared by diluting a concentrated ^{241}Am solution (5×10^{-3} M in 1 M HCl) with Millipore water. The purity of the resulting ^{241}Am stock solution was checked by α- and γ-ray spectroscopy.

2.2 Analytical techniques

α-spectroscopy: The concentrations of ^{239}Pu, ^{242}Pu, and ^{237}Np in solutions were determined by α-spectroscopy. A silicon surface barrier detector (ORTEC, USA) with an active area of 450 mm^2 and a detector resolution of < 25 keV at 5.5 MeV was used. The detector efficiency was about 14%. It was controlled regularly by measuring a standard ^{241}Am source. Special sample preparation was required. Therefore, a small volume ~ (10 - 20) µL of the sample was deposited on a titanium or tantalum foil and evaporated to dryness. Counting times up to 24 h were chosen.

γ-ray spectroscopy: Concentrations and purity of ^{237}Np, ^{239}Np, ^{241}Am, and ^{22}Na solutions were determined by γ-ray spectroscopy using the γ-lines at 29.4 and 86.5 keV for ^{237}Np, 103.4

and 106.1 keV for ^{239}Np, 59.5 keV for ^{241}Am, and 1274.5 keV for ^{22}Na. All measurements were accomplished on a spectroscopic system consisting of a HPGe (GMX-13180-S, EG and G ORTEC, USA) coaxial γ-ray detector, Canberra Inspector 2000 (model IN2K, Canberra Industries, Inc., USA) analyzer, and a PC equipped with Genie 2000 gamma acquisition and analysis software (V. 3.0, Apr 05, 2004; Canberra Industries, Inc., USA). The mixed radionuclide γ-ray standard reference solution QCY48 (Solution number: R6/50/38, Amersham, AET Technology QSA GmbH, Germany) was used for calibration of the spectroscopic system. All samples were counted until an error level of about 3% was achieved at a confidence level of 2σ. In the case of ^{237}Np, the results were also confirmed by liquid scintillation counting

UV-vis spectroscopy: The purity of the oxidation states of ^{237}Np and ^{239}Pu was verified by UV-vis absorption spectroscopy using a high-resolution UV-vis spectrometer (Cary 50 Bio, Varian, USA (for Np) and Tidas 100, J&M Analytik AG, Germany (for Pu)). The samples were measured in 1.5 mL polymethylmethacrylat semi-microcuvettes (Brand GmbH, Wertheim, Germany).

Liquid scintillation counting (LSC): ^{232}Th/^{228}Th, ^{237}Np, ^{239}Pu concentrations were determined using LSC (home built scintillation counter) by measuring 1 mL sample in 10 mL scintillation cocktail Ultima Gold™ AB (for sorption experiments) or Ultima GOLD XR (for diffusion experiments) (PerkinElmer LAS GmbH, Rodgau-Jügesheim, Germany). The samples were counted until a 2σ error of 2% was attained. The activities of HTO and $^{22}Na^{+}$ were measured using a Beckman LS6800 liquid scintillation counter (Beckman Coulter, USA).

Inductively coupled plasma - mass spectrometry (ICP-MS): ^{238}U and ^{232}Th concentrations in the samples were determined by ICP-MS measurements using an Agilent 7500ce unit (Agilent Technologies, Waldbronn, Germany).

Capillary electrophoresis (CE): CE was coupled online to ICP-MS to separate the different oxidation states of Pu and Np in various solutions. The coupling of the homemade CE to the ICP-MS was performed as described in [22, 23]. Standard LSC vials (20 mL), or for small sample volumes, 300 µL PE vials were used for the buffer and sample solutions. For hydrodynamic sample injection, 60 – 100 mbar was applied for 4 – 10 s. A fused-silica

capillary with an inner diameter of 50 μm (PolyMicro Technologies, Phoenix, AZ) and 60 – 80 cm length was used. Before use, the capillary was purged for 5 min at 1 bar with 0.1 M HCl, 0.1 M NaOH, and for 10 min at 1 bar with Milli-Q deionized water and the electrolyte solution (1 M acetic acid at pH ≈ 2.4). Using a MiraMist CE nebulizer (Burgener Research Inc., Mississauga, Canada), a detection limit of 0.5 ppb for Pu [23] and Np has been obtained.

Resonance ionization mass spectrometry (RIMS): For the speciation of Pu and Np at ultratrace level, an experimental setup of offline coupling CE and RIMS was developed and optimized [23 - 26]. The RIMS setup consisted of a high repetition rate solid-state laser system (three titanium-sapphire lasers pumped by a pulsed Nd:YAG laser (Clark-MXR ORC-1000 or DM-60, Photonics Industries, Bohemia, NY, USA)) and a reflectron time-of-flight (TOF) mass spectrometer. The high selectivity and sensitivity of the CE-RIMS allowed the determination of the oxidation as well as the isotope ratios of Pu at ultratrace level, e.g., under environmental conditions. The limit of detection of RIMS is about 10^6 atoms for Pu [24, 25] and about 10^7 atoms for Np [26]. Compared to CE-ICP-MS this method should yield an improvement in the detection of at least two orders of magnitude.

pH and Eh measurements: The pH of solutions was measured using a pH meter inoLab or Cond pH 720 (WTW GmbH, Weilheim, Germany) equipped with a pH electrode (blue line 16 pH, Schott, Mainz, Germany) and a temperature sensor (TFK 150, WTW, Weilheim, Germany). The pH meters were calibrated with certified commercial (DIN) buffers (pH 4.01, 6.87, and 9.18 from Schott, Mainz, Germany). The redox electrode (blue line 31 RX, reference system: Ag/AgCl, Schott, Germany) was used for Eh measurements. It was checked with a standard solution of known redox potential (240 mV, HI 7021 ORP solution, HANNA instruments, USA).

Liquid-liquid extraction: Chemical extraction was applied in combination with LSC to determine the redox behavior of Np in aqueous solutions after sorption experiments. As extracting agents, a solution of 0.5 M di(2-ethylhexyl) phopshoric acid (HDEHP) (Merck) diluted in toluene was used. A 0.5 mL portion of the supernatant was shaken together with 2 mL 1 M HCl and 2.5 mL 0.5 M HDEHP (in toluene) solutions for 5 min. The phases were separated by centrifugation at 4.030 g and 2 mL of each phase were analysed by γ-ray spectroscopy (Np(V) in H_2O, and Np(IV) in organic solution). The oxidation state of Np

sorbed on OPA was investigated analogously by shaking the dried clay powder with 2.5 mL 1 M HCl and 2.5 mL of HDEHP solution for 5 minutes.

3 Experimental

3.1 Sorption (batch experiments)

The sorption behavior of the actinides Th, U, Np, Pu, and Am on OPA (Mont Terri) was investigated by batch experiments. The effects of different parameters such as pH, solid-to-liquid ratio (S/L), nuclide concentration, aerobic/anaerobic conditions, partial pressure of CO_2 ($p(CO_2)$), background electrolyte, ionic strength, temperature, and presence/absence HA were investigated. An overview of the performed batch experiments is presented in Tab. 3.

Table 3: Overview of the performed batch experiments.

Actinide	**Investigated parameters**
Th(IV)	pH, S/L ratio, background electrolyte
U(IV)	concentration
Np(V)	pH, S/L ratio, concentration, aerobic/anaerobic cond., $p(CO_2)$, background electrolyte, ionic strength, temperature, presence/absence HA
Pu(III)	S/L ratio
Pu(IV)	pH, S/L ratio, background electrolyte
Pu(VI)	pH, S/L ratio, background electrolyte, temperature, , presence/absence HA
Am(III)	S/L ratio

In most batch experiments, suspensions of well characterized aerobic and anaerobic dry powders of OPA (typically 2 - 20 g/L for amount isotherms, 15 g/L for concentration isotherms and other experiments) were prepared in synthetic pore water at pH 7.6, 0.1 M $NaClO_4$ or saturated $CaCO_3$ solution (only for experiments with Np(V)) in closed 10 mL polycarbonate (Np batch experiments) or 50 mL polyallomer (Pu batch experiments) centrifuge tubes (Beckman Coulter, USA) at room temperature under aerobic and anaerobic conditions. Experiments under anaerobic conditions were performed in the absence of CO_2 in

a glove box (Unilab, MBraun, Garching, Germany) filled with high purity Ar gas (> 99.99%) in order to avoid oxidation processes, i.e. Pu(III) to Pu(IV).

Some Np(V) sorption experiments were also done under anaerobic conditions at high partial pressure of CO_2 ($10^{-2.3}$ atm). The samples were sealed and preconditioned by shaking in an end-over-end rotator (SB 3, Stuart Scientific, UK) for 72 h. After that aliquots of the stock nuclide solution of $^{232}Th/^{228}Th$ (^{228}Th was added as a tracer), ^{238}U, $^{237}Np/^{239}Np$ (^{239}Np was used as tracer in the concentration isotherm experiment, and in pH dependence experiments at 7×10^{-12} M concentration), ^{239}Pu, and ^{241}Am were added individually to the samples and the pH was adjusted immediately with $HClO_4$ and NaOH solutions of different concentrations to the desired value (Δ pH = ± 0.05). The total concentrations of actinides were about 8×10^{-9} M $^{232}Th(IV)$, 2×10^{-4} - 1×10^{-7} M $^{238}U(VI)$, 5×10^{-5} - 1×10^{-11} M $^{237}Np(V)/^{239}Np$ (for concentration isotherm), 8×10^{-6} M $^{237}Np(V)$ (for amount isotherm, and other experiments), 7×10^{-12} M $^{239}Np(V)$, 1×10^{-7} M $^{239}Pu(III)$, 9×10^{-8} M $^{239}Pu(IV)$, 1×10^{-7} M $^{239}Pu(VI)$ and 9×10^{-9} M ^{241}Am. The concentration of 8×10^{-6} M Np in 0.1 M $NaClO_4$ is below the solubility of any solid phase, e.g., $NaNpO_2CO_3(s)$ [27]. Then, the samples were shaken for at least 60 h. During this time, the pH of the solutions was checked twice and was readjusted if necessary. Afterwards the solid and liquid phases were separated by centrifugation at 108.800 g for one hour in a centrifuge Avanti J-30I (Beckman Coulter, USA). The actinides uptake was determined by γ-ray spectroscopy, LSC or ICP-MS of the supernatants.

Temperature dependent investigations up to 80 °C were carried out using the same procedure, except that the samples were placed on a heatable multipoint magnetic stirrer (IKA RT 10 power IKAMAG, IKA, Staufen, Germany) equipped with a massive aluminum block with boreholes for the samples. The block was heated to the desired temperature with a fluctuation of less than ± 3 °C. The samples were stirred with stirring bars of 5 mm length (VWR, Germany). Blank samples were run along with all batch experiments. The loss of Np and Pu to the walls of the centrifuge tubes was found to be negligible (≈ 1 - 2% of the initial Np conc. and max. 5% of the Pu conc.). The oxidation state of Np after the sorption experiments under anaerobic conditions was checked via liquid-liquid extraction using HDEHP (Merck, Germany) as extracting agent.

For the LSC measurements of ^{228}Th, the supernatants were stored for more than 3 months until the decay products of ^{228}Th were in equilibrium.

During the sorption experiments with Np and Pu, the Eh under aerobic conditions was approximately equal to + 350 ± 25 mV (SHE). In the case of anaerobic conditions, the Eh was equal to - 60 ± 25 mV and - 120 ± 25 mV (SHE) for Np and Pu(III), respectively.

The percentage of the actinide sorbed was calculated by using the following equation:

$$\text{Sorption}\% = \left(1 - \frac{[\text{An}]_{eq}}{[\text{An}]_0}\right) \times 100\% \quad (1)$$

A convenient representation of sorption data is the sorption coefficient, K_d, which is defined by the following equations:

$$K_d = \frac{V}{m} \times \left(\frac{[\text{An}]_0 - [\text{An}]_{eq}}{[\text{An}]_{eq}}\right) \quad (2)$$

or

$$K = \frac{\frac{x}{m}}{[\text{An}]_{eq}^n} \quad (3)$$

where $[An]_{eq}$ and $[An]_0$ (mol/L) are the equilibrium and initial concentrations of the sorbate in solution, respectively; V is the volume of experimental solution in m^3; x (mol) is the amount of sorbate; m is the mass of sorbent (kg), and n is a constant. For n = 1, K equals the distribution coefficient K_d (m^3/kg).

3.2 Diffusion

For the diffusion experiments, a cylinder of about 25 mm diameter and 11 mm height was cut out from the aerobic OPA bore cores (BAE 25/10 or BLT 14). The orientation of the cylinder in the diffusion cell was so that the direction of transport (diffusion) was perpendicular to the bedding. The density of the intact and dry OPA samples was between 2402 und 2429 kg/m³. All diffusion experiments were carried out in artificial pore water (pH = 7.6) as mobile phase under aerobic conditions in presence/absence of HA (M42) at room temperature (20 ± 2 °C) [28] and 60 ± 2 °C. For the diffusion experiments, 0.003 M NaN_3 was added to the pore water to avoid bacterial growth. The diffusion setup and the experimental procedures were the same as those used for the through-diffusion experiments by Van Loon et al. [29]. A schematic drawing and a photograph of the experimental setup of the diffusion experiment are shown in Fig. 1. The set up comprises a diffusion cell (stainless steel, RM-Stahlhandel GmbH, Flörsheim am Main, Germany), an 8-channel peristaltic pump (Ismatec, Ecoline VC-MS/CA8-6, IDEX Health & Science GmbH, Wertheim-Mondfeld, Germany), a 250 mL container and a 25 mL container (Schott Duran, Mainz, Germany). The OPA sample was sandwiched between two stainless steel filter plates (stainless steel: 316 L, pore diameter: 10 µm, diameter: 25.4 mm, thickness: 1.57 mm, Ligacon AG, Switzerland) and mounted in a

diffusion cell. The large container was filled with 210 mL artificial OPA pore water and the small one with 20 mL. The sample was saturated by circulating the OPA pore water solutions against both ends of the sample for at least 5 weeks. Subsequently, the solutions were replaced by fresh ones and the solution in the large container was spiked with the desired tracer. The radiotracers studied in this work were: HTO, $^{22}Na^{+}$, $^{237}Np(V)$, $^{237}Np(V)$-HA M42, and $^{242}Pu(VI)$ (used only for spectroscopic investigations).

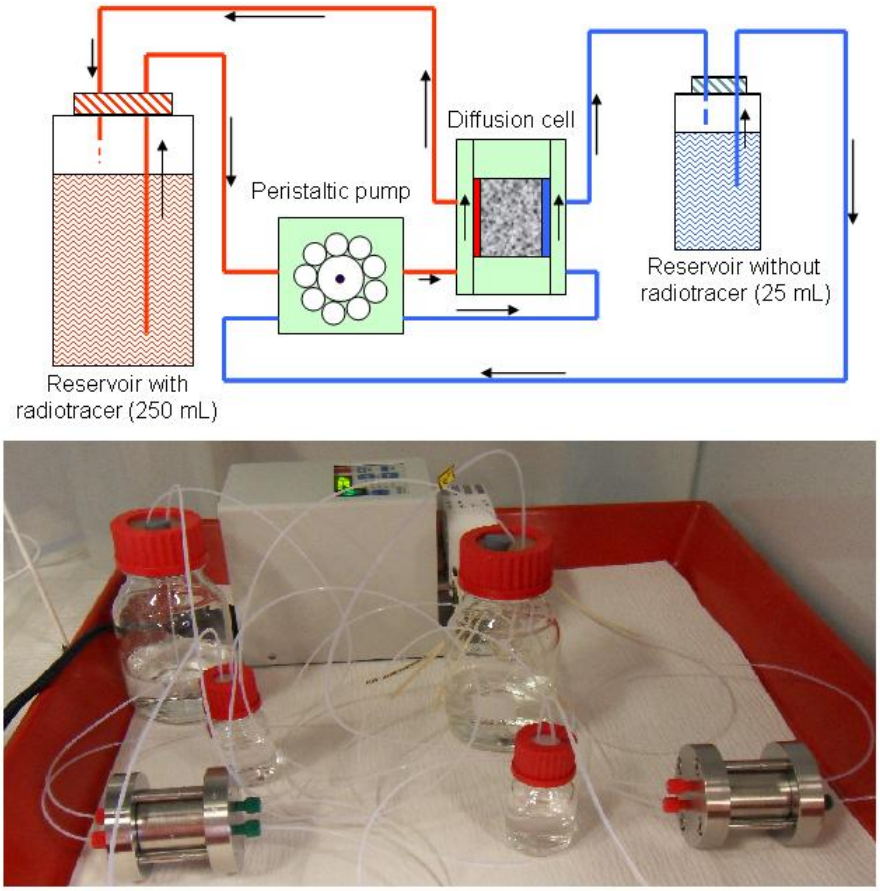

Figure 1: Schematic drawing (adapted from [29]) and a photograph of the experimental setup of the diffusion experiment.

Table 4: Overview of the tracers used and their activities.

Cell Nr.	OPA	ρ (kg/m^3)	Temp. (°C)	[HTO] (MBq/L)	[^{22}Na] (MBq/L)	[^{237}Np(V)] (MBq/L)	[HA] (MBq/L)
1 [28]	BAE 25/10	2420	20	1.23	1.00	0.05	-
2	BLT 14	2412	20	1.30	5.10	0.05	-
3	BLT 14	2429	20	1.30	5.10	0.05	0.06
4	BLT 14	2402	60	1.30	5.10	0.05	-

After the completion of HTO or $^{22}Na^+$ through-diffusion experiments, the solutions in both containers were replaced by artificial pore water without tracer and out-diffusion was started. At given time intervals, the activity in the solutions was measured, and the solutions were replaced by fresh ones. The activities of HTO and $^{22}Na^+$ in the samples were measured by LSC. This procedure was repeated until all the activity in the OPA sample had diffused out. Once this had been achieved, a new radiotracer, in particular ^{237}Np, ^{237}Np-HA (M42), and ^{242}Pu(VI) was added to the large container and diffusion of the new tracer was started. In case of experiments with HA, HA was added simultaneously with Np to the reservoir. The high-concentration reservoir was filled with 210 mL of artificial pore water and spiked with 50×10^6 Bq/m^3 Np (see Tab. 4). The diffusion time was in all cases up to 35 days. During this time, the Eh in the high-concentration reservoir was controlled (SHE ≈ + 350 mV) and no significant changes were observed. In order to check the evolution of the concentration of ^{237}Np(V) as a function of diffusion time in the high concentration reservoir, 0.5 mL of solution were withdrawn regularly from this reservoir and measured by γ-ray spectroscopy. After this time, the high concentration reservoir was exchanged by a smaller one (20 mL) containing artificial pore water with 1 - 5×10^9 Bq/m^3 $^{22}Na^+$ and the same concentration of ^{237}Np(V) as in the replaced high-concentration reservoir. The diffusion experiment was terminated about one day after adding $^{22}Na^+$ to the reservoir. The OPA sample was then removed from the diffusion cell and mounted on a sample holder for abrasive peeling with P220 abrasive paper (MATADOR Silicon Carbide Paper, waterproof P220 Article-No. 971 C, Starck GmbH & Co. KG, Germany). The abrasive peeling technique has been described elsewhere [30]. The activities of ^{237}Np and ^{22}Na in the peeled OPA layers were measured by γ-ray spectroscopy.

For diffusion experiemnts at 60 °C, the diffusion cell was heated in an incubator (INE-200 heating incubator, Memmert GmbH, Germany) with a temperture fluctuation of less than ± 2 °C. The experimental data processing of through-, out-, and in-diffusion experiments of

HTO, ^{22}Na, and ^{237}Np was performed with a home made computer code and has been described in detail elsewhere [7, 28].

3.3 Speciation

3.3.1 XAS, µ-XAS, µ-XRF, and µ-XRD

For synchrotron based X-ray absorption spectroscopy (XAS) measurements, the sorption samples were centrifuged after a contact time of at least 60 h and the solid and liquid phases were separated by centrifugation at 108,000 g for 1 h. Np wet paste samples were prepared under air and Ar atmosphere. The samples were put in Perspex sample holders with Kapton windows. For measurements of Np and Pu at about 15 K, the solid residues were dried for 3 days either under aerobic or Ar atmosphere. Then all powders were grinded and loaded into special PE XAS sample holders (SH-01c) and heat sealed. Anaerobic XAS samples were prepared in a glove box (Ar box > 99.99%). The transport of anaerobic samples was performed in an anaerobic transport container (Anaerobic jar, Schuett-biotec GmbH, Göttingen, Germany), which was purged with argon, or in a special dewar filled with liquid nitrogen (Voyageur 12, AIR LIQUIDE Deutschland GmbH, Germany), where the samples were shock frozen until measurement.

Both Np and Pu L_{III}-edge absorption spectra (Np: 17630 eV, Pu: 18070 eV) were collected in fluorescence mode at the Rossendorf beamline ROBL [31] at the European Synchrotron Radiation Facility (ESRF) in France using a 13-element Ge solid-state detector. A Si(111) double-crystal monochromator was used for tuning the energy of the incident X-ray beam. Yttrium foil was used for calibrating the X-ray energy. The EXAFS analysis was performed with the software packages Athena [32] and EXAFSPAK [33]. Backscattering phase and amplitude functions required for data fitting were calculated with FEFF 8.20 [34] using crystal structures of $(UO_2)_2SiO_4 \cdot 2H_2O$ [35], $K_3NpO_2(CO_3)_2 \cdot 0{,}5\ H_2O$ [36], NpO_2 [37], $Eu_{1.3}Fe_{0.7}O_{6.3}Ti_{2.0}$ [38]. For modeling possible interactions of Np or Pu with Si, Fe, etc., U or Eu were replaced in the crystal structures by Np or Pu. The shift in threshold energy, ΔE_0, was allowed to vary as a global parameter in the fits.

µ-XAS, µ-XRF, and µ-XRD measurements were performed at the MicroXAS beamline at the Swiss Light Source, Paul Scherrer Institut (PSI), Switzerland [39]. For these investigations, several OPA samples were prepared by contacting with ^{237}Np(V) or ^{242}Pu(VI) solutions (at about pH = 7.6). Three kinds of samples were prepared: (i) Np or Pu solutions were deposited directly by pipetting on the OPA thin sections. The solution was given time to evaporate

completely before the procedure was repeated until the whole amount of solution was placed on the thin section, (ii) Np or Pu was sorbed on OPA thin sections using a sorption cell (homemade) with a contact time of at least three days, (iii) small pieces of OPA were taken from an in-diffusion experiment with Np(V) or Pu(VI), which lasted for more than one month. Np and Pu loadings in all OPA thin sections were between 96 and 1389 ng/mm². Thin sections were prepared on glass slides from OPA batches (BAE 25/10 for aerobic samples and BLT 14 for anaerobic and diffusion samples). The preparation of these samples was performed at the Max-Planck-Institut für Chemie in Mainz. The thickness of the clay was approximately 20 to 30 µm, the contacted area was always smaller than 1 cm².

µ-XRF and µ-XAS measurements of all samples were performed using a Kirkpatrick-Baez mirror microfocusing system and a double-crystal monochromator with three different crystal pairs (Si (111), Si (311) and Ge (111)). In this experiment, a pair of Si(111) crystals was used. The ring current during the measurement was about 400 mA. X-ray fluorescence was measured using a Ketek single-element Si-detector. µ-XRF mappings of elements of interest (i.e. Ca, Fe, Sr, As, Np, Pu) were collected at an excitation energy above the Np or Pu L_{III}-edge. Overview maps were taken at a step size of 20 - 10 µm, fine mappings were performed in 5 - 1 µm steps. All measurements were done with a beam size (h × w) of ≈ 1 - 2 × 2 - 4 μm^2. A Zr foil (17998 eV) was used for energy calibration. As Np has a similar fluorescence energy ($E(L_\alpha)$ = 13950 eV) compared to Sr ($E(K_\alpha)$ = 14160 eV), which is present at amounts of ≈ 235 ppm in OPA [16], potential hot spots of Np were remapped at an excitation energy of 17550 eV to exclude Sr interferences. XRF maps were analyzed using a PSI intern MATLAB code. Np and Pu hot spots were studied by Np or Pu L_{III}-edge µ-XANES in fluorescence mode. Deadtime corrections for the measured XANES spectra were performed using an in-house java applet code. Background and energy correction of the spectra were performed with the software package Athena [32].

The XANES spectra were analyzed using a software package for ITFA [40] and reference spectra of Np(IV) and Np(V). ITFA allows to determine the relative amount of different Np oxidation states in the sample from XANES spectrum.

The µ-XRD measurements were performed using the above mentioned beam size and a Pilatus 100K detector. Experimental parameters such as sample-detector distance, detector plane orientation, etc., were refined by measuring different reference powders or foils (i.e., Al_2O_3, SiO_2, Si-Zr). The analysis of the diffraction patterns was performed with the program Area Diffraction Machine [41].

Element maps of two thin sections were obtained with the Jeol JXA 8200 electron microprobe of the Max-Planck-Institut für Chemie, Mainz, Germany, which is equipped with one energy dispersive (EDX) and five wave length dispersive detectors (WDX). An acceleration voltage of 15 kV, a beam current of 30 nA, and a dwell time of 0.2 s were used. In order to get an overview, the entire sample was mapped with a beam diameter of 15 µm and a step size of 20 µm. Mg, Al, Ca, Si, and Fe were measured with WDX spectrometers, Ti with an EDX spectrometer and, in addition, the BSE (back-scattered electrons) image was recorded.
Areas of particular interest were mapped with a beam diameter of 2 µm and step sizes of 2.5 or 1.5 µm. Al, Na, Ca, Si, and Fe were measured with WDX spectrometers, Ti, Mg, K with an EDS spectrometer and, in addition, the BSE image was recorded.

3.3.2 CE-ICP-MS

The redox behavior of individual Pu oxidation states (i.e. Pu(III) and Pu(IV)) in OPA pore water (pH = 7.6), HNO_3 (pH = 0.9), and $NaClO_4$ (pH = 7.6) was investigated under aerobic and anaerobic conditions using CE-ICP-MS. In all experiments Pu(III) and Pu(IV) were freshly prepared from a Pu(VI) stock solution by potentiostatic electrolysis and checked by UV-vis spectroscopy. Then, a defined amount of Pu(III) or Pu(IV) from the stock solution was added to the corresponding solutions. The pH/Eh values were measured directly after addition and checked again after 5 - 7 days. The Pu concentration in all samples was about 30 - 50 ppb or ~ 1 - 2 × 10^{-7} mol/L. The speciation of Pu was analyzed by CE-ICP-MS after 60 min, 80 min, and 7 days.

3.3.3 CE-RIMS

The principle of the off-line coupling CE to ICP-MS is based on collecting fractions of the different oxidation states of Pu eluted from the capillary at different retention times. From each fraction, a separate filament is prepared and studied by RIMS on its Pu content. In a first validation of the method, it was possible to determine successfully the oxidation state composition of a known Pu mixture (6 × 10^9 atoms) [42]. In this work, the development and optimization of CE coupled to RIMS for the speciation of Pu at ultratrace level was performed and successfully applied to sorption samples from batch experiments of Pu(III) and Pu(IV) on OPA. The memory effect of Pu(IV) sorbed on the capillary inner surface was also shown by this method. The Pu detection limit by CE-RIMS was about 10^6 atoms [23]. For the detection of ultratrace amounts of Np by RIMS, extensive spectroscopic investigations have been carried out. Five excitation/ionization schemes involving autoionizing states for efficient and

selective resonant excitation and ionization were identified, which can be used for RIMS measurements of Np. An overall efficiency of 0.3% was determined with a synthetic sample of a known number of ^{237}Np atoms [26].

4 Results and discussion

4.1 Batch experiments

4.1.1 Batch experiments with Np(V) [16]

The sorption behavior of Np(V) on OPA was investigated in batch experiments by varying different parameter such as pH (6 - 10), Np(V) concentration (10^{-12} - 10^{-4} M), solid to-liquid ratio (S/L = 2 - 20 g/L), partial pressure of CO_2 ($10^{-3.5}$ and $10^{-2.3}$ atm), temperature (20 - 80 °C) in the absence and presence of HA under aerobic and anaerobic conditions in saturated calcite solution and using synthetic OPA pore water (pH 7.6, I = 0.4 M), $NaClO_4$, NaCl, $CaCl_2$, and $MgCl_2$ as background electrolytes. All batch experiments were carried out with well characterized aerobic (BHE 24/1) and anaerobic (BDR 2) dry powders of OPA (see also Tab. 1).

4.1.2 Sorption isotherms

The sorption isotherms were measured with saturated calcite solutions as background electrolyte to avoid partial dissolution of the calcite contained in OPA. Following the procedure described above (Sect. 3.1), two sorption isotherms under aerobic conditions using aerobic OPA powder (BHE 24/1) were measured at pH 8.2 by varying the S/L ratio between 2 - 20 g/L (at [Np(V)] = 8×10^{-6} M) and the Np(V) concentration between 10^{-12} and 10^{-4} M using ^{237}Np and ^{239}Np as tracer (at S/L ratio = 15 g/L), respectively. At picomolar concentration, only ^{239}Np was used. The percentage of sorbed Np(V) and the distribution coefficient (K_d) were calculated by using eqs. 1 and 2. Table 5 shows the distribution coefficient K_d (m^3/kg) for the sorption of 8×10^{-6} M Np(V) on aerobic OPA in saturated calcite at pH 8.2 under aerobic conditions as a function of the S/L ratio.

Table 5: K_d values for the sorption of 8×10^{-6} M Np(V) on OPA (BHE 24/1) as a function of the S/L ratio at pH = 8.2 under calcite saturation and aerobic conditions.

S/L / g/L	**K_d / m^3/kg**
2	0.141 ± 0.029
4	0.120 ± 0.017
6	0.135 ± 0.012
8	0.120 ± 0.011
10	0.123 ± 0.008
15	0.120 ± 0.008
20	0.123 ± 0.008

As shown in Tab. 5, the K_d is not influenced by the S/L ratio under these experimental conditions; the mean value of K_d equals 0.126 ± 0.013 m^3/kg. A constant K_d for this Np(V) concentration and range of S/L ratio was reported also for the sorption of Np(V) on other minerals [43, 44].

In the second batch series, the sorption of Np on OPA was measured at pH 8.2 under aerobic conditions by varying the Np(V) concentration between 10^{-12} and 10^{-4} M and using ^{239}Np as tracer. The S/L ratio of this series was 15 g/L corresponding to ≈ 65% sorption. The result is shown in Fig. 2, where the data of Tab. 5 are included as well.

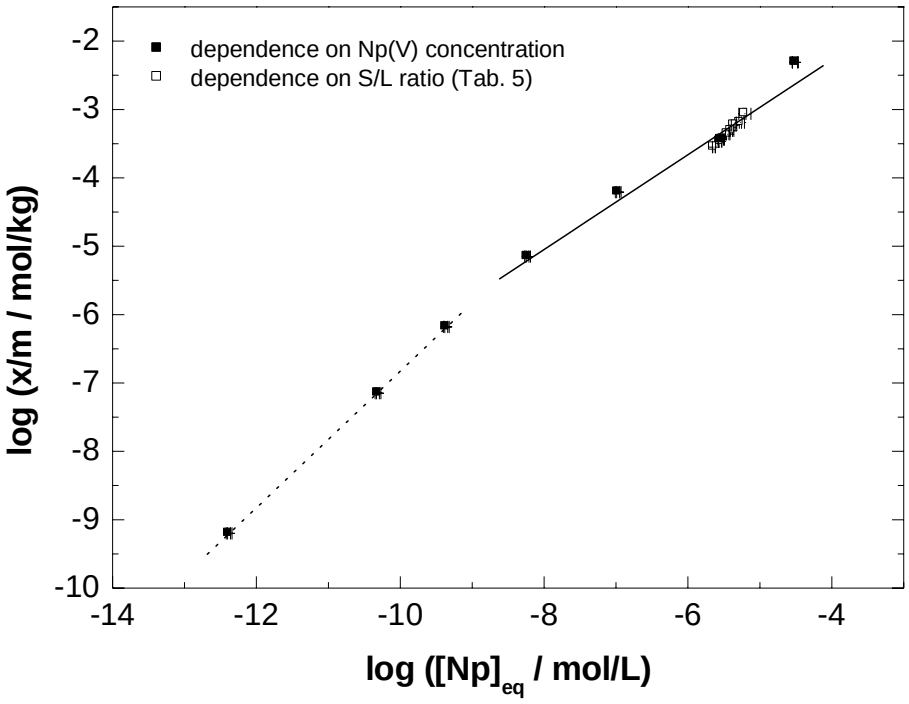

Figure 2: Sorption of Np(V) on OPA (BHE 24/1) as a function of Np(V) concentration and S/L ratio at pH = 8.2 under calcite saturation and aerobic conditions. For all points the error bars (calculated from the 1σ error of the measured activity) are smaller than the symbols (smaller than 0.1 log units).

The sorption isotherm (Fig. 2) can be described by the Freundlich type formalism given by eq. 3 [45]. The isotherm in Fig. 2 can be divided into two parts. The linear part below 10^{-8} M provides a slope of 1.00 ± 0.01 (dotted line). In this concentration range, sorption remains constant with a related K_d value of 1.445 ± 0.033 m^3/kg. The data between 10^{-8} and 10^{-4} mol/L show a slope of 0.69 ± 0.04 (solid line), reflecting a non-linear sorption behavior of Np(V) on OPA. The decrease in the relative amount of Np sorbed with increasing Np concentration may be explained by different affinities of the sorption sites for Np(V) due to different sorption characteristics of the various minerals contained in OPA. Apparently enough sorption sites with a high affinity are available at concentrations below 10^{-9} M Np(V) and the system is far away from site saturation. At higher Np concentrations, the high affinity sites are already occupied and low-affinity sites are accessed resulting in a weaker sorption of Np(V).

A similar isotherm measurement at a lower pH of 7.6 in synthetic OPA pore water did not show such a behavior [46]. In this case, sorption of 10^{-5} - 10^{-11} M Np(V) on OPA was lower by up to two orders of magnitude. On one hand, lower sorption can be explained by the lower pH value as Np(V) sorption decreases with decreasing pH (see next Sect.). On the other hand, the Ca^{2+} concentration in OPA pore water (see Tab. 2) exceeds the corresponding concentration in saturated calcite solution at pH = 8.2 by two orders of magnitude (as calculated with Visual MINTEQ V. 2.52 [19]). The ionic strength of pore water is ≈ 0.4 M compared to < 0.01 M in saturated calcite solution. Probably, the deviations in pH, electrolyte composition, and ionic strength are the reasons for the different sorption behaviors.

4.1.3 Influence of pH and pCO_2

Neptunium

For sorption experiments at different pH (pH 6 - 10) and pCO_2 ($10^{-3.5}$ and $10^{-2.3}$ atm), saturated calcite solutions as background electrolyte were used. Batch experiments were performed under aerobic conditions (aerobic OPA powder (BHE 24/1)) and anaerobic conditions (anaerobic OPA powder (BDR 2), Ar glove box, $pCO_2 = 10^{-2.3}$ atm) using a S/L ratio of 15 g/L. Fig. 3 shows the sorption of Np(V) on OPA at initial concentrations of 7×10^{-12} and 8×10^{-6} M under aerobic and anaerobic conditions. At both concentrations under aerobic conditions, the sorption edge occurs between pH 7.0 - 7.5. In the absence of oxygen under a higher partial pressure of CO_2 ($10^{-2.3}$ atm), which has been estimated for the OPA host rock formation [47], the sorption edge and sorption maximum are shifted to lower pH due to higher carbonate concentrations resulting from the increased pCO_2, which has a significant influence on Np(V) speciation (see Fig. 4). The sorption maximum under aerobic conditions is between pH 8 - 9. In the case of the micromolar Np(V) concentration, maximum sorption is reached at pH 8.9 with 66% Np(V) sorbed. The curve with picomolar Np concentration exhibits maximum sorption at pH 8.3 with 95% Np(V) sorbed. In both cases, sorption decreases at pH > 9.5 due to the complexation of Np with carbonate in aqueous solution (see Fig. 4). The K_d for a Np(V) equilibrium concentration of 3×10^{-13} M at pH 8.3 amounts to 1.343 ± 0.105 m^3/kg and exceeds the corresponding value for $[Np]_{eq} = 3 \times 10^{-6}$ M (K_d = 0.110 ± 0.008 m^3/kg) by one order of magnitude.

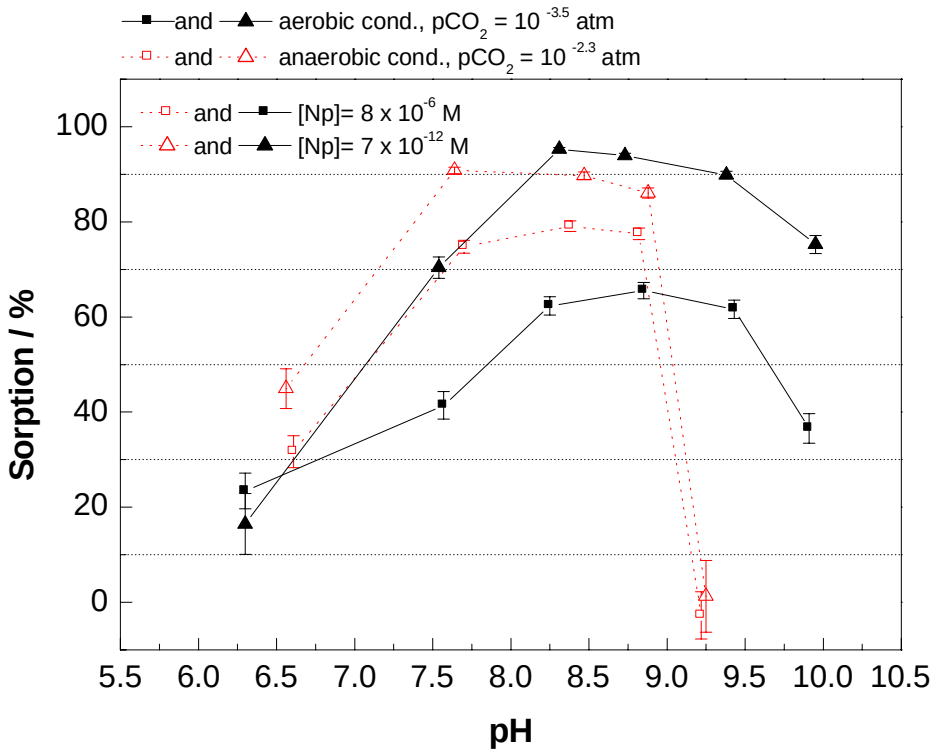

Figure 3: Sorption of 8×10^{-6} and 7×10^{-12} M Np(V) on 15 g/L OPA as a function of pH in saturated calcite solution under aerobic and anaerobic (p_{CO2} $10^{-2.3}$ atm) conditions.

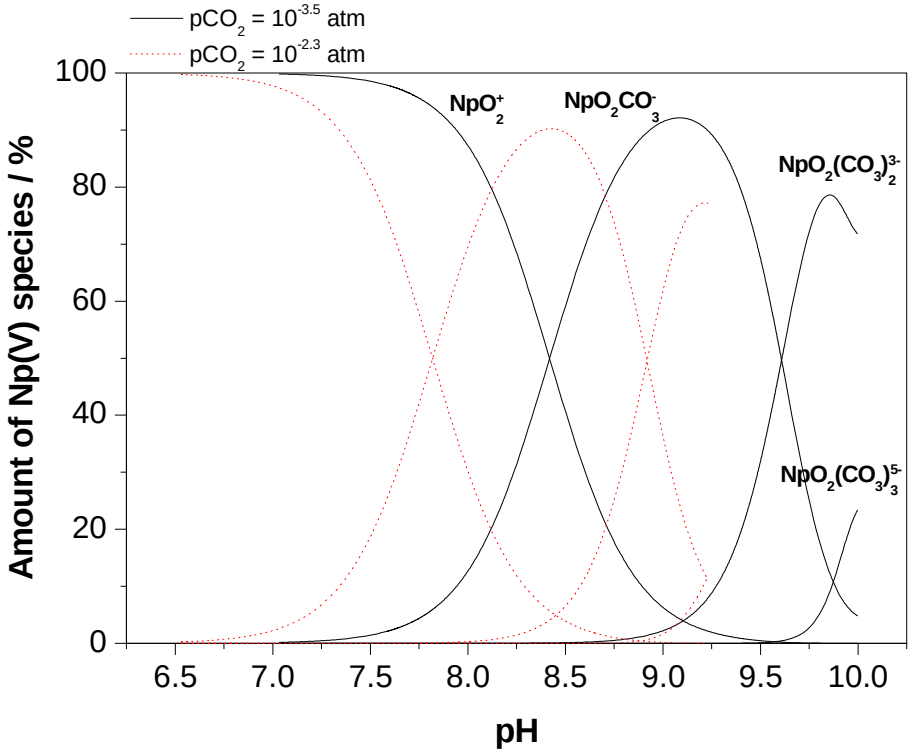

Figure 4: Np(V) speciation in aqueous solution under calcite saturation condition as a function of pH for 8×10^{-6} M Np(V) and pCO_2 equal to $10^{-3.5}$ atm (solid lines) and $10^{-2.3}$ atm (dotted lines); species present at a level less than 1% are not shown. The distribution of Np(V) complexes was calculated with the geochemical equilibrium speciation software Visual MINTEQ V. 2.52 [19]. The thermodynamic data contained in the database of MINTEQ are those given in [10] and the NIST (National Institute of Standards and Technology, USA) database 46.6.

Under anaerobic conditions, the percentage of Np(V) sorbed is almost constant between pH 7.5 - 9 with maximum sorption occurring at pH 8.4 for 8×10^{-6} M Np(V) (80% sorbed) and pH 7.6 – 8.6 for 7×10^{-12} M Np(V) (90% sorbed), respectively. There is no sorption of Np(V) at pH > 9.25 at both Np concentrations due to the formation of negatively charged Np-carbonate species, which are predicted from speciation calculations (see Fig. 4). The maximum K_d value at micromolar Np(V) concentration (0.252 m^3/kg at pH 8.4, Fig. 5) exceeds the corresponding value under aerobic conditions by a factor of 2. At lower Np concentration, the highest K_d of 0.660 m^3/kg occurs at pH 7.6. The stronger sorption of 8×10^{-6} M Np(V) in the absence of oxygen was found to be caused by a partial reduction of

Np(V) to Np(IV) as determined by liquid-liquid extraction using HDEHP as extracting agent. This result is supported by Eh measurements in the near neutral pH range, indicating a lower redox potential of ≈ 100 mV under anaerobic conditions compared to ≈ 400 mV (SHE) under aerobic conditions. The decrease in the redox potential might be caused by the dissolution of iron(II) containing minerals (pyrite and siderite), which make up 4.1% of OPA. Due to the lower solubility of Np(IV) compared to Np(V) [10], a precipitation of Np(IV) in this pH range can not be excluded. It has also to be taken into account that aerobic and anaerobic OPA samples are from different bore cores. Therefore, differences in the sorption behavior may be related to minor differences in the mineralogy and specific surface areas of the two OPA samples.

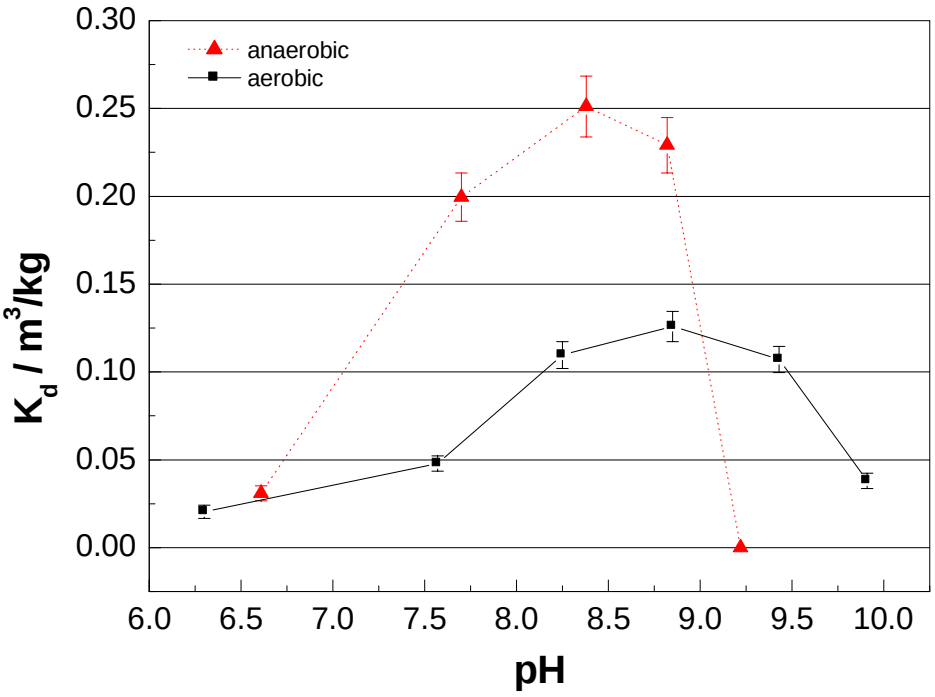

Figure 5: Sorption of 8×10^{-6} M Np(V) on 15 g/L OPA as a function of pH under aerobic and anaerobic (p_{CO2} $10^{-2.3}$ atm) conditions in saturated calcite solution.

Plutonium

The sorption of Pu(IV) and Pu(VI) on OPA (BHE 24/1) has been studied by batch experiments as a function of pH in 0.1 M $NaClO_4$ solution. A similar experiment was conducted with Th(IV) as an oxidation state analogue. Experiments were performed with a S/L ratio of 1 g/L (Pu(IV) and Th(IV)), and 2 g/L (Pu(VI)) in the pH range 1 - 8 with

concentrations of 4×10^{-7} M for Pu(IV) and Th(IV) and 1×10^{-7} M for Pu(VI). The obtained results are shown in Fig. 6. The sorption of Pu(IV) and Pu(VI) as well as of Th(IV) on OPA is strongly influenced by the pH. The sorption increases with increasing pH up to pH 4 (for Pu(IV) and Th(IV) and to pH 6 (for Pu(VI)). For Pu(IV) and Th(IV), a similar sorption behavior was found as a function of pH. The sorption edges of Pu(IV) and Th(IV) are both at about pH 1.5 with maximum sorption of 99% between pH 4 and 8. The sorption edge of Pu(VI) is shifted to a higher pH value (pH = 2.5) with maximum sorption of 99% between pH 6 and 8. In case of Pu(VI) a partial reduction to Pu(IV) can not be excluded. Due to the strong sorption of Pu(IV) and Pu(VI) on OPA in the natural pH range (7 – 9), this would lead to an enhanced immobilization and retardation of the aqueous plutonium. A similar behavior was found for Pu(IV) and Th(IV) sorption on kaolinite [48].

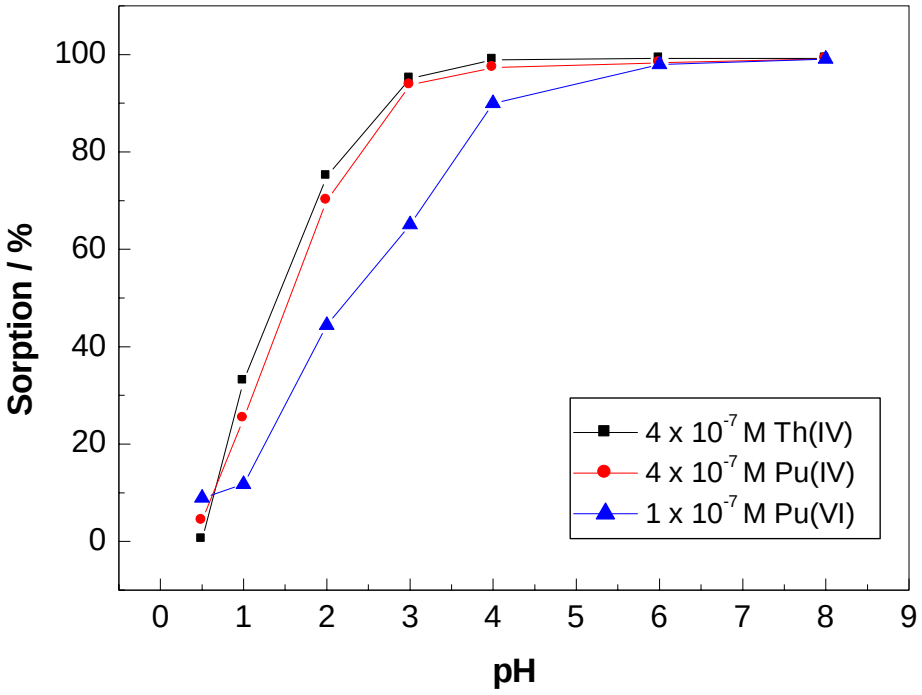

Figure 6: Sorption of Pu(IV), Pu(VI), and Th(IV) on OPA in 0.1 M $NaClO_4$ as a function of pH at S/L ratio of 1 g/L for Pu(IV) and Th(IV)), and 2 g/L for Pu(VI) under aerobic conditions.

4.1.4 Influence of humic acid (HA)

Neptunium

^{14}C labelled synthetic HA (M42) [18] was used at a concentration of 10 mg/L to study the influence of HA on the sorption of Np(V) onto OPA as a function of pH under the same experimental conditions as in the Chapter 4.1.3. The preparation of the samples was carried out analogously to the other batch experiments. HA was added instantly after addition of ^{237}Np(V) or ^{239}Np(V).

Figures 7 and 8 show the sorption of 7×10^{-12} M and 8×10^{-6} M Np(V) on OPA under aerobic and anaerobic (p_{CO2} $10^{-2.3}$ atm) conditions in the presence of HA, respectively. For comparison, data for Np uptake in the absence of HA are also shown.

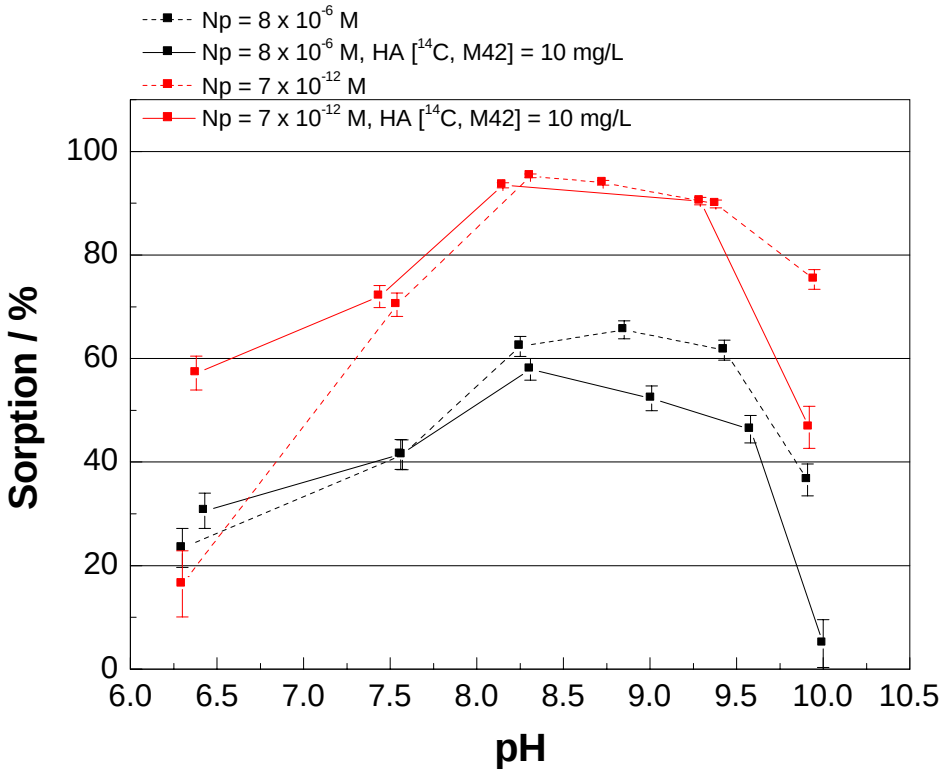

Figure 7: Sorption of 8×10^{-6} M and 7×10^{-12} M Np(V) on 15 g/L OPA in the presence/absence of HA as a function of pH under aerobic conditions in saturated calcite solution.

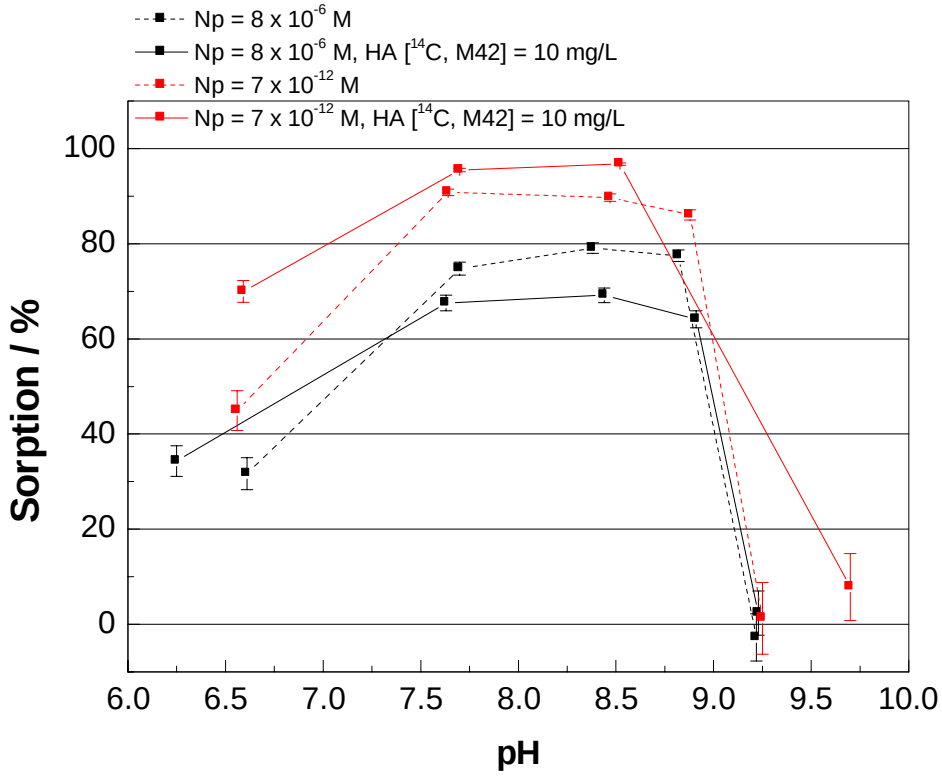

Figure 8: Sorption of 8×10^{-6} and 7×10^{-12} M Np(V) on 15 g/L OPA in the presence/absence of HA as a function of pH under anaerobic conditions (p_{CO2} $10^{-2.3}$ atm) in saturated calcite solution.

At 8×10^{-6} M Np(V) and $p(CO_2) = 10^{-3.5}$ atm, the presence of HA reduces slightly the amount of Np sorbed on OPA in the pH range of 8 – 10, probably due to formation of Np humate or ternary Np humate-carbonate complexes [27, 49]. This effect of HA is less pronounced at 7×10^{-12} M Np(V).

Plutonium

The Pu(IV) sorption onto OPA (BHE 24/1) was also investigated in the presence and absence of HA under aerobic conditions in OPA pore water (pH = 7.6). Analogous to Np batch experiments with HA, ^{14}C (M42) was used at a concentration of 10 mg/L. Pu(IV) sorption isotherms were measured as a function of the S/L ratio between 2 - 20 g/L at constant Pu(IV) concentration of 1×10^{-7} M. After preconditioning the batch samples, aliquots of $^{239}Pu(IV)$ and HA stock solution were added and mixed at same time with the suspensions. After 62 h contact time, the solid and liquid phases were separated by centrifugation. Then aliquots of

the suspensions were taken and analyzed by LSC. The influence of HA on the sorption of Pu(IV) on OPA is shown in Tab. 6.

Table 6: K_d values for the sorption of Pu(IV) on OPA in absence / presence (10 mg/L) of HA under aerobic conditions as a function of S/L ratio in OPA pore water at pH = 7.6.

S /L / g/L	**K_d / m^3/kg**	
	With HA	**Without HA**
2	4.64 ± 0.35	70.50 ± 4.88
4	6.49 ± 0.47	122.46 ± 8.64
6	8.88 ± 0.63	125.71 ± 9.00
8	10.94 ± 0.78	40.56 ± 2.84
10	13.07 ± 0.93	97.48 ± 6.99
15	30.18 ± 2.14	78.69 ± 5.52
20	14.56 ± 1.03	47.97 ± 3.38

HA significantly affects the sorption of Pu(IV) on OPA in pore water at pH 7.6 and reduces the averaged K_d value from 83.3 ± 33.7 m^3/kg in the absence of HA to 12.7 ± 8.5 m^3/kg in the presence of HA. This effect is probably due to the formation of Pu humate complexes, since tetravalent actinides form strong complexes with HA [49]. Pu(IV) is significantly mobilized in the presence of HA under these experimental conditions. Our results are in good agreement with sorption data reported for Pu(III/IV) on kaolinite in the presence of HA compared to the HA-free system [48, 50].

4.1.5 Influence of temperature [51, 52]

Neptunium

The German concept for nuclear waste disposal proceeds on the assumption that the temperature at the contact surface of the containers with the host mineral will stay below 100 °C [53]. This increase in temperature might change the physical properties of the host rock formation and influence the sorption and migration of the radionuclides. Therefore, the effect of temperature has to be taken into account. Until now, the effect of temperature on radionuclide sorption, especially on clay minerals has not been investigated in much extent and only few studies have been reported on Np and Pu sorption up to 80 °C [54, 55]. More information is available for the sorption of non-radioactive heavy metals or lanthanides (Ni^{2+},

Cs^{+}, Cd^{2+}, Co^{2+}, and Eu^{3+}) onto several clay minerals such as smectite, montmorillonite, and kaolinite [56 - 59]. Therefore, the sorption of micromolar Np(V) on OPA (BHE 24/1) at temperatures up to 80 °C in synthetic OPA pore water (pH = 7.6, I = 0.4) under aerobic conditions was studied and the results were compared with our data at room temperature [28]. Figure 9 shows the percentage of Np(V) sorbed on OPA in dependence of S/L ratio and temperature compared to the results at 20 °C [28].

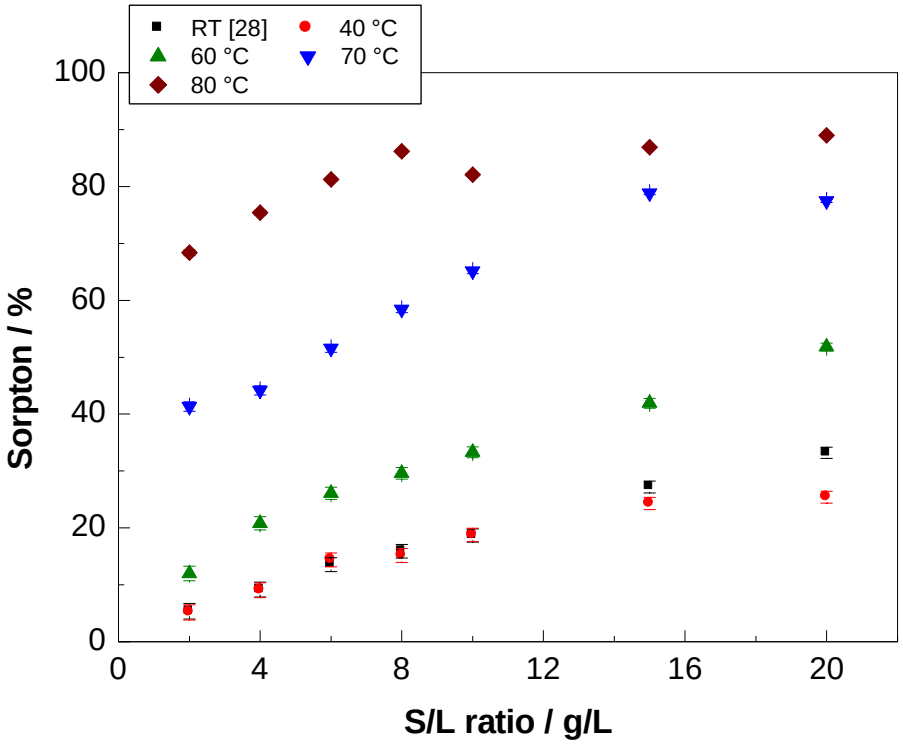

Figure 9: Sorption of 8×10^{-6} M Np(V) on OPA (BHE 24/1) as a function of S/L ratio and temperature in OPA pore water under aerobic conditions.

The sorption of Np does not change as temperature is raised from room temperature to 40 °C. Between 40 and 80 °C, sorption increases continuously with increasing temperature. At 80 °C an average K_d value of 0.678 ± 0.254 m^3/kg is reached which exceeds the corresponding value at room temperature by a factor > 27. The average K_d values for different temperatures are summarized in Tab. 7.

Table 7: Averaged K_d values for the sorption of Np(V) on OPA (S/L = 2 - 20 g/L) in OPA pore water in dependence of temperature under aerobic conditions.

Temperature / °C	pH	$[Np]_0$ / mol/L	K_d / m^3/kg
20 [28]	7.6	8×10^{-6}	0.025 ± 0.005
40	7.6	1×10^{-5}	0.023 ± 0.004
60	7.5	8×10^{-6}	0.056 ± 0.005
70	7.5	1×10^{-5}	0.235 ± 0.072
80	7.5	8×10^{-6}	0.678 ± 0.254
preconditioned at 60 °C sorption at 20 °C	7.5	8×10^{-6}	0.028 ± 0.009

To exclude the possibility that a change of the surface structure of OPA due to higher temperature causes the observed increase in Np(V) sorption, one batch series was performed in which the preconditioning of OPA was carried out at 60 °C. After cooling of the suspension to room temperature, the K_d values were determined as described before. As can be seen from Tab. 7, the preconditioning of the clay suspension at elevated temperature had no effect on the neptunium sorption on OPA. Within experimental uncertainties, the K_d values are identical. Higher sorption at elevated temperature might be caused by an increase of the negative charge on the clay surface as it was reported for other clay minerals, e.g., kaolinite [60]. For rutile it was also reported that the point of zero net proton charge (pH_{znpc}) is shifted by 0.7 units to lower pH values as temperature increases from 25 to 100 °C; for pH values above the pH_{znpc}, the negative surface charge also increased with increasing temperature [61]. During the experiment, we observed that the heating of the clay suspension was followed by a decrease in pH (at 80 °C with 20 g/L OPA the pH decreased from 7.6 to 7.0). This effect is possibly the result of a stronger deprotonation of the surface and therefore supports the assumption of an increase in the negative surface charge.

Our results indicate that Np(V) sorption on OPA is an endothermic reaction. This trend is in good agreement with studies of Runde et al. [55], who investigated Np(V) sorption on hematite, montmorillonite, and silica. For all minerals, neptunium sorption increased when temperature was raised up to 80 °C.

By using the Van't Hoff equation (4), the apparent sorption enthalpy of Np(V) on OPA can be calculated:

$$\log(K_d) = \frac{\Delta_r S^{App}}{2.3R} - \frac{\Delta_r H^{App}}{2.3R} \times \frac{1}{T}, \qquad (4)$$

where $\Delta_r H^{App}$ is the apparent reaction enthalpy in kJ/mol, $\Delta_r S^{App}$ the apparent entropy in J/K mol, T the absolute temperature in Kelvin and R the universal gas constant. By performing an Arrhenius plot ($\log(K_d)$ vs. 1/T) between 40 and 80 °C as shown in Fig. 10, an apparent sorption enthalpy of 77.3 ± 15.8 kJ/mol was derived for the sorption of Np(V) on OPA. This value lies in the same order of magnitude as those reported for the sorption of Ni^{2+} (33 ± 10 kJ/mol) and Eu^{3+} (39 ± 10 kJ/mol) on montmorillonite at pH = 7.0 ± 0.5 [57, 58] or Co^{2+} (27 - 42 kJ/mol) and Cd^{2+} (26 - 40 kJ/mol) on kaolinite at pH 7.0 and 7.5, respectively [59].

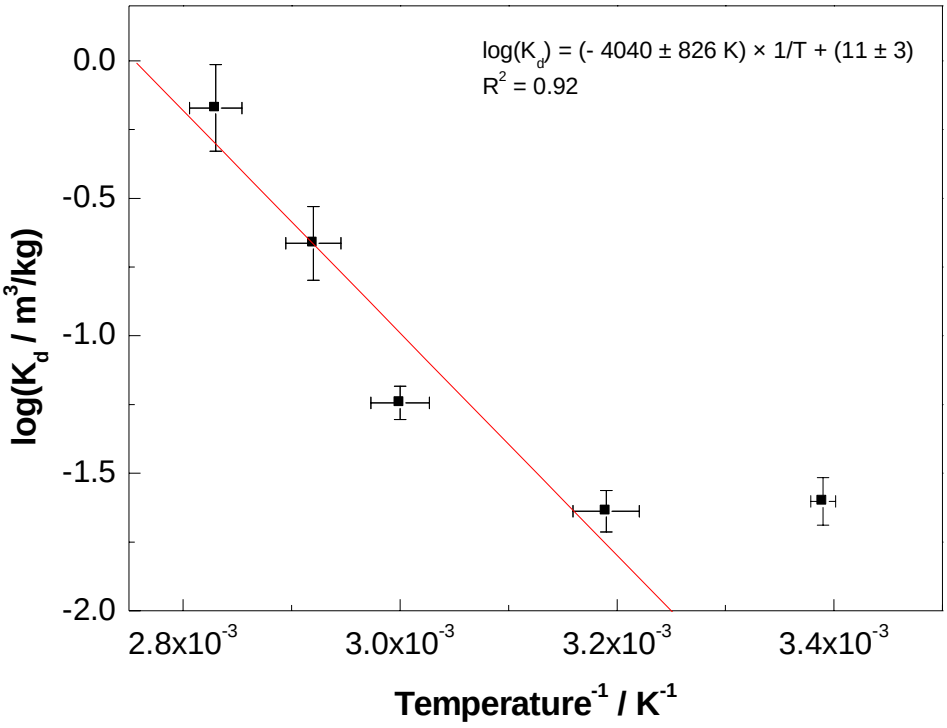

Figure 10: Arrhenius plot for the sorption of Np(V) on OPA in OPA pore water at pH = 7.6 under aerobic conditions using the average K_d values shown in Table 7.

Plutonium

Analogous to Np, the influence of temperature on the sorption of Pu(VI) on OPA (BHE 24/1) was investigated. Sorption isotherms at room temperature (20 °C) and 60 °C were carried out with a Pu(VI) concentration of about 1×10^{-7} M as a function of S/L ratio (2 - 20 g/L) under aerobic conditions using OPA pore water (pH = 7.6) as a background elektrolyte. Table 8 presents the obtained K_d values at both temperatures as a function of the S/L ratio. The

sorption of Pu(VI) increases with increasing temperature. The K_d value at 60 °C is about 6 times higher than at 20 °C (12.5 ± 3.3 m^3/kg). This result is in good agreement with the data for Np(V) sorption on OPA and indicates that Pu(VI) sorption on OPA is an endothermic reaction, which would have a positive implication for the nuclear waste disposal in OPA.

Table 8: K_d values for the sorption of Pu(VI) on OPA at room temperature (20 °C) and 60 °C under aerobic conditions as a function of S/L ratio in OPA pore water at pH 7.6.

S/L / g/L	**K_d / m^3/kg**	
	20 °C	**60 °C**
2	11.28 ± 0.87	94.20 ± 6.81
4	7.83 ± 0.60	96.02 ± 6.92
6	10.62 ± 0.79	96.98 ± 4.93
8	11.26 ± 0.85	65.09 ± 4.70
10	13.26 ± 0.97	60.48 ± 4.21
15	15.69 ± 1.21	52.73 ± 3.78
20	17.7 ± 0.87	72.95 ± 4.96

A partial reduction of Pu(VI) to Pu(IV) under these experimental conditions can not be excluded.

4.1.6 Influence of ionic strength and background electrolyte [51, 52]

Since pore water consists of several constituents (mainly NaCl, $CaCl_2$, and $MgCl_2$), the influence of ionic strength at both 0.1 M and 0.4 M $NaClO_4$, NaCl, $MgCl_2$, and $CaCl_2$ electrolytes on the sorption of 8×10^{-6} M Np(V) onto OPA was studied in individual batch experiments at room temperature and pH 7.6.

Figure 11 shows the log(K_d) values for different background electrolytes as a function of S/L ratio. In all cases, Np(V) sorption does not depend on the amount of OPA, which is in good agreement with results mentioned above [16] and studies reported elsewhere [43].

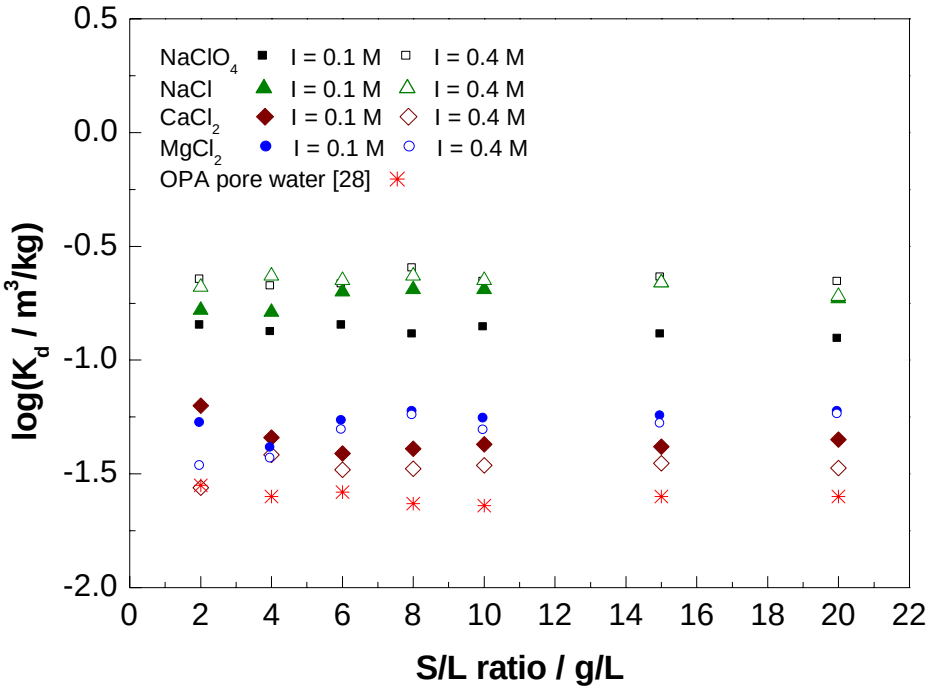

Figure 11: Log K_d values of the sorption of ~ 8×10^{-6} M Np(V) on OPA as a function of S/L ratio and background electrolyte at pH ≈ 7.6 under aerobic conditions at room temperature. For clarity error bars (typically between 0.1 and 0.4 log units) are omitted.

In Fig. 11, two groups of log(K_d) can be distinguished. Background electrolytes containing Na^+ gave log(K_d) values above - 1.0, while electrolyte solutions with divalent cations have log(K_d) values around - 1.5. The values reported for synthetic OPA pore water [28] lie in the same range as for the $CaCl_2$ and $MgCl_2$ electrolytes, independent from ionic strength (0.1 or 0.4 M). Small differences in K_d might be explained by the slightly different pH values. The average K_d values and the corresponding standard deviations (1σ) are presented in Tab. 9. Furthermore, in $NaClO_4$ solution, a weak, but pronounced dependence of Np(V) sorption on ionic strength was noticed. The K_d for sorption of Np(V) in $NaClO_4$ solution increased by a factor of two from 0.133 ± 0.009 m^3/kg to 0.231 ± 0.013 m^3/kg with increasing ionic strength from 0.1 to 0.4 M. In case of kaolinite, the sorption of Np(V) increased by ~ 10% in the near neutral pH range when the ionic strength increased from 0.01 to 0.1 M $NaClO_4$ [43, 49].

Table 9: Averaged K_d values for the sorption of Np(V) on OPA (S/L = 2 - 20 g/L) as a function of different background electrolytes and ionic strength under aerobic conditions at room temperature.

Electrolyte	Ionic strength / M	K_d / m^3/kg	pH	$[Np]_0$ / mol/L
$NaClO_4$	0.1	0.133 ± 0.009	7.8	1×10^{-5}
	0.4	0.231 ± 0.013	7.7	1×10^{-5}
NaCl	0.1	0.214 ± 0.012	7.8	9×10^{-6}
	0.4	0.224 ± 0.017	7.8	9×10^{-6}
$CaCl_2$	0.1	0.045 ± 0.008	7.4	8×10^{-6}
	0.4	0.034 ± 0.003	7.2	8×10^{-6}
$MgCl_2$	0.1	0.054 ± 0.006	7.8	9×10^{-6}
	0.4	0.037 ± 0.008	7.7	9×10^{-6}
Synthetic OPA pore water[28]	0.4	0.025 ± 0.005	7.6	8×10^{-6}

From speciation calculations using Visual MINTEQ V. 2.52 [19], differences in neptunium speciation in investigated background electrolytes at different ionic strength can be excluded as reason for these different K_d values.

4.1.7 Sorption isotherms of Th, U, Np, Pu, and Am in OPA pore water

The migration behavior of actinides in OPA pore water at environmentally-relevant conditions is essential for repository safeguarding, especially because only few sorption studies concerning the actinide sorption on OPA have been published [28, 15].

In this work, the distribution coffecients (K_d values) were determined by batch experiments for Th(IV), U(VI), Np(V), Pu(III, IV, VI), and Am(III)) on OPA (BHE 241) using pore water (pH = 7.6) as background electrolyte under aerobic conditions (except for Pu(III) under Ar atmosphere) as a function of S/L ratio (2 - 20 g/L) and actinide concentration (only U(VI) and Np(V), see Fig. 12) at constant S/L of 15 g/L. Batch experiments were performed as described in Sect. 3.1. Results from batch sorption experiments (sorption isotherms) are expressed through the K_d values. When n = 1 in eq. 3, $K = (x/m) / [An]^n_{eq} = K_d$, which is the slope of the isotherm at the origin. In case of the Freundlich isotherm [45], the constants K and n can be determined from a linear fit of eq. (5) to the experimental data.

$$\log \frac{x}{m} = \log K + n \log[An]_{eq} \qquad (5)$$

The intercept of the line then equals log K_d and the slope is n.

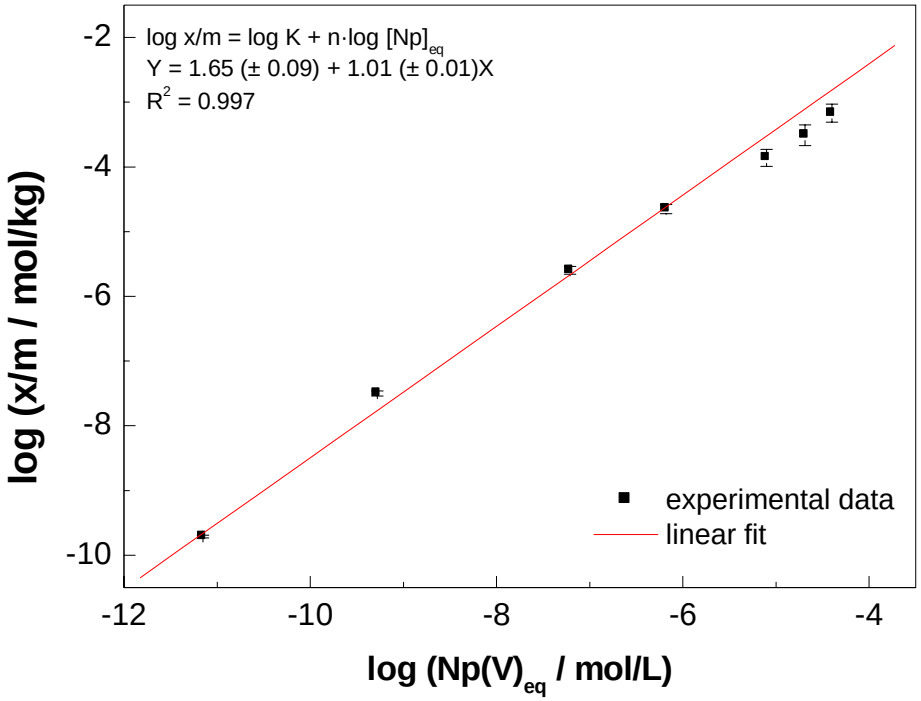

Figure 12: Freundlich isotherm of Np(V) sorption on OPA as a function of Np(V) concentration at S/L ratio 15 g/L in OPA pore water (pH = 7.6) under aerobic conditions.

The slope of the fit line is n = 1.01 (± 0.01), the intercept is log K_d = 1.65 (± 0.09) and the related K_d value is equal to 0.04 ± 0.01 m^3/kg. The obtained K_d value agrees well with the previously determined K_d value (0.025 ± 0.005 m^3/kg) for Np sorption in dependence of S/L (2 - 20 g/L) [28].

In the same way, the sorption of U(VI) on OPA in pore water was investigated by varying the U(VI) concentration between 1.6 × 10^{-4} - 1.3 × 10^{-7} M at constant S/L ratio of 15 g/L under aerobic conditions. The results show a linear sorption behavior (Frendlich isotherm) resulting in a K_d value of 0.05 ± 0.01 m^3/kg. By using eq. 2, an average K_d value of 0.03 ± 0.01 m^3/kg was determined, which agrees well with data from Joseph et al. [15] (K_d = 0.02 ± 0.01 m^3/kg). Since experimental K_d values for Pu sorption on OPA are missing and estimated K_d values were derived from chemical analogous (Th(IV) and Am(III) [62]), we measured the K_d values of Pu(III, IV, VI) and its analogous Th(IV), Am(III) as well as for Np(V) and U(VI) for the first time under identical experimental conditions in pore water at pH 7.6. Figure 13

shows the sorption isotherms of Th, Np, Pu, and Am in pore water at pH 7.6 by varriation of the S/L ratio between 2 - 20 g/L.

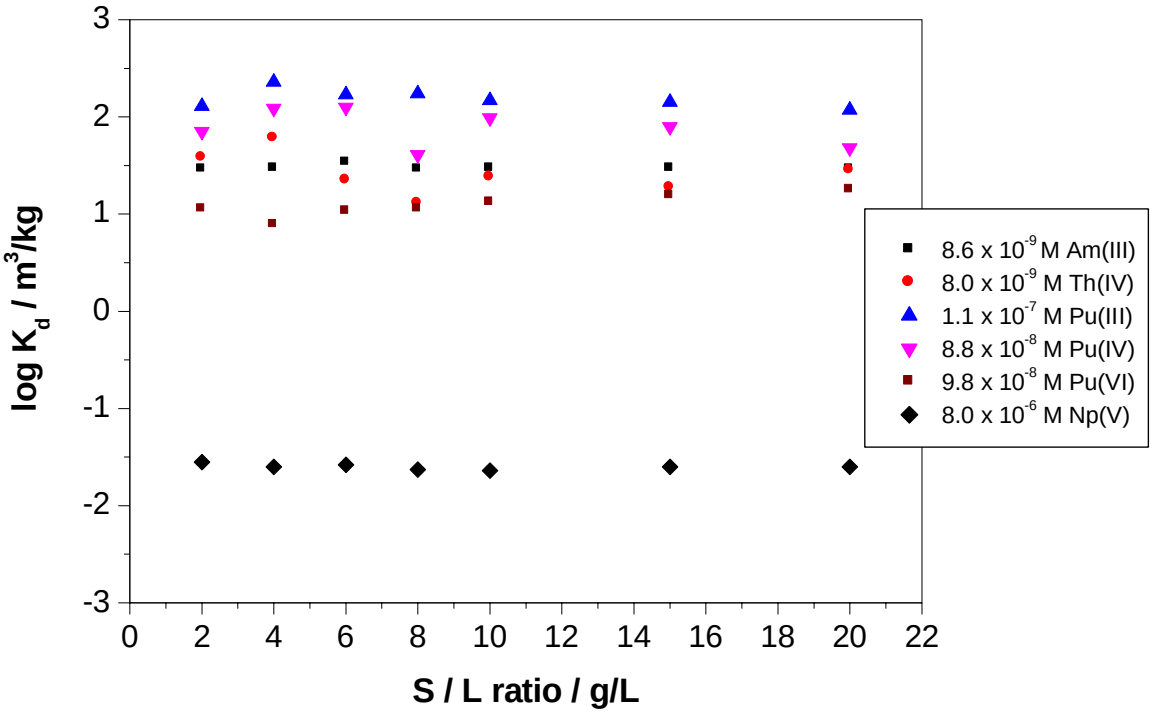

Figure 13: Log K_d values for the sorption of Th(IV), Pu(III, IV, VI), Np(V) and Am(III) on OPA in pore water (pH = 7.6) as function of S/L ratio (2 - 20 g/L) (uncertainty in log K_d values is < ± 0.4 log units).

Linear sorption behavior under these experimental conditions was observed in all cases. The sorption data of Np(V), Pu(III), Am(III) can also be fitted by using the Freundlich isotherm (not shown). The average K_d values of all studied actinides obtained from sorption isotherms in comparison to published data [62] are summarized in Tab. 10.

Table 10: Averaged K_d values for the sorption of actinides on OPA in OPA pore water (pH = 7.6).

Actinide	S/L ratio g/L	[actinide] mol/L	K_d / m^3/kg		
			This work	Ref. [62]	
			pH = 7.8	pH = 7.2	pH = 7.6
Am(III)	2 - 20	8.6×10^{-9}	29.8 ± 1.8	17.0	63.0
Pu(III)	2 - 20	1.1×10^{-7}	158.7 ± 37.1	22.6	75.2
Th(IV)	2 - 20	8.0×10^{-9}	29.0 ± 15.6	55.4	55.4
Pu(IV)	2 - 20	8.8×10^{-8}	83.3 ± 33.7	-	-
Np(V)	2 - 20 15	8.0×10^{-6} 5.0×10^{-5} - 1.0×10^{-11}	0.03 ± 0.01	-	-
U(VI)	15	1.6×10^{-4} - 1.3×10^{-7}	0.03 ± 0.01	-	-
Pu(VI)	2 - 20	9.8×10^{-8}	12.5 ± 3.3	-	-

As can be seen from Tab. 10, the measured K_d values depend on the oxidation state of the actinide element. K_d values for the tri- and tetravalent actinides are in the range of 30 - 159 m^3/kg, indicating strong sorption on OPA in pore water at pH 7.6. The measured K_d values for Th(IV), Pu(III/IV) and Am(III) are in the same order of magnitude with the corresponding K_d values from literature [62]. The K_d value of Pu(VI) is lower than those for Th(IV), Pu(III, IV), and Am(III), but it is about three orders of magnitude higher than the K_d values of U(VI) and Np(V). This is probably due to a partial reduction of Pu(VI) to Pu(IV) during the batch experiments, which causes the higher sorption on OPA (confirmed by EXAFS). U(VI) and Np(V) are weakly sorbed on OPA with K_d values of 0.03 ± 0.01 m^3/kg. As a conclusion, tri- and tetravalent actinides will be immobilized in the host rock OPA in comparison to penta- und hexavalent actinides, which will be more mobile.

4.2 Diffusion experiments

Because OPA has a very low hydraulic conductivity, diffusion is considered to be the main process responsible for the transport of radionuclides released from a repository [7]. Due to little diffusion data available for actinides, the main objective of our investigation was to study the diffusion of Np(V) as a function of temperature in the presence/absence of HA by

using OPA pore water (pH = 7.6) as a mobile phase to determine diffusion parameters needed for transport modeling.

The distribution coefficient K_d, as one of the most important parameters to evaluate the migration behavior of radionuclides in argillaceous rocks, can be also obtained by diffusion experiments [7, 28]. Diffusion experiments may be a more representative method to simulate the migration behavior of radionuclides transported from the nuclear repository into the environment, but they take a longer time and are more complicated to perform compared to batch experiments. During diffusion experiments, it is also difficult to change and control physicochemical parameters such as pH, Eh, etc. of the contact solutions. Due to many problems in diffusion experiments, only few studies showed a good agreement between K_d values obtained by batch experiments and diffusion measurements [63 - 69]. One of the goals was to compare K_d values from batch experiments on suspended material with the values derived from in-diffusion experiments. To make this comparison as close as possible, several chemical parameter were identical during both the batch and diffusion experiments, i.e., Np(V) concentration (8×10^{-6} M), pore water (pH = 7.6), HA (M42) concentration 10 mg/L, and aerobic conditions. The experimental setup for the diffusion experiments is shown in Fig. 1 and an overview of the used tracers and their concentrations can be found in Tab. 4 (see Sect. 3.2). The experimental data processing of through-, out-, and in-diffusion experiments has been described in [7, 28]. A computer code based on Mathematica 6.0 has been developed for modeling through-, out-, and in-diffusion experiments. It was used to determine the diffusion coefficients (D_e) and the rock capacity factors (α) for tritiated water (HTO), $^{22}Na^+$, Np, and the distribution coefficient (K_d) of $^{22}Na^+$ and Np in OPA. Since HTO can be considered as a nonsorbing tracer, i.e., $K_d = 0$, α is equal to porosity (ε). Making the assumption that the pore space determined for HTO is accessible for $^{22}Na^+$ [7], the K_d value for $^{22}Na^+$ can be calculated by eq. 6. ε is obtained from the through diffusion experiment with HTO.

$$\alpha = \varepsilon + \rho \cdot K_d \tag{6}$$

where ε is the diffusion-accessible porosity; ρ (kg/m^3) is the bulk dry density.

The values for D_e and α for HTO and $^{22}Na^+$ were obtained by fitting the results of experimental data of both transient and steady-state phases to the analytical solution of accumulated activity. The quality of the parameters D_e and α was tested by using them as input parameters in the equation of flux (eq. 7).

$$J(L,t) = \frac{1}{S} \cdot \frac{\partial A}{\partial t}, \tag{7}$$

where J(L, t) is the flux at the low-concentration boundary (x = L) at diffusion time t, A (Bq/m^3) is the radionuclide activity in solution, t (s) is the diffusion time, and S (m^2) is the cross section area of the sample.

Figure 14 shows as an example the flux and the accumulated activity of cell 1 (Tab. 4) as a function of diffusion time obtained by through-diffusion of HTO and ^{22}Na. As can be seen, the flux increases with diffusion time at the transient phase and becomes constant at the steady phase. In the transient phase, the flux depends on diffusion time, D_e, ε, and α, while in the steady state the flux depends only on D_e. The accumulated activity increases with time, becoming a linear function of time at the steady phase.

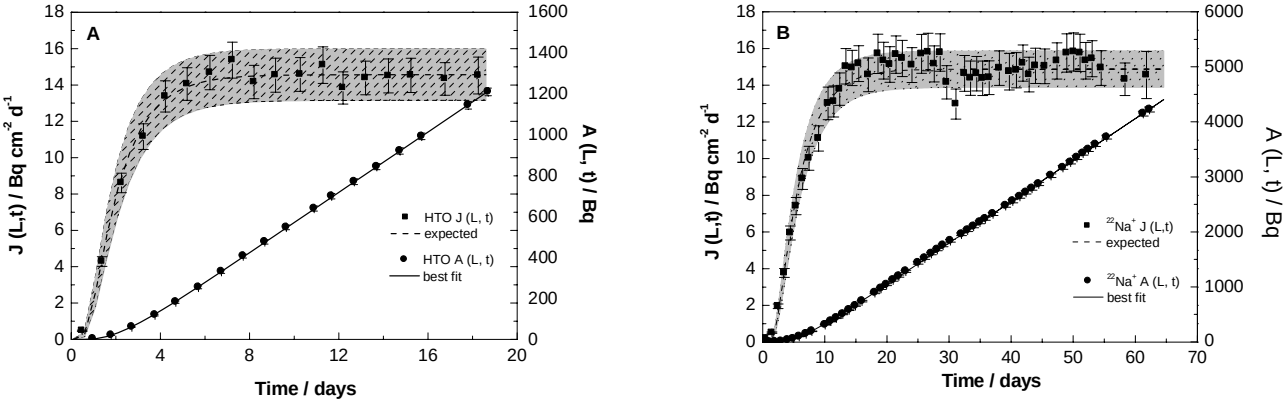

Figure 14: Through-diffusion curves of cell 1 for HTO (A) and $^{22}Na^+$ (B) with flux (J(L, t)) and accumulated activity (A_{cum}) as a function of diffusion time through OPA in pore water at aerobic condition (The shaded area represents the uncertainty of the calculated curve).

As can be seen from Fig. 14, the experimental data of flux J for both HTO and $^{22}Na^+$ as a function of diffusion time are in good agreement with the calculated data. The non-sorbing tracer HTO reached steady state after about 6 days, while the weak sorbing cation $^{22}Na^+$ took longer time (about 15 days) to reach it. Moreover, the diffusion parameters of HTO and $^{22}Na^+$ were determined also by out-diffusion experiments and similar values for D_e and α were obtained. In case of $^{22}Na^+$, the diffusion parameters D_e and K_d were also obtained by in-diffusion experiments after diffusion of Np and were in excellent agreement with those obtained by the through-diffusion technique, indicating that both methods can be used to study the diffusion behavior of radionuclides in the clay. The obtained diffusion parameters (D_e, ε, α, and K_d) for HTO and $^{22}Na^+$ are summarized in Tab. 11.

Table 11: Diffusion parameters (D_e) for HTO and (D_e and D_a**)** for $^{22}Na^+$ in OPA by through- and in-diffusion experiments, respectively.

Cell	Temp. (°C)	HTO		$^{22}Na^+$			
		ε	D_e ($\times 10^{-11}$ m^2/s)	α	D_e ($\times 10^{-11}$ m^2/s)	D_a ($\times 10^{-11}$ m^2/s)	K_d ($\times 10^{-3}$ m^3/kg)
1	20 ± 2	0.15 ± 0.01	1.50 ± 0.10	0.50 ± 0.02[a] 0.44 ± 0.03[b]	1.9 ± 0.1[a] 1.8 ± 0.2[b]	3.8 ± 0.2[a] 4.1 ± 0.4[b]	0.15 ± 0.03[a] 0.14 ± 0.01[b]
2	20 ± 2	0.20 ± 0.01	1.97 ± 0.14	0.44 ± 0.01	2.5 ± 0.4[a]	5.7 ± 0.9[a]	0.10 ± 0.01[a]
3[c]	20 ± 2	0.14 ± 0.01	1.73 ± 0.12	0.40 ± 0.01	3.1 ± 0.7[a]	7.8 ± 1.8[a]	0.11 ± 0.01[a]
4	60 ± 2	0.19 ± 0.01	3.13 ± 0.22	0.40 ± 0.01	3.5 ± 0.7[a]	8.8 ± 1.8[a]	0.11 ± 0.01[a]
[29]	23 ± 2	0.09 ± 0.02	1.48 ± 0.07	0.44 ± 0.01			
[63]	23 ± 2			0.33 ± 0.03	1.6 ± 0.1[a]	4.8 ± 0.3[a]	0.10 ± 0.02[a]

[a] Values measured in through-diffusion experiments, [b] values measured in in-diffusion experiments, and [c] presence of HA

As shown in Tab. 11, all samples have a similar porosity, which is representative for OPA from Mont Terri [29]. The D_e values of HTO for cells 1 to 3 are in the same range as values from the literature [29]. The obtained D_e of cell 4 at 60 °C is higher by a factor of about 1.5 than for those at room temperature. From the literature, it is known that the diffusion of HTO increases with increasing temperature. Our D_e value at 60 °C agrees well with the corresponding experimental data from Van Loon et al. [7] (55 °C: 2.95 ± 0.22 × 10^{-11} m^2/s; 65 °C: 3.63 ± 0.35 × 10^{-11} m^2/s). In the case of $^{22}Na^+$ similar diffusion parameters were obtained in all experiments. The K_d values were constant within the experimental errors. The obtained D_e or D_a values (apparent diffusion coefficient $D_a = D_e / \alpha$) are for all cells comparable (within experimental error). The presence of HA (cell 3) and an increase in temperature up to 60 °C (cell 4) had no significant effect on the diffusion of $^{22}Na^+$ in OPA.

In all diffusion experiments, stainless steel filter plates were used to confine the clay in the diffusion cell. The filters have retarding and sorption effects which can be important at the clay boundary. Since the amount of Np(V) sorbed on the filter plates was very low, the sorption effect is negligible and only the retardation effect of the filter was taken into account by introducing the diffusion coefficient (D_f) of Np(V) in the filter. The parameter D_f (m^2/s) can be estimated by $D_f = (D_w/10)$ [70], where D_w (m^2/s) is the diffusion coefficient of Np(V) in water (OPA pore water). Using the capillary method [71], D_w values of $^{237}Np(V)$ in OPA pore water in presence/absence of HA and at elevated temperature (60 °C) were determined to be 6.0 ± 1.0 × 10^{-10} m^2/s in absence of HA, 7.0 ± 1.0 × 10^{-10} m^2/s in presence of HA, and

$2.8 \pm 0.5 \times 10^{-9}$ m^2/s at 60 °C. These values were used for correcting the retardation effect of the filter plates in the in-diffusion experiment with Np(V).

The in-diffusion experiments with $^{237}Np(V)$ were started after the through- and out-diffusion studies of HTO had been completed (for cell 1 after HTO and $^{22}Na^+$ through- and out-diffusion). The Np(V) concentration in all diffusion experiments was 8×10^{-6} M, the HA (M42) concentration was 10 mg/L, and the diffusion time was about 35 days. Figure 15 shows the concentration profile of $^{237}Np(V)$ and $^{22}Na^+$ in OPA of cell 1. The diffusion distance for $^{237}Np(V)$ and $^{22}Na^+$ were less than 1 mm in 35 days and 17 h, respectively.

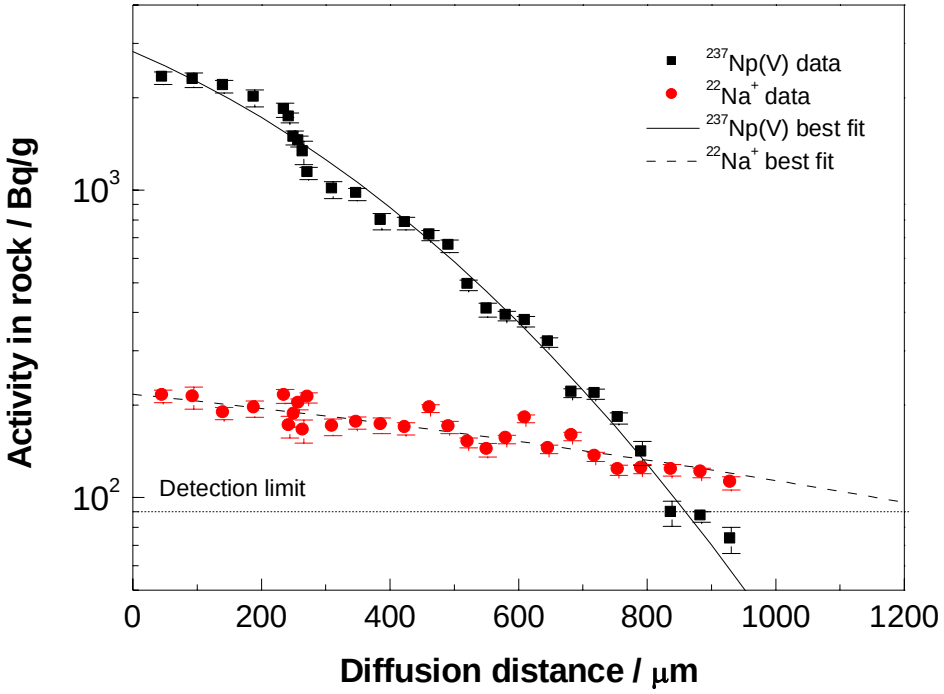

Figure 15: Diffusion profile of 8×10^{-6} M $^{237}Np(V)$ and 2×10^{-10} M $^{22}Na^+$ in OPA of cell 1 in OPA pore water under aerobic conditions.

The values for D_e and α were obtained by modeling the obtained data using our developed Mathematica code. The distribution ratio K_d was deduced by eq. 6, where ε was obtained from the through-diffusion experiment with HTO. In case of Np(V), α is mainly impacted by K_d due to the strong sorption of Np(V) on OPA. The quality of the parameters D_e and α is tested by using them as input parameters for the calculation of the radionuclide concentration in the high-concentration reservoir. Figure 16 shows for example the activity of $^{237}Np(V)$ in the source reservoir of cell 1 as a function of diffusion time.

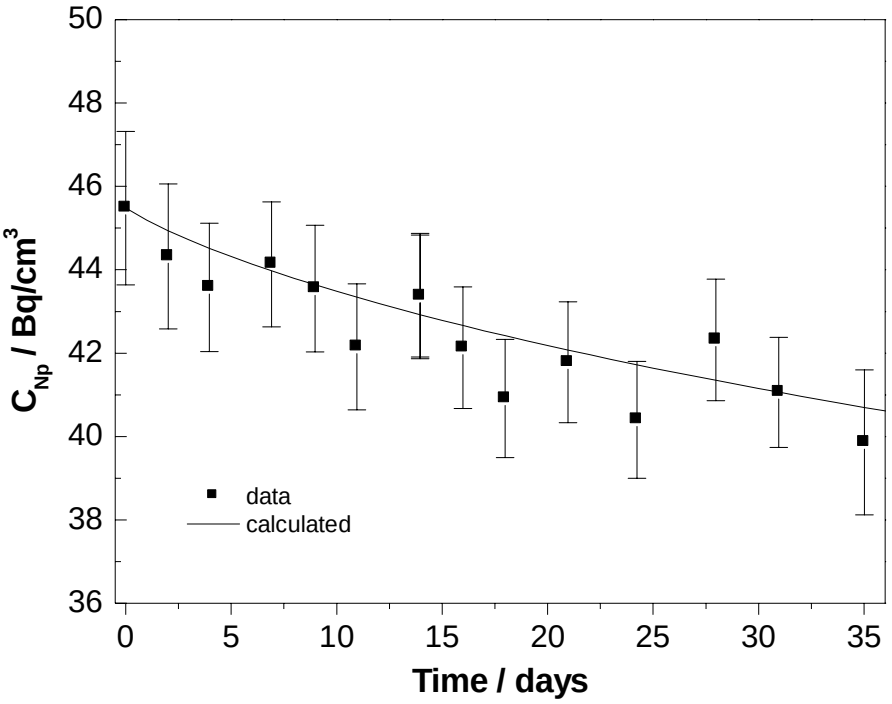

Figure 16: Concentration of ^{237}Np(V) in the source reservoir of cell 1 during in-diffusion.

As can be seen from Fig. 16, the calculated data for the Np(V) concentration in the high-concentration reservoir are in fairly good agreement with the experimental data. While Np(V) diffusion at room temperature (cells 1 and 2) could be fitted very well by the same evaluation procedure as described above, it was not possible to describe the data obtained at 60 °C well by the same model (black line in Fig. 17). It seems that the curve at 60 °C consists of two parts, one with slow diffusion at the beginning and a part of faster diffusion at distances > 500 µm. Using two fit curves (red lines) the experimental data can be better described. One possible explanation of this effect would be a change of Np speciation during diffusion in OPA. A temperature gradient within the clay can be excluded from the experimental conditions. Nevertheless, both fits result in K_d values that are at least five times smaller compared to the results of our batch experiments at 60 °C (see Tab. 13). To understand and explain this effect, further diffusion experiments are required.

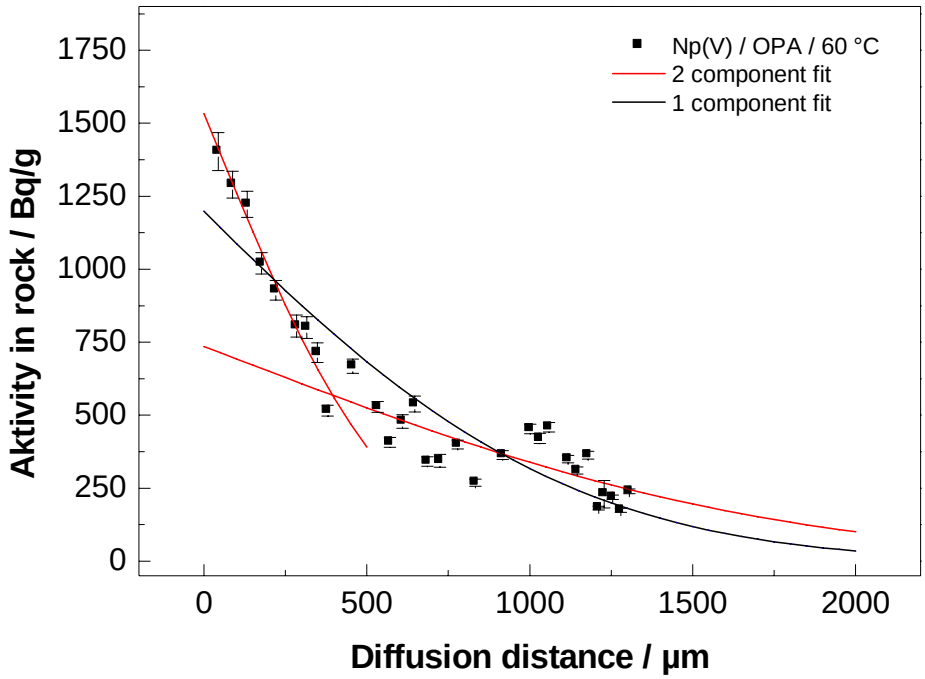

Figure 17: Diffusion profile of 8 × 10^{-6} M ^{237}Np(V) in OPA at 60 °C in OPA pore water under aerobic conditions (cell 4).

The obtained diffusion parameters for all in-diffusion experiments with Np(V) in absence (cell 1 and 2)/presence of HA (cell 3) at room temperature and at 60 °C (cell 4) are summarized in Tab. 12.

Table 12: Diffusion parameters for 8 × 10^{-6} M ^{237}Np(V) in OPA by in-diffusion experiments of cells 1 - 4.

Cell	Np(V)			
	α	**D_e / (× 10^{-11} m^2/s)**	**D_a / (× 10^{-13} m^2/s)**	**K_d / m^3/kg**
1 [28]	243 ± 4	0.7 ± 0.1	2.8 ± 0.1	0.10 ± 0.01
2	110 ± 3	2.3 ± 0.2	2.1 ± 0.2	0.049 ± 0.003
3 [c]	78 ± 2	1.5 ± 0.1	1.9 ± 0.1	0.032 ± 0.002
4	48 ± 2[a]	1.0 ± 0.1[a]	2.1 ± 0.2[a]	0.019 ± 0.001[a]
	69 ± 2[b]	0.2 ± 0.02[b]	0.30 ± 0.03[b]	0.029 ± 0.002[b]
	34 ± 2[b]	1.0 ± 0.07[b]	2.9 ± 0.2[b]	0.014 ± 0.001[b]

[a] Values obtained from 1 component fit, [b] values obtained from 2 component fit, and [c] presence of HA

As can be seen from Tab. 12, the K_d and D_a values obtained for Np diffusion in the presence of HA (cell 3) are slightly decreased compared to experiments in the absence of HA (cells 1 and 2). However, the α value in case of cell 3 is by about 30% lower. D_a values for cells 2 - 4 are similar within experimental errors (considering only the values obtained from 1 component fit for cell 4 at 60 °C). In contrast to batch experiments, the K_d values obtained from diffusion experiment decreased with increasing temperature. This trend was also shown by in-diffusion studies in compacted montmorillonite [72]. The difference between cell 1 and 2 in the obtained diffusion parameters, which are both performed only with Np(V), can be explained by the usage of two different OPA batches (cell 1: BAE 25/10, cell 2: BLT 14) and the lower porosity of OPA in the cell 1.

The K_d value of 0.10 ± 0.01 m^3/kg obtained by the in-diffusion experiment of cell 1 in intact OPA is four times the value of 0.025 ± 0.005 m^3/kg obtained by batch experiments using OPA suspensions. A possible reason for this difference could be that two different OPA batches BHE 24/1 and BAE 25/10 were used in batch and diffusion experiments, respectively. In addition, a small part of Np(V) could be reduced to Np(IV) after diffusion into the intact clay (see Sect. 4.3).

To better compare the diffusion results of cells 2 - 4, three new batch experiments with the same OPA batch (BLT 14) were performed. Therefore, one cylinder of OPA batch BLT 14 was pulverized and sieved to a particle size of less than 150 µm. This powder was used for batch experiments with 8×10^{-6} M Np(V) under aerobic conditions in OPA pore water (pH = 7.6) at room temperature, 60 °C, and in the presence of HA (M42). In the sorption experiments, the S/L ratio was varied between 2 and 20 g/L. The results of the batch experiments performed at room temperature, 60 °C, and in the presence of HA (M42) in comparison to the diffusion results are shown in Tab. 13.

Table 13: Averaged K_d values for the sorption of 8×10^{-6} M Np(V) on OPA (BLT 14, S/L ratio of 2 - 20 g/L) in OPA pore water as a function of temperature and HA under aerobic conditions in comparison to diffusion results.

Cell	**Averaged K_d / m^3/kg**	
	Batch exp.	**Diffusion exp.**
2	0.034 ± 0.010	0.049 ± 0.003
3	0.023 ± 0.002	0.032 ± 0.002
4	0.157 ± 0.052	0.019 ± 0.001

As shown from Tab. 13, slightly lower K_d values were obtained for cell 2 and 3 in the case of batch experiments in comparison to the related diffusion experiments. In contrast to diffusion experiment, the K_d value for the OPA suspension increased significantly with increasing temperature (endothermic process). HA causes a slight mobilization of Np(V), which, however lies in the range of experimental error. Therefore, it can be concluded that the interaction mechanisms between Np(V) and OPA during sorption and diffusion are significantly different, pointing out that the processes that determine the endothermic behavior in batch experiments are almost not relevant in diffusion experiments. With respect to the safety assessment of a nuclear waste repository, the usage of sorption data would lead to an overestimation of Np(V) uptake by OPA at 60 °C, while room temperature data seem to be sufficient for conservative estimates.

4.3 Speciation experiments

4.3.1 XAS, µ-XAS, µ-XRF, and µ-XRD

The uptake mechanism of Np and Pu by OPA as a function of different chemical parameters such as pH, metal concentration, S/L ratio, background electrolyte, and presence/absence of HA was studied by micro-spectroscopic investigations using synchrotron based X-ray techniques such as µ-XAS, µ-XRF, and µ-XRD. These methods have been used to determine the speciation of Np and Pu on OPA after sorption and diffusion processes. The spatially resolved investigations were complemented by EXAFS measurements of wet and dried powder samples from batch experiments to determine the structural parameters of the near neighbour environment of sorbed Np or Pu on the OPA surface. In the literature, there is no information regarding XAS, µ-XAS, µ-XRF, and µ-XRD studies of Np or Pu sorption on OPA. Until now, only few speciation studies of Np and Pu sorption on natural clays were performed. Duff et al. studied Pu sorption on tuff by µ-XRF and µ-XANES [73, 74].

XAS measurements of Np

The sorption of Np(V) on OPA has been investigated as a function of pH in the absence/ presence of HA (M42) or dissolved $FeCl_2$ in different background electrolytes such as 0.1 M $NaClO_4$ (pH 8.5), OPA pore water (pH = 7.6), and saturated calcite solution (pH = 8.5) under aerobic and anaerobic conditions. Samples were prepared with a total $^{237}Np(V)$ concentration of 8×10^{-6} M, S/L ratio of 15 g/L, 10 mg/L HA (M42), 1×10^{-3} M $FeCl_2$. The Np L_{III}-edge

(17630 eV) EXAFS data were collected in fluorescence mode at room and low temperatures (about 15 K) at the Rossendorf beamline ROBL [31] at ESRF using a 13-element Ge solid state detector. Table 14 shows an overview of the measured XAFS samples.

Table 14: Details of the Np samples measured by XAS.

Sample	OPA / (CO_2/Ar)[a]	pH	Electrolyte	OPA batch	HA	Np loading ppm	State[c]	Temp.	Transport
1	aerobic/CO_2	8.5	sat. $CaCO_3$ solution	BHE 24/1	-	91	WP	RT	under air
2	anaerobic/CO_2[b]	8.5	sat. $CaCO_3$ solution	BDR 2	-	109	WP	RT	
3	aerobic/CO_2	8.5	0.1 M $NaClO_4$	BHE 24/1	-	108	WP	RT	
4	anaerobic/Ar	8.5	0.1 M $NaClO_4$	BDR 2	-	121	WP	RT	
5	aerobic/Ar	8.5	0.1 M $NaClO_4$	BHE 24/1	-	110	WP	RT	
6	anaerobic/Ar	7.6	pore water	BDR 2	-	52	WP	RT	
7	aerobic/CO_2	8.5	sat. $CaCO_3$ solution	BHE 24/1	yes	93	WP	RT	anaerobic jar filled with Ar
8	anaerobic/Ar	8.5	sat. $CaCO_3$ solution	BHE 24/2	yes	94	WP	RT	
9	anaerobic/Ar	8.5	sat. $CaCO_3$ solution	BHE 24/2	-	105	P	15 K	
10	anaerobic/Ar	7.6	pore water	BHE 24/2	-	43	P	15 K	
11	anaerobic/Ar	8.5	0.1 M $NaClO_4$ + 10^{-3} M $FeCl_2$	BHE 24/2	-	267	P	15 K	Voyageur 12 filled with LN_2
12	anaerobic/Ar	8.5	0.1 M $NaClO_4$	BHE 24/2	-	151	P	15 K	
13	anaerobic/Ar	8.5	sat. $CaCO_3$ solution	BHE 24/2	-	101	P	15 K	
14	anaerobic/Ar	7.6	pore water	BHE 24/2	-	57	P	15 K	

[a] CO_2: $pCO_2 = 10^{-3.5}$ atm, [b] CO_2: $pCO_2 = 10^{-2.3}$ atm, [c] WP: wet paste, P: powder, RT: room temperature

Figure 18 shows the raw Np L_{III}-edge k^3-weighted EXAFS data, the fit with the best theoretical model, and the corresponding Fourier transform magnitudes (FT) of samples 1 - 6. All FTs are uncorrected for scattering phase shifts (R + Δ), causing peaks to appear at shorter distances.

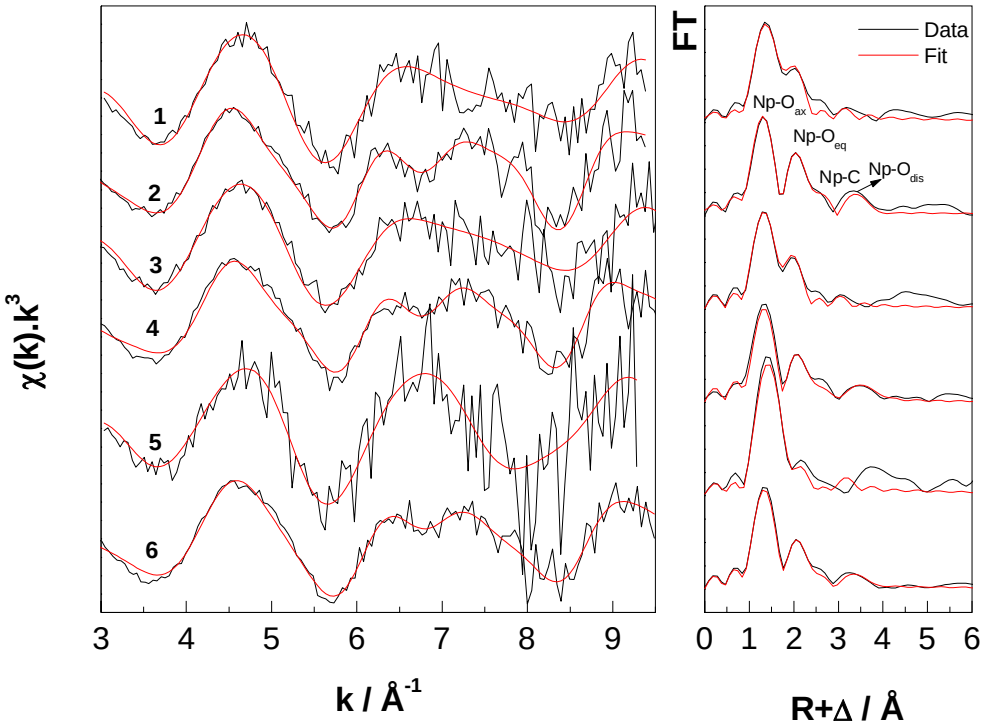

Figure 18: Np L_{III}-edge k^3-weighted EXAFS spectra (left) and the corresponding Fourier transform magnitudes (right) of samples 1 - 6.

As can be seen from Fig. 18, samples 2, 4, and 6 of anaerobic OPA prepared under anaerobic conditions in different background electrolytes show similar EXAFS spectra and have different EXAFS pattern compared to samples 1, 3, 5 of aerobic OPA. They show a double oscillation structure between k 6 - 8 $Å^{-1}$, which is a characteristic for carbonate species. The Fourier transform spectra of samples 2, 4, and 6 show four coordination shells at 1.83 Å, 2.52 Å, 2.98 Å, and 4.25 Å, which are related to Np-O_{ax} axial, Np-O_{eq} equatorial, Np-C, and Np-O_{dis} distal (distal oxygen atom of the CO_3^{2-} group), respectively. In the samples 1, 3, 5 only two coordination shells were observed (Np-O_{ax} and Np-O_{eq}). Table 15 summarizes the structural parameters derived from the EXAFS fits. The average Np-O_{eq} bond distance of samples 1, 3 and 5 is somewhat shorter than in the Np(V) aquo ion [75]. This could indicate inner-sphere sorption of a Np(V) at the OPA surface. The neptunium coordination shells and bond distances of samples 2, 4, and 6 are consistent with the formation of a Np(V) carbonato species at the OPA surface [76], which is also in good agreement with our previous result for Np(V) sorption on kaolinite [77].

In all samples, the obtained distances of both Np-O_{ax} and Np-O_{eq} indicate that the pentavalent oxidation state of Np was dominant. The reduction of Np(V) to Np(IV) under anaerobic conditions could not be confirmed (possible oxidation during transportation).

Table 15: EXAFS structural parameters for the Np samples 1 – 6 in Tab. 14.

Sample	2x O_{ax}	5x O_{eq}	C^d		O_{dis}		ΔE_0 / eV	red. error
	R / Å	R / Å	N	R / Å	N	R / Å		
1	1.85	2.46					- 8.1	0.64
2	1.83	2.52	2.4	2.98	2.4	4.25	- 8.9	0.51
3	1.83	2.45					- 10.3	0.87
4	1.85	2.54	2.5	3.00	2.5	4.26	- 6.6	0.38
5	1.86	2.41					- 9.2	3.60
6	1.85	2.51	1.9	3.00	1.9	4.24	- 9.5	0.33
$NpO_2(H_2O)_4^{+}$ [75]	1.82	2.49						
$NpO_2(CO_3)_3^{5-}$ [76]	1.86	2.53	2.7	2.98	3.0	4.22		

During fit the coordination numbers for $O_{ax,}$ and O_{eq} were held constant and the coordination numbers for C and $O_{dis,}$ were linked together and adjusted as one parameter. The average value of the Debye-Waller factors σ^2 for O_{ax}, O_{eq}, and O_{dis} were 0.0026 $Å^2$, 0.011 $Å^2$, and 0.008 $Å^2$, respectively. Debye-Waller factor σ^2 for C was held constant at 0.003 Å.

Using an iterative transformation factor analysis (ITFA) method [40], the oxidation state of Np in the measured XANES spectra was checked and the amount of Np(IV) to Np(V) in each spectrum was determined and compared to reference spectra of Np(IV) and Np(V) taken from [75]. In case of a mixture of Np(IV) and Np(V), the percentage of both oxidation states was taken into account in the fitting of the related EXAFS spectra. The amount of Np(IV) in samples 1 - 6 was less than 14% (duo to data quality the error can be estimated to about ± 10%) and therefore, the reduction of Np(V) to Np(IV) was not considered. Samples 7 - 10 were transported in an anaerobic transport container filled with Ar gas. Samples 11 – 14 were shock frozen and transported in a liquid nitrogen dewar. By using these two transport options, the reduction of Np(V) to Np(IV) in most of the samples (7 - 12) was clearly observed as can be seen in Tab. 16.

Table 16: Amount of Np(IV) and Np(V) in EXAFS samples 7 - 14 determined using ITFA [40].

Sample	Np(IV) / %[a]	Np(V) / %[a]
7	25	75
8	38	62
9	47	53
10	49	51
11	64	36
12	18	82
13	11	89
14	9	91

[a] Error value from ITFA is about 10%

As shown in Tab. 16, the reduction of Np(V) to Np(IV) was most significant in samples 8 - 11 under anaerobic conditions, independent of the background electrolyte or presence of HA. In the presence of solved $FeCl_2$ (sample 11), the maximum amount of Np(IV) was reached (64%). EXAFS spectra of samples 7 - 10 together with the best fit to the data and their corresponding Fourier transform magnitudes are shown in Fig. 19.

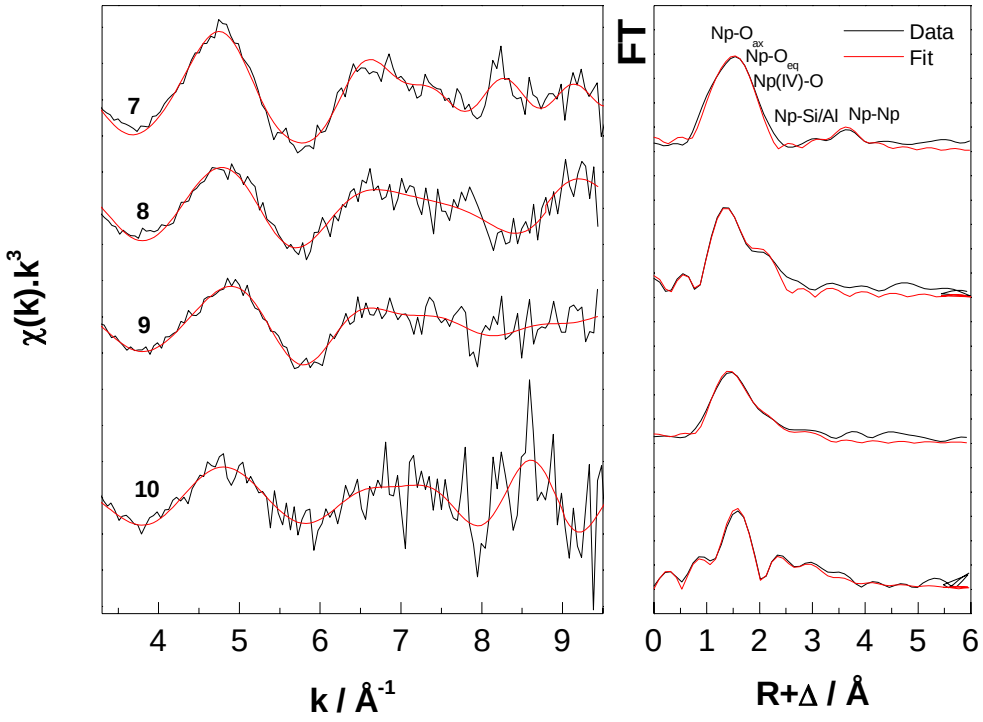

Figure 19: Np L_{III}-edge k^3-weighted EXAFS spectra (left) and the corresponding Fourier transform magnitudes (right) of samples 7-10.

Samples 7 and 8, which were prepared in presence of HA under aerobic and anaerobic conditions, respectively, show similar EXAFS pattern with minor differences. In both cases, the structural parameters derived from the EXAFS fits show three coordination shells Np-O_{ax}, Np-O_{eq}, and Np(IV)-O at distances about 1.80 Å, 2.45 Å, 2.27 Å, respectively. One additional peak at about 3.84 Å was observed in sample 7 (above the noise level), which can be assigned to Np-Np interaction. The Np(IV)-O distance at about 2.27 Å is in good agreement with the characteristic distance of Np(IV) [78]. Similar Np-O distances as for samples 7 and 8 were found for sample 9 with an additional Np-Si/Al coordination shell at distances of 3.19 Å. The obtained Np-O and Np-Al/Si distances for sample 10 were at 1.78 Å (Np-O_{ax}), 2.60 Å (Np-O_{eq}), 2.32 Å (Np(IV)-O), and 3.28 Å/3.55 Å (Np-Al/Si). EXAFS spectra of samples 11 - 14 are presented in Fig. 20 together with the corresponding Fourier transform magnitudes.

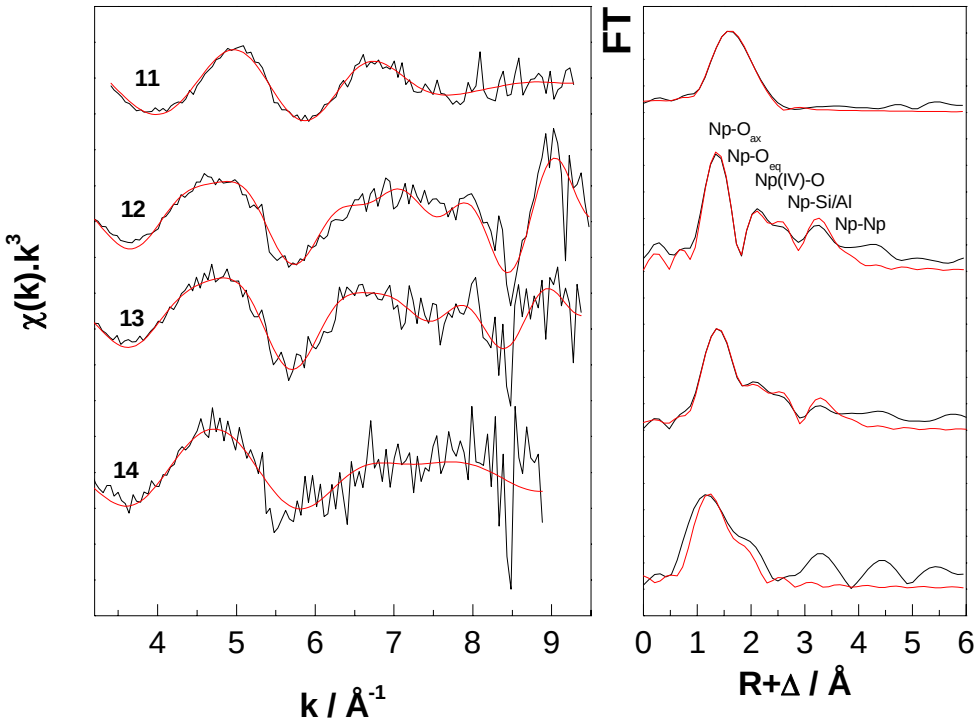

Figure 20: Np L_{III}-edge k^3-weighted EXAFS spectra (left) and the corresponding Fourier transform magnitudes (right) of samples 11 - 14.

Unfortunately, all fours EXAFS spectra show a poor signal-to-noise ratio compared to the previous samples. These spectra were collected using 6-bunch mode (max. current 80 mA), where pervious samples were collected using 7/8 multi-bunch operation mode (max. current 200 mA). Due to the addition of solved $FeCl_2$ in sample 11, the reduction of Np was confirmed with 64% of Np(IV) (see Tab. 16). Three Np-O coordination shells at 1.85 Å, 2.41 Å, 2.21 Å were obtained from the EXAFS measurements of sample 11. Similar distances were obtained for samples 12 and 13 with an additional Np-Np coordination shell at about 3.55 Å. In samples 11 - 13 a Np-Al/Si interaction at about 3.14 Å was also observed. However, this Np-Np coordination shell did not improve the reduced error of the fit significantly. According to the lower beam intensity and lower Np loading (57 ppm) of sample 14, it was only possible to analyze the Np-O_{ax} and Np-O_{eq} coordination shells of this sample. Finally, from all EXAFS results, we can conclude that under both aerobic and anaerobic conditions a partial reduction of Np(V) to Np(IV) occurred, clearly pronounced under anaerobic conditions as well as in the presence of solved $FeCl_2$. HA and background electrolyte had not influence on the Np speciation on OPA. Formation of Np carbonate

species at the OPA surface was detected under anaerobic conditions, probably due to the increase of CO_2 partial pressure. Formation of Np polynuclear species was detected in some anaerobic samples, in which Np(IV) was detected.

µ-XAS, µ-XRF, and µ-XRD measurements of Np(V)

By EXAFS measurements on bulk samples, it was possible to determine the structural parameters of Np sorbed on OPA as a function of several chemical parameters. However, these EXAFS investigations provide only an average over all Np species present in the sample. Microscopic techniques may allow a more selective approach for the speciation. Using µ-XAS and µ-XRF analysis one can attain information on elemental correlations and the distribution of contaminant. Therefore, these techniques are well suited to study heterogeneous materials such as OPA. By using µ-XRD it is also possible to identity crystalline mineral phases within a complex mixture on a micro scale. In this study, the uptake of Np by OPA was investigated by a combination of these synchrotron based methods. As already mentioned, all investigations were performed at the MicroXAS beamline at SLS. The elemental distributions of Np and other elements (e.g., Fe, Ca) of this heterogeneous natural sorbent were determined by µ-XRF mapping. The distribution of mineral phases near Np enrichments (hot spots) was investigated using µ-XRD. Np hot spots located on the samples were analyzed by µ-XANES to determine its oxidation state after uptake or diffusion processes. An overview of all Np samples measured at SLS is shown in Tab. 17.

Table 17: Details of the Np samples measured at SLS.

Sample	**Preparation**	**Activity Bq**	**Np loading ng/mm^2**
1	deposition of 8×10^{-6} M ^{237}Np(V) on OPA thin section under aerobic conditions	107	96
2		823	792
3		2379	1389
4		118	69
5	sorption of 8×10^{-6} M ^{237}Np(V) on OPA under anaerobic conditions	11	22
6	diffusion of 8×10^{-6} M Np(V) in an intact OPA bore core under aerobic condition	86	-

The Np loading in all samples was between 96 ng/mm^2 and 1389 ng/mm^2. For the diffusion sample it was not possible to determine the Np concentration on the surface due to the shape of this massive piece of clay. The focus will primarily be put on samples 1, 3, and 6 as representatives for other measured samples.

Figure 21 shows a ≈ 500 × 500 µm mapping of sample 1 measured by µ-XRF and electron microprobe. The Fe mapping was measured by both methods with good statistics and therefore chosen to align both measurements. Slight differences in the signal intensity can probably be a result of topographic differences on the sample due to swelling of the clay when contacted with Np solution. As can be seen from Fig. 21, Fe and Np are distributed heterogeneously on the thin section and several spots of Fe and Np enrichments are present. The interference between Np (L_α) and Sr (K_α) was considered, since Sr is present in OPA with a concentration of up to 235 ppm [16]. For verification of Np, the Np-L_{III} edge absorption spectrum of the interested spot was measured below 17550 eV and at an energy of 17630 eV. Due to the high-energy used by µ-XRF analysis, it was not possible to measure the lighter elements such as Al and Si contained in OPA simultaneously with Np and Fe. Furthermore, it was also not possible to perform any µ-XRD measurements on the areas of interest to get further information about the mineralogical environment of Np due to high impurities in the standard glass object slides used for the preparation of sample 1. Therefore, only electron microprobe analysis was done in sample 1 to determine the distributions of Al, Si, Ca, Na, and Ti (see Fig. 21). While Al and Si are present on the whole sample as it can be expected, based on the mineral composition of OPA, the mappings of Ca and Fe show certain hot spots, probably calcite and siderite/pyrite, respectively. The Fe distribution determined by both µ-XRF and microprobe analysis fit very well and were used to identify the areas measured by µ-XRF.

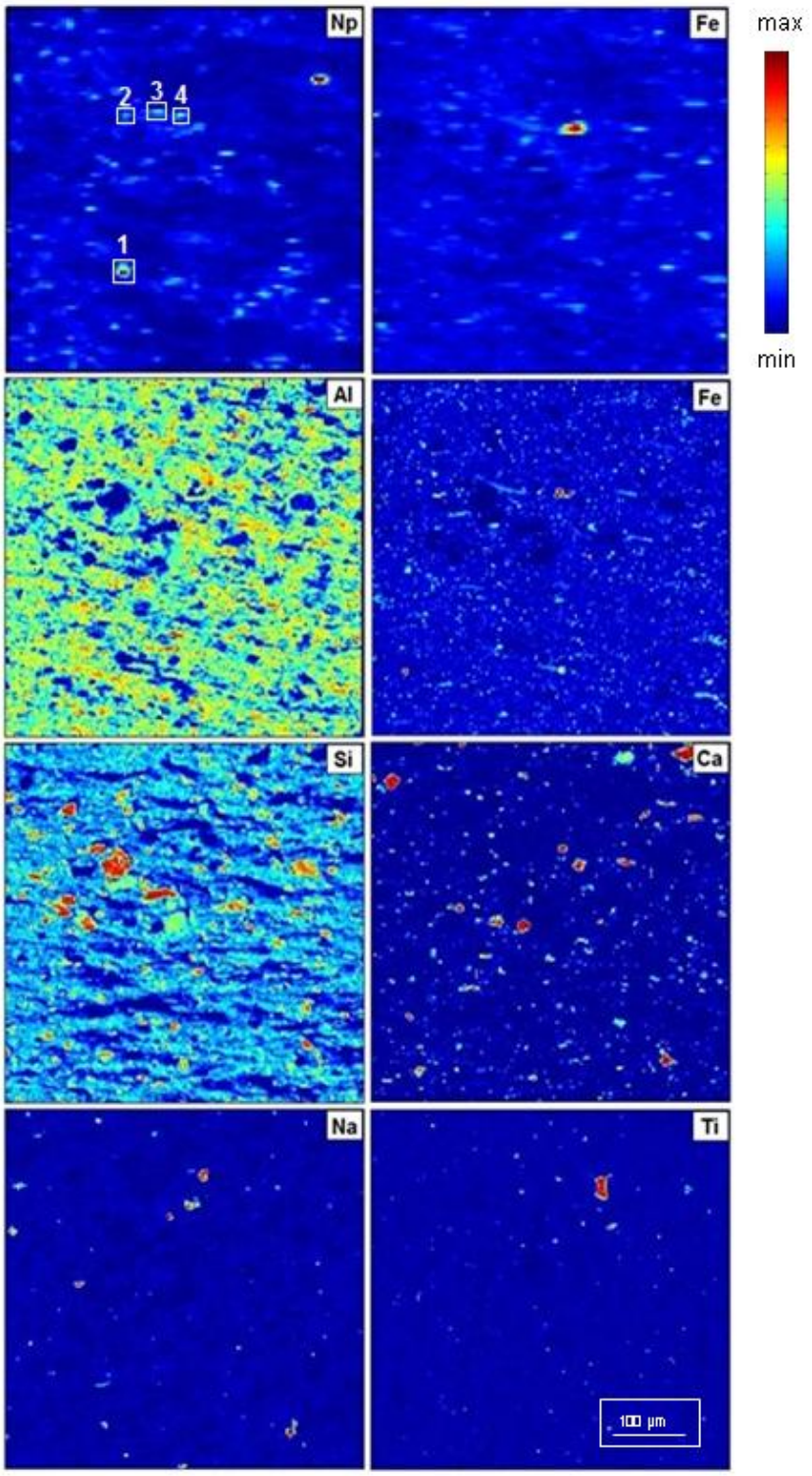

Figure 21: µ-XRF mappings (≈ 500 × 500 µm, step size: 5 µm) of Fe and Np (two upper mappings) compared to electron microprobe measurements (step size: 2.5 µm) of Al, Fe, Si, Ca, Na, and Ti. XANES spectra were recorded at spots 1 – 4 (Fig. 22).

Four Np hot spots on sample 1, whose positions are marked in Fig. 21, were selected and measured by µ-XANES (see Fig 22). Using ITFA [40] normalized XANES spectra were compared to reference spectra of Np(IV) and Np(V) [75] and their amounts were determined.

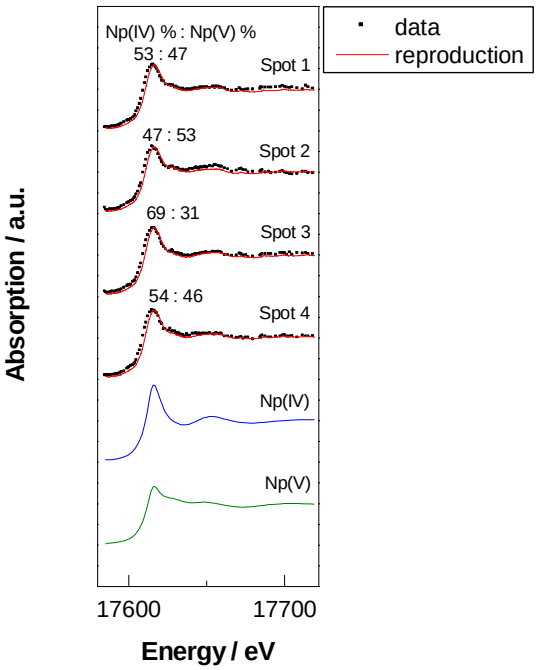

Figure 22: Normalized Np L_{III}-edge XANES spectra measured on spots 1 - 4 marked in Fig. 21 together with the reproductions from IFTA using reference spectra of Np(IV) and Np(V).

A mixture of Np(IV) and Np(V) was found in all XANES spectra. The amount of Np(IV) was determined by ITFA and was between 47% and 69%, although the experiment was carried out under aerobic condition. Np(V) has been partly reduced to Np(IV), probably by iron(II) baring minerals contained in OPA. µ-XRF measurements (Fig. 21) do not show a clear correlation between Np and other measured elements. This correlation was also not confirmed by scatter plots (not shown) using the program XY-MAP display [79]. The fact that spots of Np(IV) are not located directly on Fe hot spots may be explained by the short contact time between Np and Fe during sample preparation. At high Np concentration as in sample 3 (10 times more than in sample 1), it was also not possible to see any correlations between the measured elements. Np was distributed homogenously on the whole sample surface. Additionally, Np(V) was the dominating species on OPA. In both samples the precipitation of Np on the OPA thin sections during evaporation cannot be excluded. To prevent any Np precipitation during sample preparation, a thin section (sample 5) was prepared using a sorption cell under anaerobic conditions. High purity quartz glass object slides (Heraeus Holding GmbH, Hanau, Germany) were used to eliminate any impurities and allow us to perform µ-XRD investigations. Unfortunately, under aerobic conditions the sorption of Np on

OPA thin section was very low and it was not possible to measure this sample. For sample 5, which was prepared under anaerobic condition, the Np loading was sufficient (22 ng/mm^2) for the measurements and several Np hot spots were detected (see Fig. 23). As can be seen in the upper right corner of the Np and Fe mappings in Fig. 23, a clear correlation between Np and Fe can be found. Two points from this mapping were selected to study the speciation of Np.

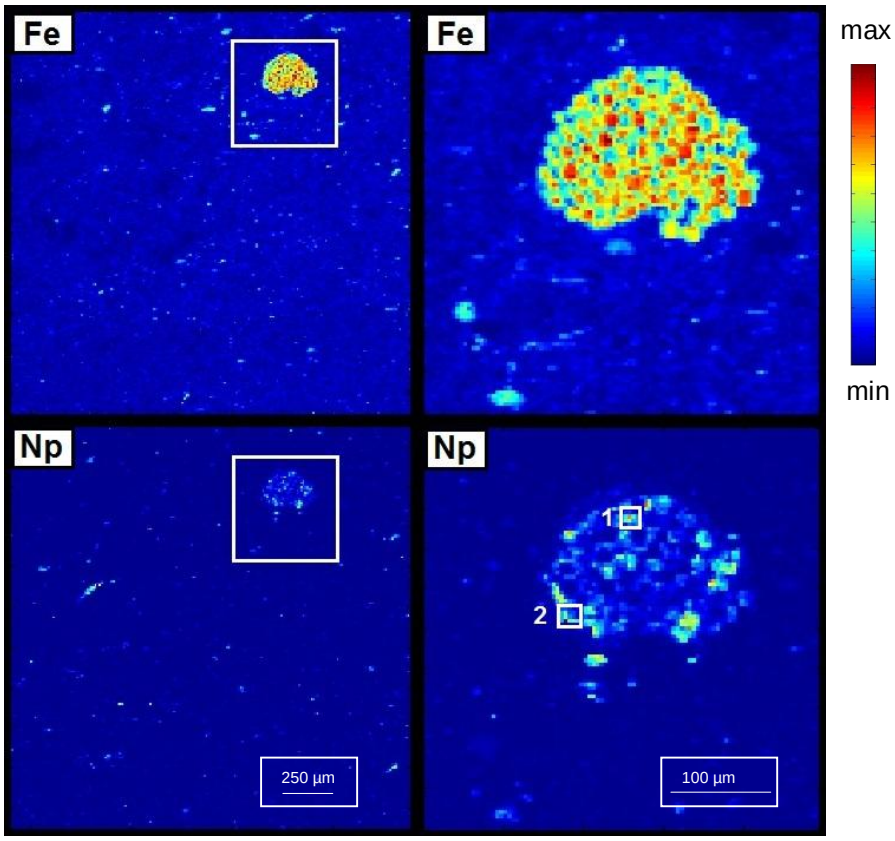

Figure 23: Left: µ-XRF mappings (2 × 2 mm, step size: 10 µm) of Fe and Np of an anaerobic sample prepared by sorption of 8 × 10^{-6} M ^{237}Np on OPA thin section. Right: Same element distributions for 500 × 500 µm mappings (step size 1 µm). XANES spectra were recorded at spots 1 and 2 (Fig. 24).

Figure 24 show the normalized XANES spectra of spots 1 and 2 of sample 5 with the percentages of Np(IV) and Np(V) determined by ITFA.

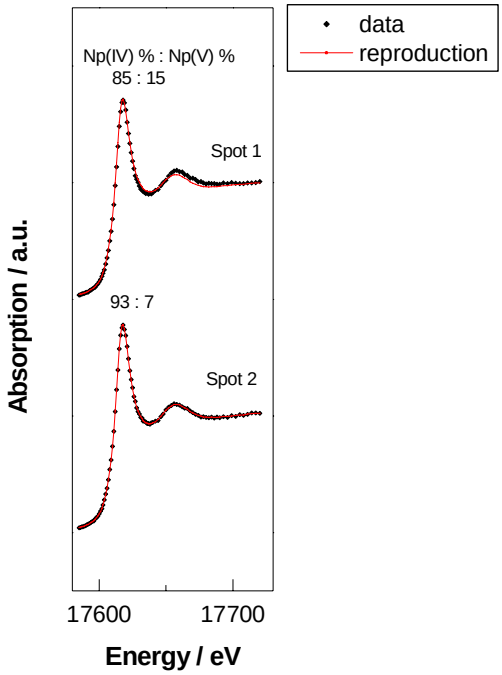

Figure 24: Normalized Np L_{III}-edge XANES spectra measured on spots 1 and 2 marked in Fig. 23 together with the reproductions from IFTA using reference spectra of Np(IV) and Np(V).

The measured XANES spectra of spots 1 and 2 of sample 5 show a similar near-edge structure, which is different from the spectra of spots 1 - 4 in sample 1 prepared under aerobic condition (see Fig. 22). The spectra of sample 1 show a broader adsorption peak and the characteristic Np(V) shoulder. Sample 5, which was prepared under anaerobic condition, shows an almost quantitative reduction of Np(V) to Np(IV) (Np(IV) ≥ 85%). The µ-XRF distribution mappings show clearly that Np reduction has occurred near the iron bearing mineral contained in OPA. To determine which iron mineral is responsible for this reduction, µ-XRD measurements were performed at spots 1 and 2. The collected XRD images (Fig. 25) at each point were analyzed using the program Area Diffraction Machine [41] and compared to the diffraction patterns of different iron bearing minerals. As can be seen from Fig 25, the collected diffraction images of spots 1 and 2 agree well with XRD pattern of pyrite (circles), which is present to about 1 - 3% in OPA [3]. Pyrite appears to be one of the redox-active mineral phases in OPA, which determine the Np speciation after the sorption process.

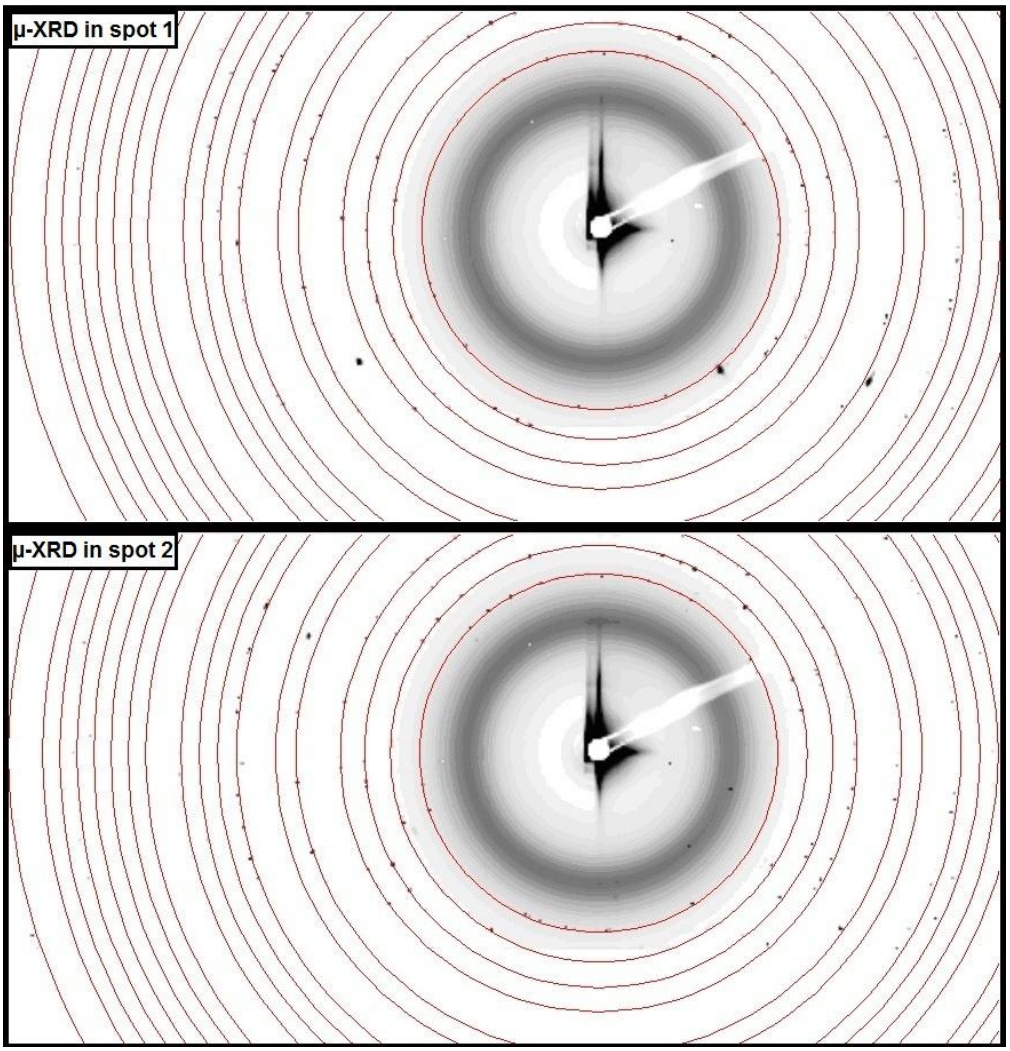

Figure 25: µ-XRD images (20 × 20 µm, step size: 1 µm, E = 17700 eV) of spots 1 and 2 presented in the µ-XRF mapping of sample 5 (Fig. 23). µ-XRD patterns of pyrite are shown as circles.

To investigate the Np speciation on OPA after diffusion, sample 6 was prepared from an intact OPA bore core that was contacted with 8×10^{-6} M ^{237}Np in OPA pore water (pH = 7.6) for more than one month. Figure 26 show the element distributions of Ca, Fe, and Np on this sample.

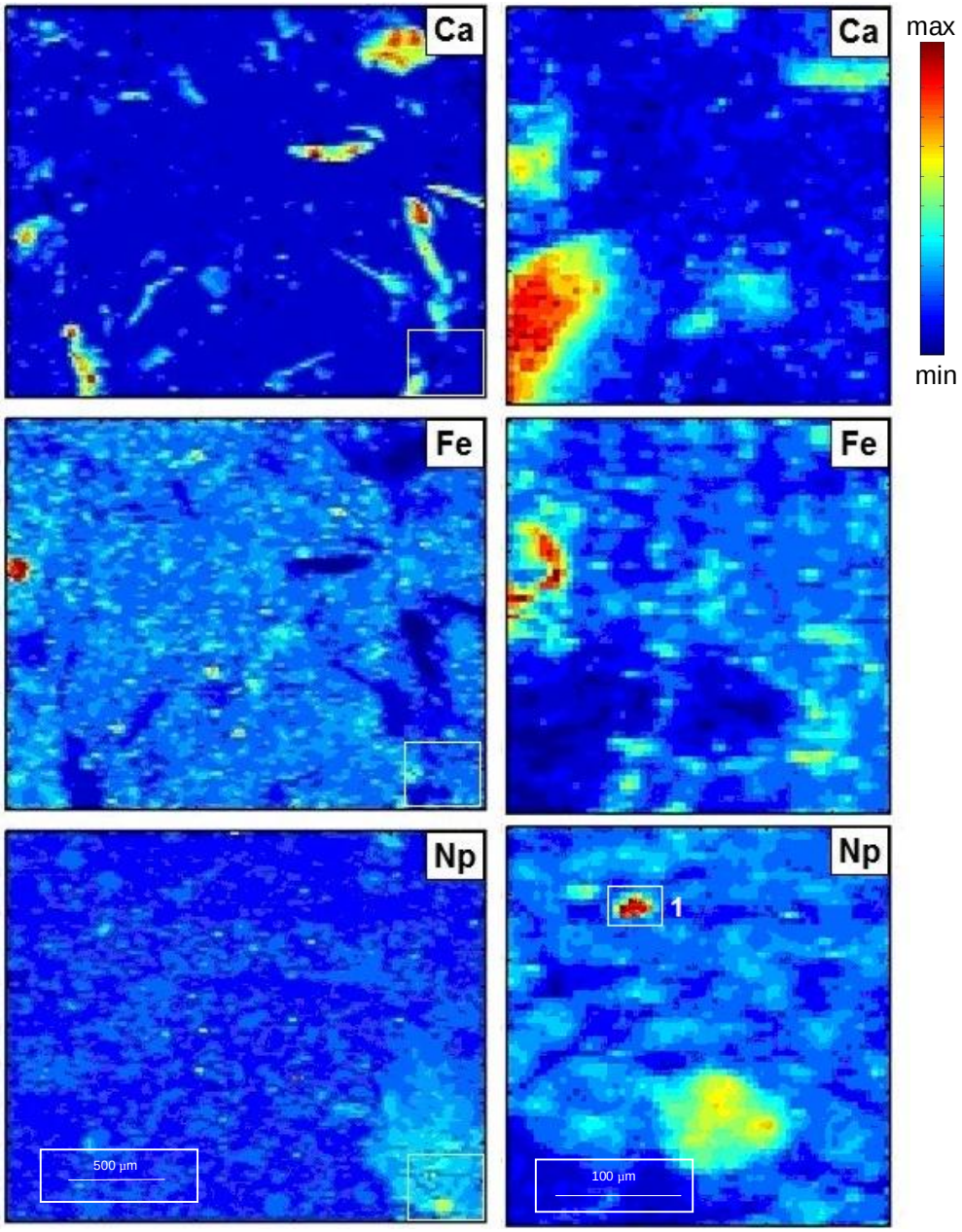

Figure 26: Left: µ-XRF mappings (2.0 × 2.5 mm, step size: 20 µm) of Ca, Fe, and Np of an aerobic sample prepared from in an intact OPA bore core after diffusion of 8×10^{-6} M ^{237}Np for one month. Right: Same element distributions for 300 × 300 µm mapping (step size 5 µm). A XANES spectrum was recorded at spot 1 (Fig. 28).

Due to lower Np loading in the diffusion sample and the sample was not strongly shielded as in the case of the other samples, higher Ca concentrations with several Ca hot spots were observed. Iron was homogeneously distributed in the sample with very high concentration (10^5 counts, perhaps from the stainless steel filter used in diffusion experiment) and only few hot spots were detected. In case of Np, areas with slightly elevated Np concentrations can be

found on the lower right region of the mapping (see Fig. 26). Using XY Display program [79], tri-color (red-blue-green) mappings of Ca, Fe, and Np in the diffusion sample are presented in Fig. 27.

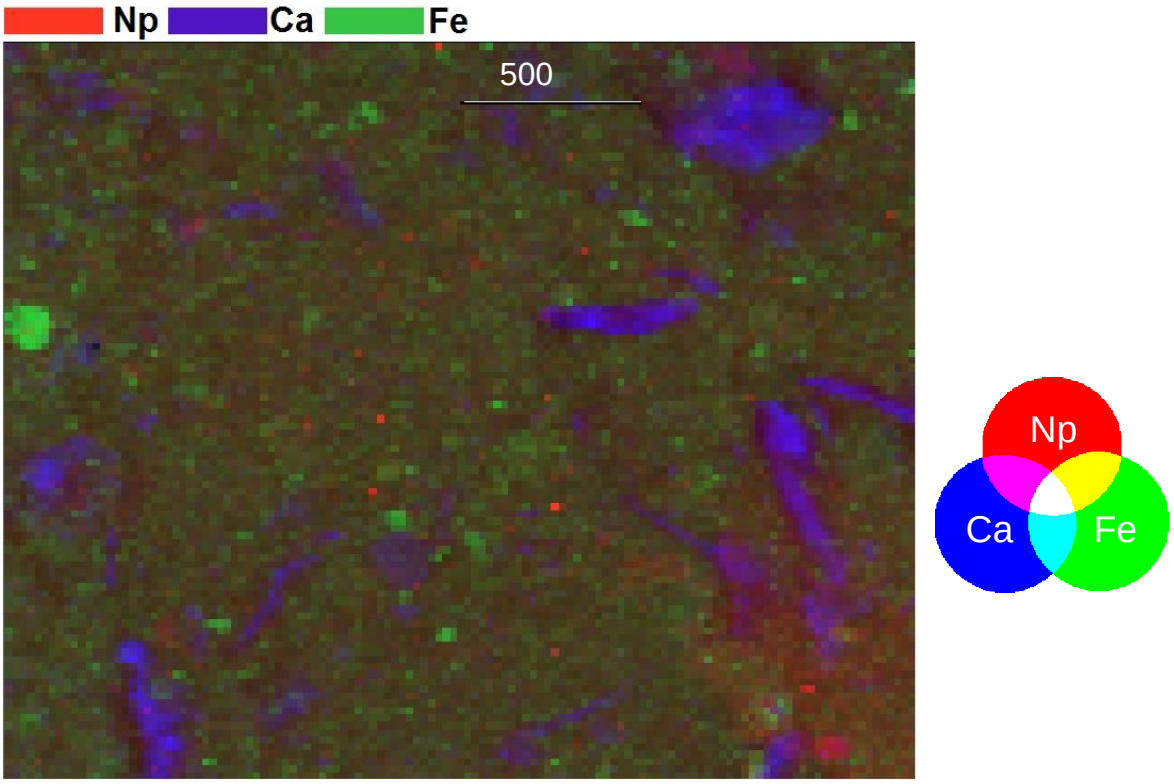

Figure 27: Tri-color mapping of the distributions of Ca, Fe, and Np in the diffusion sample from µ-XRF mapping in Fig. 26 (left).

This tri-color µ-XRF mapping indicates that Ca, Fe, and Np are distributed heterogeneously throughout the sample. The pure green, blue, and red colours of the Fe-, Ca- and Np-rich areas indicate that these elements are segregated. Ca and Fe hot spots are not associated with Np show up as numerous areas in blue and green colors. The correlation between Np, Fe, and Ca was also not confirmed by a scatter plot.

µ-XANES measurement on the Np hot spot selected in Fig. 26 (right) showed that Np(IV) is the dominating species (Fig. 28) with an amount of 82% as determined by ITFA.

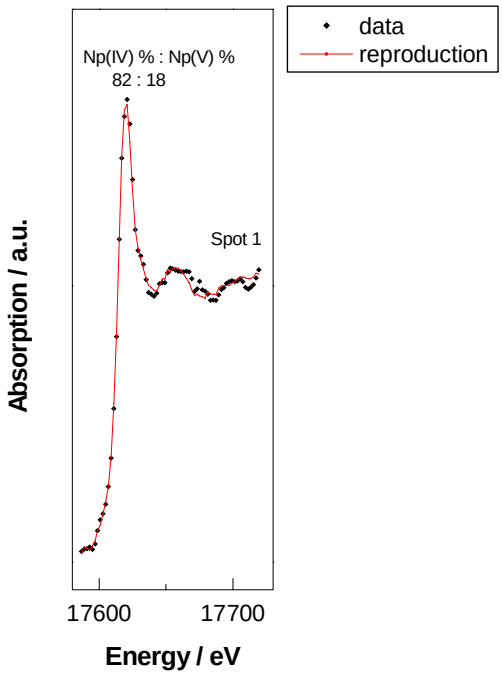

Figure 28: Normalized Np L_{III}-edge XANES spectrum measured on spot 1 marked in Fig. 26 together with the reproduction from IFTA using reference spectra of Np(IV) and Np(V).

Because the diffusion sample was a thick one (not a thin section), it was not possible to perform µ-XRD measurements at the Np hot spot.

As conclusion, from spectroscopic investigations with synchrotron based techniques, it was possible to determine the elemental distributions of Ca, Fe, and Np in OPA samples prepared form sorption and diffusion experiments by using µ-XRF analysis. µ-XANES investigations on Np hot spots of thin sections and diffusion samples showed that Np(V) is partly reduced to Np(IV) under both aerobic and anaerobic conditions. The reduction was more pronounced under anaerobic condition and in diffusion experiments. These results are in good agreement with our pervious diffusion [28] and sorption [16] investigations. Furthermore, µ-XRD data confirm that pyrite is one of the redox-active mineral phases of OPA determining the speciation of Np after uptake on OPA. This indicates that the reduction process takes place on the OPA surface and not in solution. With respect to the assessment of the long-term safety of a nuclear waste repository, even if Np(V) is formed in the near field of the storage containers, the reduction to Np(IV) by OPA will immobilize Np and thus prevent its transport to the far field, showing OPA as a suitable host rock.

XAS measurements of Pu

The sorption of Pu on OPA has been investigated by XAS as a function of pH, Pu oxidation state (III, IV, V, and VI) in the absence and presence of HA (M42), $Na_2CO_3/NaHCO_3$, dissolved $FeCl_2$, in different background electrolytes such as 0.1 M $NaClO_4$ (pH = 8.5), OPA pore water (pH = 7.6) under aerobic and anaerobic conditions. Samples were prepared with a total ^{239}Pu concentration of 1 - 2 × 10^{-5} M, S/L ratio of 6 g/L, 10 mg/L HA (M42), 5 × 10^{-3} M $FeCl_2$, and 2.1 M Na_2CO_3/1 M $NaHCO_3$ solution. Pu L_{III}-edge (18070 eV) XAS data were collected in fluorescence mode at low temperature (about 15 K) at the Rossendorf beamline ROBL [31] at the ESRF using a 13-element Ge solid state detector. Details of the measured XAS samples can be found in Tab. 18.

Table 18: Details of the Pu samples measured by XAS.

Sample	Pu oxid. state	OPA / (CO_2[a]/Ar)[a]	pH	Electrolyte	OPA batch	HA	Pu loading ppm	State[b]	Transport
1	VI	aerobic/CO_2	7.6	pore water	BHE 24/1	-	375	P	under air
2	IV	aerobic/CO_2	7.6	pore water	BHE 24/1	-	375	P	under air
3	IV	anaerobic/Ar	7.6	pore water	BHE 24/2	-	370	P	under air
4	III	anaerobic/Ar	7.6	pore water	BHE 24/2	-	370	P	anaerobic jar filled with Ar
5	IV	anaerobic/Ar	7.6	0.1 M $NaClO_4$	BHE 24/2	-	372	P	
6	III	anaerobic/Ar	7.6	0.1 M $NaClO_4$	BHE 24/2	-	372	P	
7	V	anaerobic/Ar	7.7	pore water	BHE 24/2	-	436	P	Voyageur 12 filled with LN_2
8	V	anaerobic/Ar	7.8	pore water	BHE 24/2	yes	436	P	
9	VI	aerobic/CO_2	7.7	pore water	BHE 24/1	yes	733	P	anaerobic jar filled with Ar
10	VI	aerobic/CO_2	8.5	pore water + Na_2CO_3/ $NaHCO_3$	BHE 24/1	-	732	P	
11	VI	anaerobic/Ar	7.5	pore water + $FeCl_2$	BHE 24/2	-	733	P	
12	VI	aerobic/Ar	7.8	pore water	BHE 24/1	-	733	P	
13	IV	aerobic/CO_2	7.7	pore water	BHE 24/1	yes	404	P	
14	IV	anaerobic/Ar	7.7	pore water	BHE 24/2	-	405	P	Voyageur 12 filled with LN_2
15	IV	anaerobic/Ar	7.7	pore water	BHE 24/2	yes	404	P	
16	III	anaerobic/Ar	7.7	pore water	BHE 24/2	yes	435	P	
17	III	anaerobic/Ar	7.5	pore water + $FeCl_2$	BHE 24/2	-	436	P	

[a] CO_2: $pCO_2 = 10^{-3.5}$ atm, [b] P: powder

XANES measurements were performed to determine the oxidation state of Pu in the sorption samples as can be seen for example in Fig. 29. The XANES spectra of samples 1 - 8 have similar shape and showed that the Pu L_{III}-edge in all spectra occurs at 18068 ± 1 eV, which agrees well with the Pu L_{III}-edge energy of the Pu(IV) aquo ion [80, 81]. The so called "-yl" shoulder, which is used to distinguish Pu(V) and Pu(VI) from other oxidation states (III and IV), can not be seen in the measured XANES spectra. The same XANES spectra (not shown) were obtained also for the other samples (9 - 17). The oxidation state of Pu in the measured XANES spectra was analyzed by ITFA. The amount of Pu(IV) was about 99% in all samples. It follows from this XANES investigation, that Pu(IV) is the dominant oxidation state in all samples (except the samples prepared with dissolved iron(II) chloride), independent on the initial Pu oxidation state (III, IV, V, and VI), the background electrolyte used, the presence/absence of HA, and the aerobic/anaerobic conditions during sample preparation. The presence of HA did not stabilize Pu(III) and the addition of dissolved iron(II) chloride did not completely reduce Pu to Pu(III).

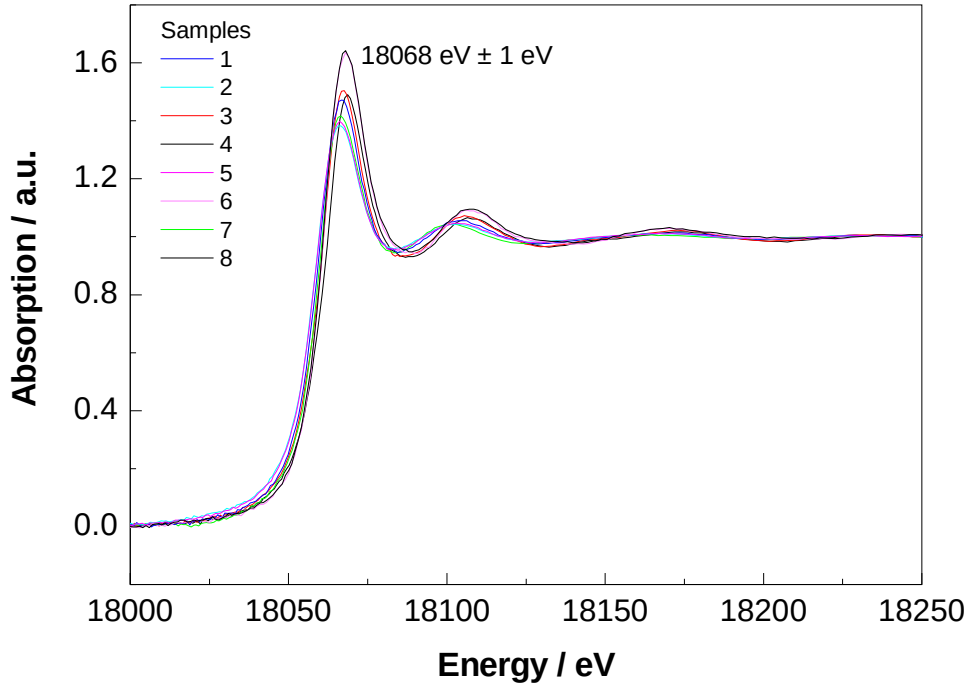

Figure 29: Pu L_{III}-edge XANES spectra of samples 1 - 8.

Figures 30 shows the raw Pu L_{III}-edge EXAFS data, the fit with the best theoretical model, and the corresponding Fourier transform magnitudes of samples 1 and 2 prepared under aerobic condition.

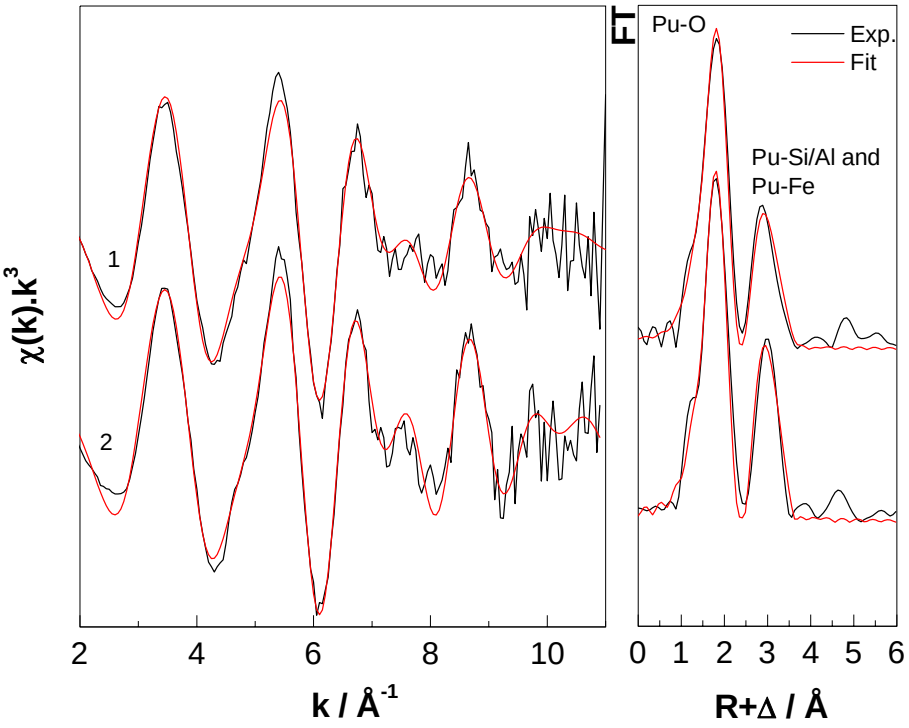

Figure 30: Pu L_{III}-edge k^3-weighted EXAFS spectra (left) and the corresponding Fourier transform magnitudes (right) of samples 1and 2 prepared under aerobic condition.

As can be seen from Fig. 30, the EXAFS spectra of samples 1 and 2 prepared under aerobic conditions show a similar EXAFS structure. The Fourier transform spectra show two main peaks. The first peak at 2.34 Å (corrected for phase shift) is related to the Pu-O coordination shell. The second peak can be modelled by two coordination shells, i.e., Pu-Al/Si and Pu-Fe at 3.13 Å and 3.46 Å, respectively.

EXAFS spectra of samples 3 - 6 prepared under anaerobic condition in different background electrolytes (OPA pore water and 0.1 M $NaClO_4$) are presented in Fig. 31. As can be seen, samples 3 - 6 have identical EXAFS patterns, which differ from the EXAFS spectra of samples 1 and 2 prepared under aerobic conditions. In the Fourier transform spectra of samples 3 - 6 only two coordination shells Pu-O and Pu-Si/Al can be found at about 2.34 Å and 3.14 Å, respectively. Comparing EXAFS spectra of sample 3 and 4 prepared in OPA pore water with samples 5 and 6 prepared in 0.1 M $NaClO_4$, no influence of the background electrolyte can be observed. Aerobic samples have a characteristic EXAFS pattern between k 6 and 9 $Å^{-1}$. In their Fourier transform spectra the amplitude of the second peak was significantly higher compared to other samples prepared under anaerobic conditions.

According to the EXAFS results the speciation of Pu by uptake on OPA is depending on the OPA batch, whether it has been prepared under aerobic or anaerobic conditions. In this context the redox-active iron-bearing mineral phase (pyrite or siderite) seems to play an important role by reduction of Pu(VI) under aerobic conditions.

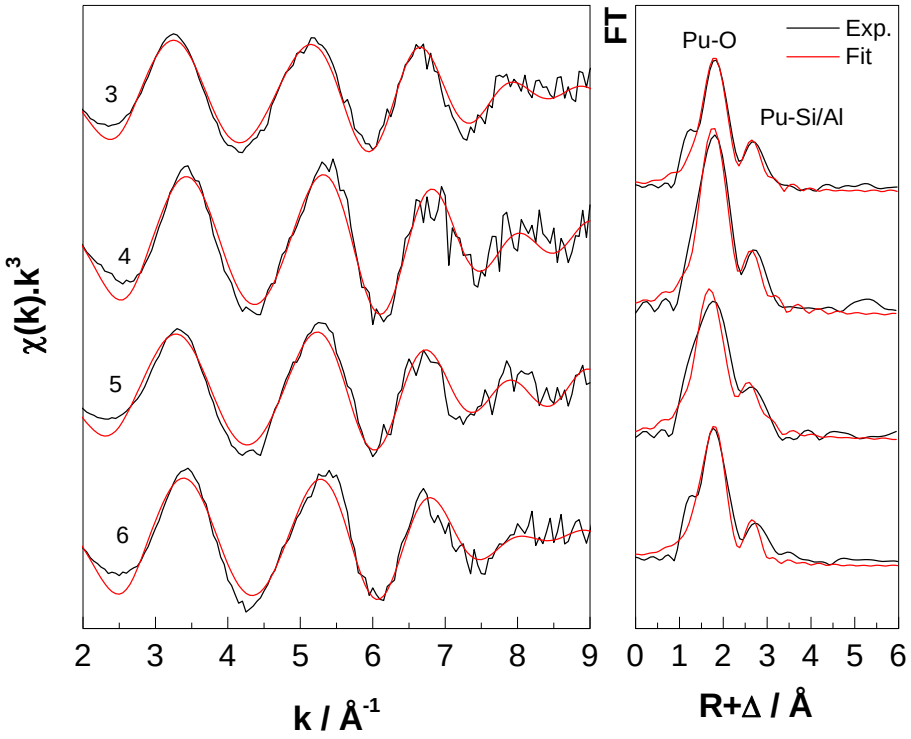

Figure 31: Pu L_{III}-edge k^3-weighted EXAFS spectra (left) and the corresponding Fourier transform magnitudes (right) of samples 3 - 6 prepared under anaerobic condition.

No influence of HA was observed on the sorption of Pu on OPA. Figure 32 shows as an example the EXAFS spectra of samples 7 and 8 for Pu(V) sorption on OPA in the absence and presence of HA, respectively. EXAFS spectra of both samples are very similar. Three coordination shells, i.e., Pu-O, Pu-Si/Al, and Pu-Pu, were observed in the Fourier transform spectra at about 2.29 Å, 3.19 Å, and 3.78 Å, respectively. The additional Pu-Pu coordination shell was observed only in these two samples because a small amount of Pu(IV) colloids remained in the Pu(V) stock solution after potentiostatic electrolysis from the initial Pu(VI) solution.

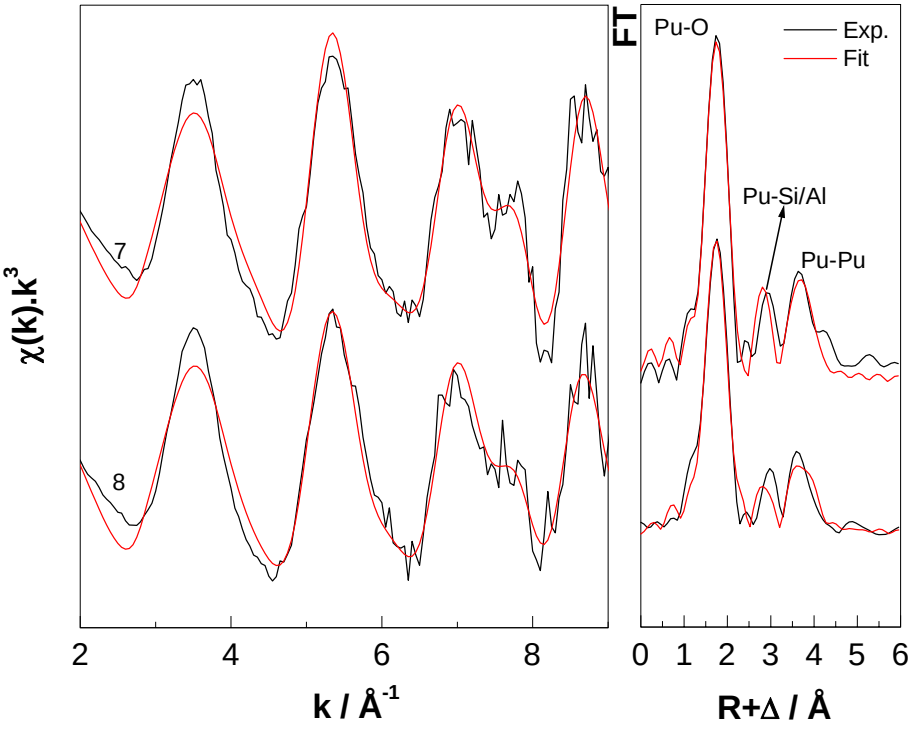

Figure 32: Pu L_{III}-edge k^3-weighted EXAFS spectra (left) and the corresponding Fourier transform magnitudes (right) of samples 7 - 8 prepared under anaerobic condition in absence and presence of HA, respectively.

The obtained structural parameters derived from EXAFS fits of samples 1 - 8 are summarized in Tab. 19.

Table 19: EXAFS structural parameters for the Pu samples 1 – 8 in Tab. 18.

Sample	Pu-O			2x Pu-Si/Al[a]		2x Pu-Fe[a]		Pu-Pu			ΔE_0 / eV	red. error
	N	R / Å	σ^2/ Å^2	R / Å	σ^2 /Å^2	R /Å	σ^2 /Å^2	N	R /Å	σ^2 /Å^2		
1	8.8	2.34	0.013	3.13	0.004	3.46	0.006				- 9.5	0.21
2	8.6	2.34	0.012	3.13	0.004	3.46	0.005				- 10.2	0.22
3	8.4	2.40	0.021	3.17	0.008						- 12.4	0.12
4	9.9	2.34	0.020	3.14	0.007						- 11.2	0.36
5	11.1	2.34	0.026	3.14	0.007						- 13.7	0.11
6	9.5	2.36	0.022	3.15	0.007						- 11.5	0.14
7	9.5	2.29	0.011	3.21	0.010			5.9	3.77	0.009	- 3.0	0.29
8	9.5	2.30	0.012	3.18	0.02			4.0	3.78	0.007	- 2.5	0.29
Pu(IV)(aq) [82]	7.8	2.39	0.007									
$Pu(OH)_4$(am.) [82]	4.6	2.32	0.011					2.2	3.85	0.006		

[a] The coordination numbers for Si/Al and Fe were held constant during the fit, $\Delta R = \pm 0.02$ Å, $\Delta\sigma^2 = \pm 0.001$ Å^2

The Pu-O distance in all samples was about 2.34 Å and agrees with that of $Pu(OH)_4$(am) [82]. A shorter Pu-O distance was found in samples 7 and 8 compared to [82], perhaps due to precipitation of Pu(IV) colloids. The obtained Pu-Pu distance in samples 7 and 8 is shorter than determined by Dardenne et al. for $Pu(OH)_4$(am.). The detection of Pu-Al/Si interactions in all samples is indicative of inner-sphere sorption of Pu(IV) on the clay minerals present in OPA. The XANES results confirm also that Pu(IV) is the dominant oxidation state after interaction of Pu(III/IV/V/VI) with OPA. Our EXAFS results are in good agreement with a previous EXAFS study on the sorption of Pu(III) and Pu(IV) onto kaolinite [77].

µ-XAS, µ-XRF, and µ-XRD measurements of Pu(VI)

The speciation of ^{242}Pu(VI) on OPA after sorption and diffusion processes has been investigated by µ-XAS, µ-XRF, and µ-XRD measurements. Fluorescence mappings of Pu, Ca, Fe, Mn, and Sr on OPA were collected. Spots of high local Pu concentration were analyzed by µ-XANES and µ-XRD to determine the oxidation state of Pu and the distribution of mineral phases near Pu enrichments. Analogous to Np, experiments with a similar set of samples were prepared. Details of the Pu samples prepared is shown in Tab. 20.

Table 20: Details of the Pu samples measured at SLS.

Sample	**Preparation (under aerobic conditions)**	**Activity Bq**	**Pu loading ng/mm^2**
1	deposition of 2×10^{-5} M ^{242}Pu(VI) on OPA thin section	750	96
2	sorption of 2×10^{-5} M ^{242}Pu(VI) on OPA thin section	917	311
3	diffusion of 2×10^{-5} M ^{242}Pu(VI) in an intact OPA bore core	400	7

As shown in Tab. 20, the Pu loading in the samples was between 7 ng/mm^2 and 311 ng/mm^2. In the following the focus will be put on samples 2 and 3. Figure 33 shows as an example the collected µ-XRF mappings for Pu, Ca, and Fe of sample 2.

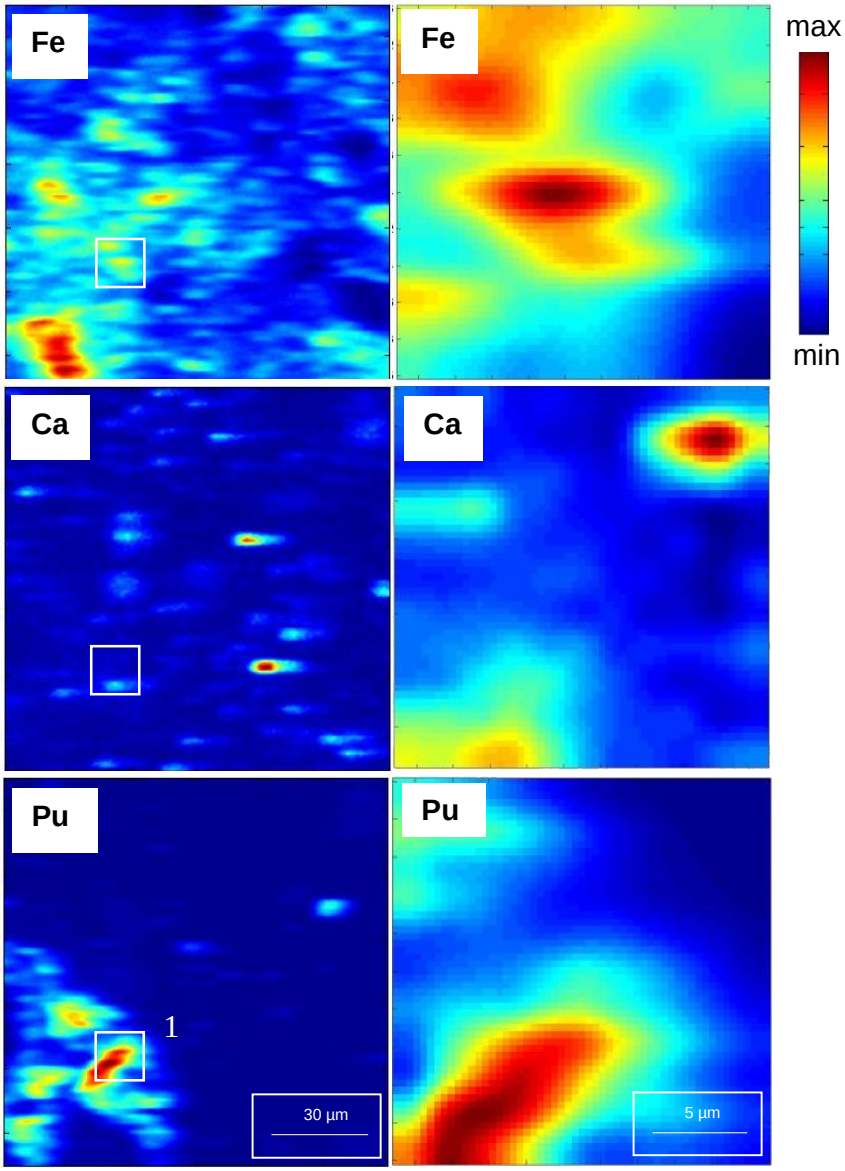

Figure 33: Left: µ-XRF mappings (120 × 120 µm, step size: 10 µm) of Fe, Ca, and Pu of sample 2 prepared by sorption of 2×10^{-5} M ^{242}Pu on OPA thin section. Right: Same element distributions for 20 × 20 µm mapping (step size 2 µm). A XANES spectrum was recorded at spot 1 (Fig. 35).

As can be seen from Fig. 33, fluorescence mappings with good signal intensity were collected for the sample 2. The elements Fe, Ca, and Pu are distributed heterogeneously on the thin section and several hot pots can be observed. In some areas, as can been seen by the presence of purple pixels in the left corner of tri-color mapping (Fig. 34), Pu is associated with Fe.

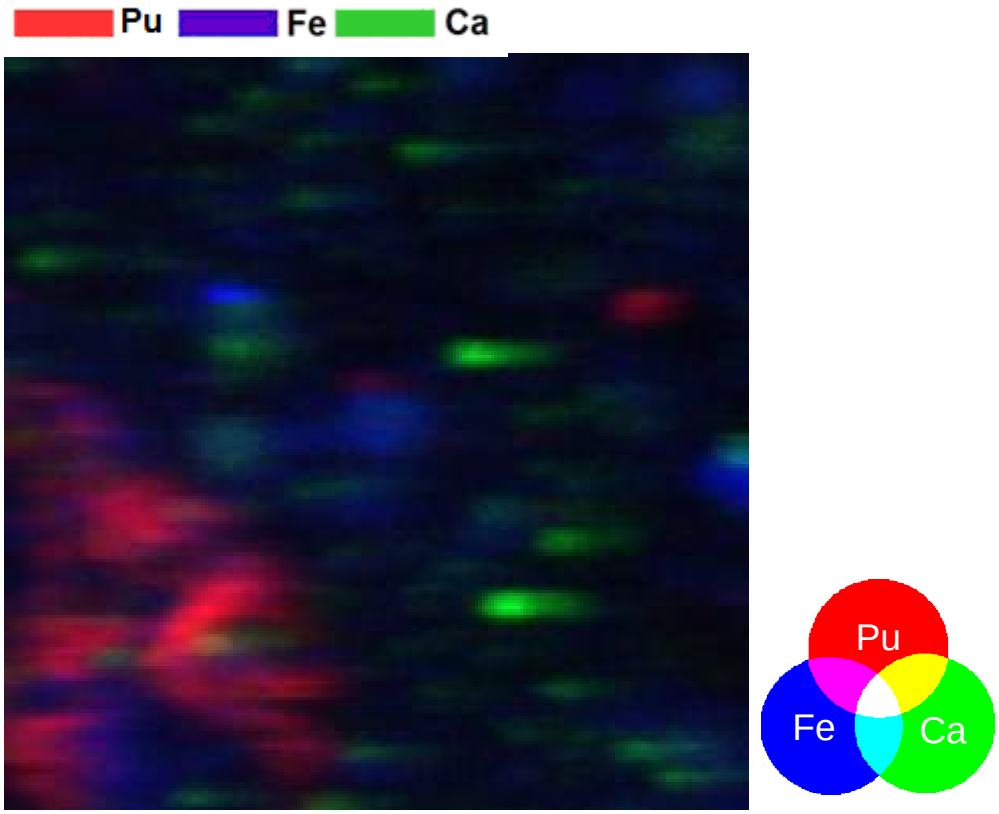

Figure 34: Tri-color mapping of the distributions of Ca, Fe, and Pu in the sorption sample from µ-XRF mapping (left) in Fig. 33.

To determine the oxidation state of Pu and the mineral phases near the Pu hot spot in sample 2 after sorption on OPA thin section, µ-XANES and µ-XRD measurements were performed on the Pu hot spot marked in Fig. 33. The normalized XANES spectrum and µ-XRD images are shown in Figs. 35 and 36, respectively. Using ITFA the amount of Pu(IV) in the XANES spectrum was determined to be 97% in the hot spot.

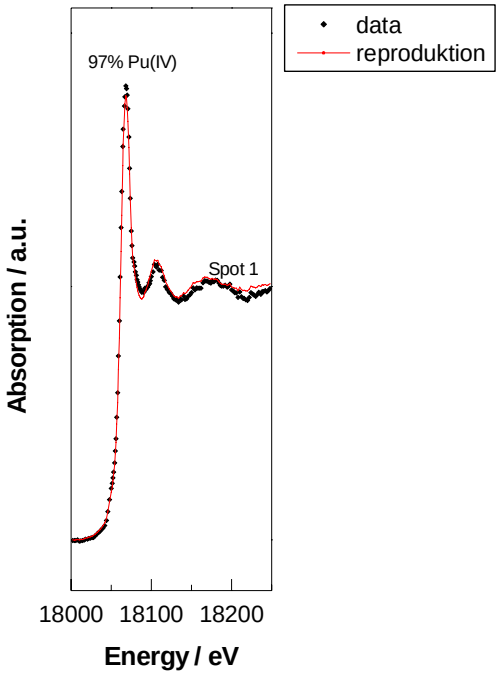

Figure 35: Normalized Pu L_{III}-edge XANES spectrum measured on spot 1 marked in Fig. 33 together with reproduction from IFTA.

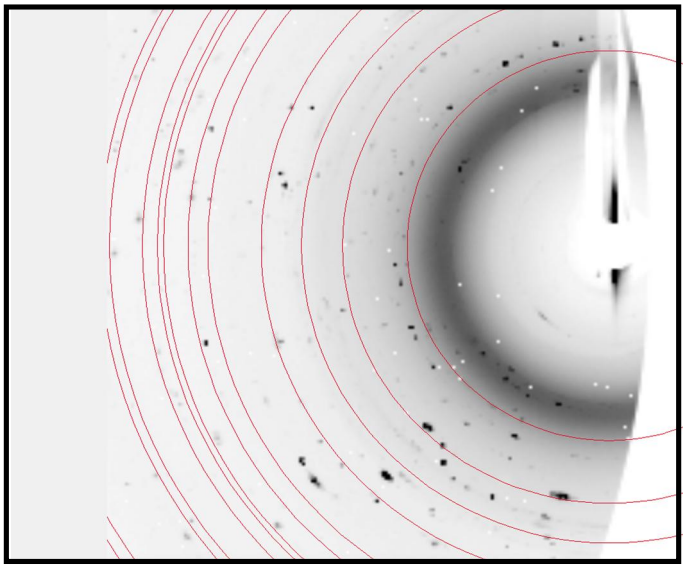

Figure 36: µ-XRD images (20 × 20 µm, step size: 2 µm, E = 18070 eV) of the Pu hot spot presented in the µ-XRF mapping of sample 2 (Fig. 33). µ-XRD patterns of siderite are shown as red circles.

As can be seen in Fig. 36, the collected XRD images near Pu hot spot 1 indicate that Pu potentially localizes on siderite mineral phases contained to about 3% in OPA [3]. Most of all other crystalline/micro crystalline phases (black points) are related to silicate mineral phases,

especially kaolinite (points in the circles close to the center). This preliminary result showed that siderite is one of the redox-active mineral phases in OPA, which determine the Pu speciation after sorption process.

For the diffusion sample with very low Pu loading (7 ng/mm^2), it was also possible to perform µ-XRF and µ-XANES measurements. Figure 37 shows the distributions of Ca, Fe, and Pu on this sample. As can be seen, several Pu and Fe hot spots can be found. Ca is heterogeneously distributed on the OPA thin section. Also in this sample, as in the sorption sample, there are some areas in which Pu was associated with Fe. The µ-XANES spectrum of the Pu hot spot showed that Pu(IV) is the dominating oxidation state after diffusion into OPA (Fig. 38). Due to the thickness of the diffusion sample, it was not possible to carry out any µ-XRD measurements.

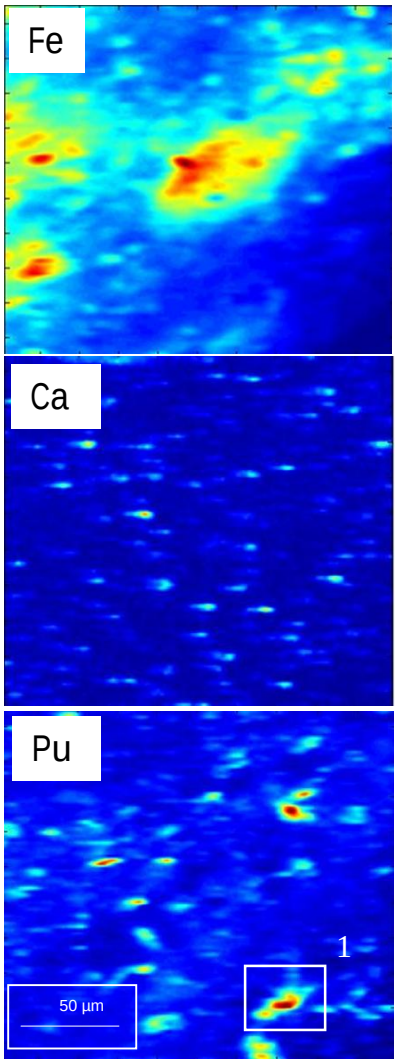

Figure 37: µ-XRF mappings (200 × 200 µm, step size: 2 µm) of Fe, Ca, and Pu of sample 3 prepared by diffusion of 2 × 10^{-5} M ^{242}Pu on OPA. A XANES spectrum was recorded at spot 1 (Fig. 38).

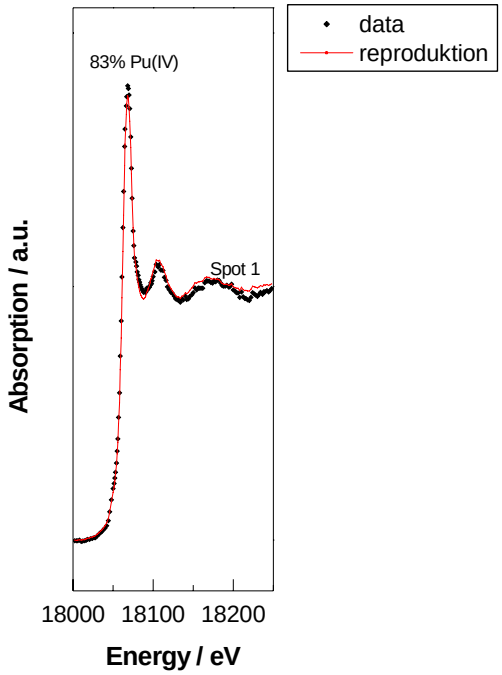

Figure 38: Normalized Pu L_{III}-edge XANES spectrum measured on spot 1 marked in Fig. 37 together with reproduction from IFTA.

In conclusion, it was possible to determine the elemental distributions of Ca, Fe, and Pu in OPA samples after sorption and diffusion experiments by µ-XRF. Bulk-XAS and µ-XANES measurments showed a complete reduction of Pu(VI) to Pu(IV) in all samples prepared under both aerobic and anaerobic conditions. These results are in good agreement with our pervious results of Pu uptake on kaolinite [77]. Furthermore, preliminary analysis of the µ-XRD patterns indicates that siderite is one of the redox-active mineral phases of OPA, which determines the speciation on Pu after uptake on OPA. The obtained results indicate that OPA is a suitable host rock for high level nuclear waste disposal.

4.3.2 CE-ICP-MS

Redox speciation of Np(IV) and Np(V)

A highly sensitive CE-ICP-MS method was developed for the speciation of Np(IV) and Np(V) in solution. The separation of the two species was performed using the homemade capillary electrophoresis described in Sect. 2.2.

A stock solution containing 3.1×10^{-5} M Np(IV) and 9.2×10^{-6} M Np(V) was prepared by partial reduction of Np(V) with hydroxlammonium chloride. The content of Np(IV) and Np(V) was checked by liquid-liquid-extraction of Np(IV) with HDEHP in toluene and subsequent measurement of the activity in the organic and aqueous phases by liquid scintillation counting (LSC).

Good separation of Np(IV) from Np(V) was possible with the described CE-setup using a solution of 1 M acetic acid with pH 2.3 as background electrolyte and a voltage of 25 kV (Fig. 39). During separation, an external pressure of 30 mbar was applied to prevent clogging of the capillary.

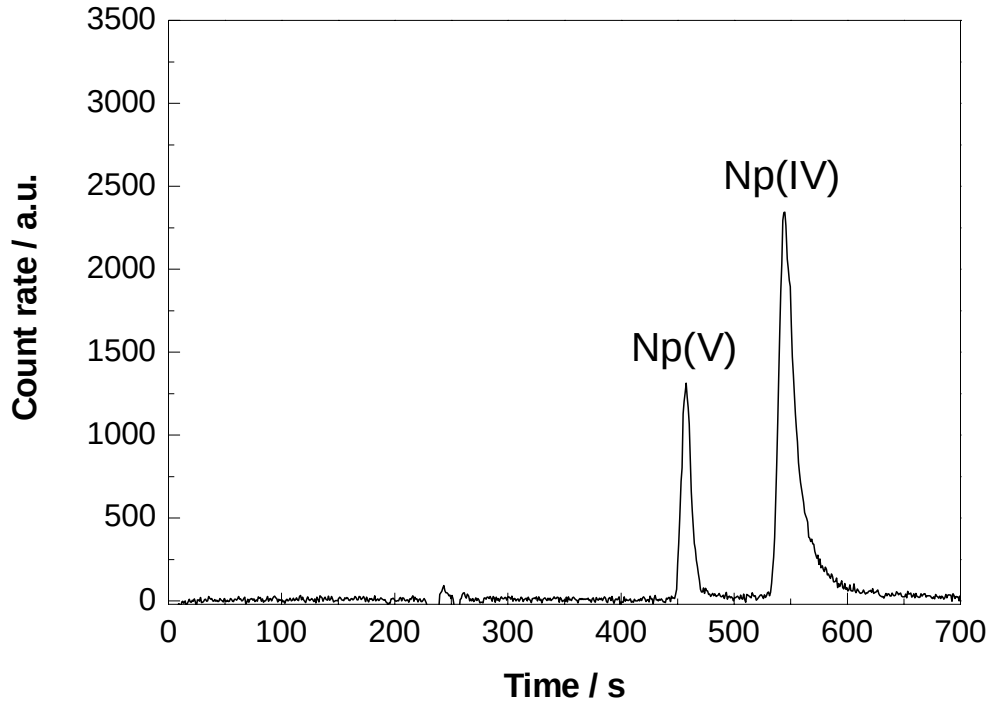

Figure 39: Electropherogram of a mixture of 3.1×10^{-8} M Np(IV) and 9.2×10^{-9} M Np(V).

A dilution series was prepared by dilution of the stock solution. After the measurement of this series, the peak areas for Np(IV) and Np(V) were calculated and plotted versus the respective concentrations (Fig. 40). As expected, a linear increase of the peak areas with the concentration was observed in both cases. Therefore, it can be concluded that there is no significant loss of Np(IV) in the given concentration range due to sorption or oxidation during the CE separation with the chosen parameters.

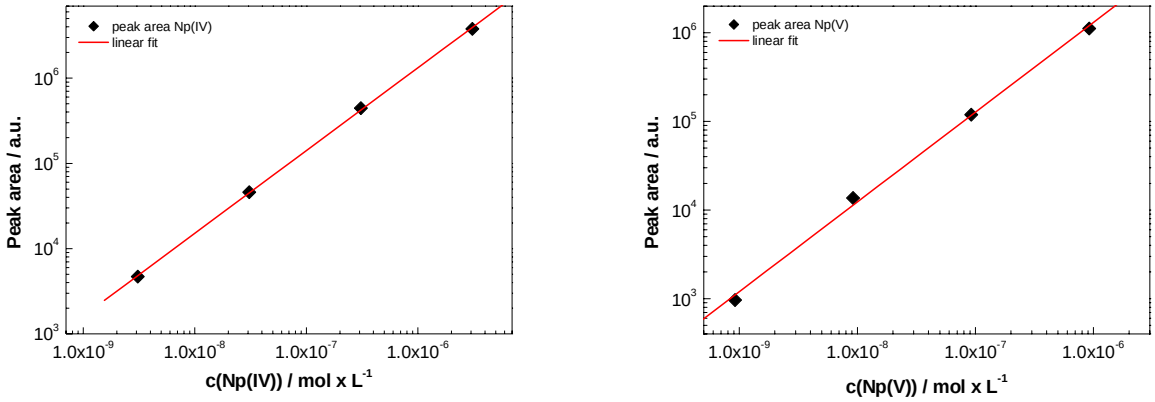

Figure 40: Results from dilution series for Np(V) and Np(IV) obtained with CE-ICP-MS.

Redox behavior of Pu(III) and Pu(IV) under aerobic condition [23]

The redox behavior of different Pu oxidation states in OPA pore water and related solutions was studied under aerobic and anaerobic conditions using on-line coupling CE-ICP-MS. Several experimental parameters and setups were tested to optimize the separation performance [23]. It was found that the sample medium has a significant influence on the separation efficiency. Experiments with 50 ppb ^{239}Pu(VI) in different mixtures of 0.2 M HNO_3 and 1 M CH_3COOH showed a better separation and a lower detection limit when the sample was prepared in a medium that had a similar composition as the electrolyte used in the capillary (1 M CH_3COOH). The speciation of Pu in a mixture of 1:4 (HNO_3/CH_3COOH) was 1.6 ± 0.1% Pu(III), 59.3 ± 3.0% Pu(IV), 33.5 ± 1.7% Pu(V), and 5.6 ± 0.3% Pu(VI).

Kinetic measurements of 50 ppb Pu(III) in 1 M CH_3COOH at pH 1.8 showed that Pu(III) is stable up to 40 minutes, i.e., during the typical measuring time for CE-ICP-MS. After a longer time Pu(III) is oxidized to Pu(IV) and Pu(VI).

The redox stability of Pu(III) and Pu(IV) in OPA pore water (pH = 7.6, I = 0.4 M), and for comparison in 0.2 M HNO_3 (pH = 0.9) and 0.4 M $NaClO_4$ (pH = 7.6) was investigated by CE-ICP-MS under aerobic conditions. Freshly prepared stock solutions of Pu(III) and Pu(IV) were added individually to the different solutions. After a contact time of 5 days, aliquots were taken and analyzed by CE-ICP-MS to determine the speciation of Pu in solution. The pH/Eh values were measured directly after Pu addition and checked again after 5 days. Figures 41 and 42 show the electropherograms of 50 ppb Pu(III) and Pu(IV), respectively, in the investigated solutions after a contact time of 5 days.

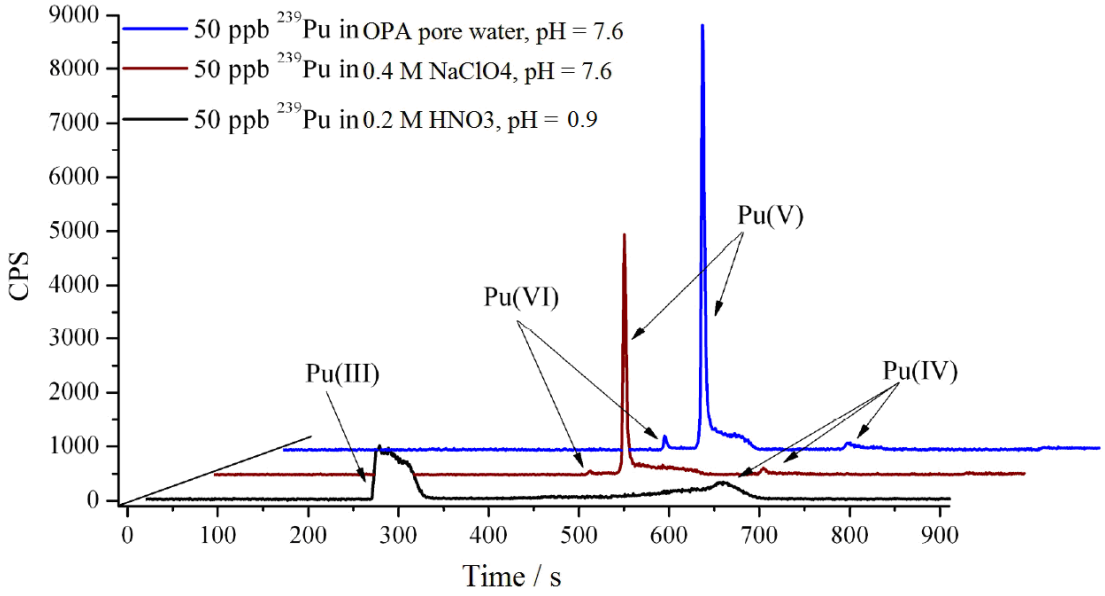

Figure 41: Electropherogram of 50 ppb ^{239}Pu(III) in different solutions after a contact time of 5 days under aerobic conditions.

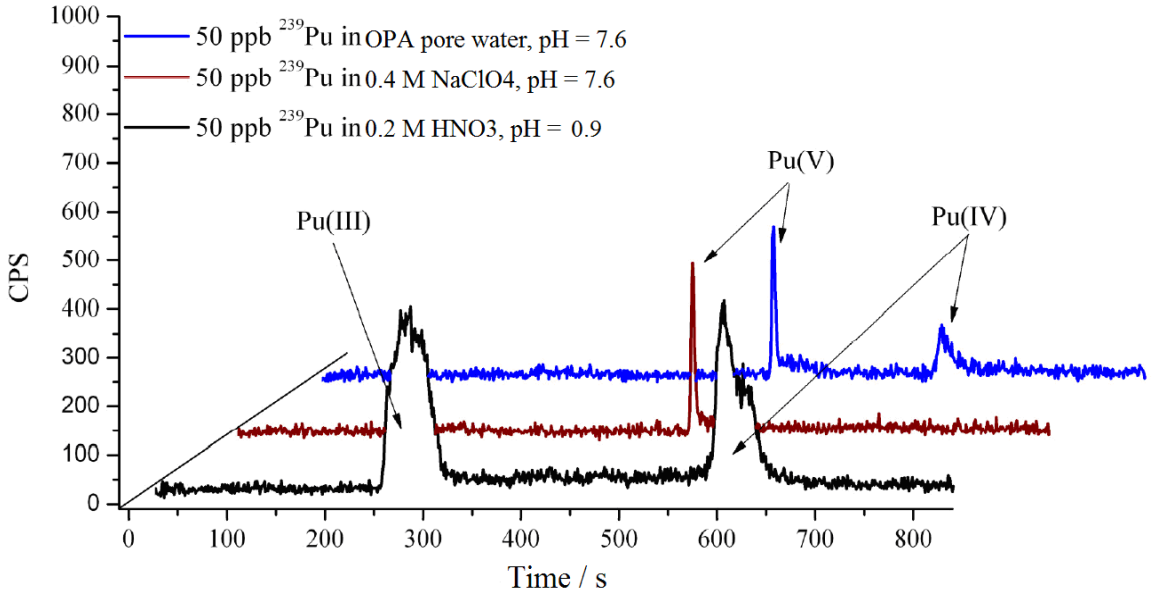

Figure 42: Electropherogram of 50 ppb ^{239}Pu(IV) in different solutions after a contact time of 5 days under aerobic conditions.

As can be seen from Figs. 41 and 42, higher signal intensities were obtained in all Pu(III) solutions compared to Pu(IV). This can be explained by the strong tendency of Pu(IV) to sorb on tube walls. In case of Pu(III) the obtained signals in both 0.4 M $NaClO_4$ and OPA pore water are more intensive and better resolved compared to 0.2 M HNO_3. The distribution of Pu

species (Tabs. 21 and 22) in each sample was obtained from the peak areas in the measured electropherograms.

Table 21: Pu species and Eh values of 50 ppb Pu(III) in 0.2 M HNO_3 (pH = 0.9), 0.4 M $NaClO_4$ (pH = 7.6), and OPA pore water (pH = 7.6) solutions after a contact time of 5 days under aerobic conditions.

Solution	**SHE Eh/mV**	**Species / %**			
		Pu(III)	**Pu(IV)**	**Pu(V)**	**Pu(VI)**
0.2 M HNO_3	792 ± 50	45 ± 3	55 ± 3	0	0
0.4 M $NaClO_4$	602 ± 50	0	9 ± 1	88 ± 5	3 ± 1
OPA pore water	520 ± 50	0	8 ± 1	89 ± 5	3 ± 1

Table 22: Pu species and Eh values of 50 ppb Pu(IV) in 0.2 M HNO_3 (pH = 0.9), 0.4 M $NaClO_4$ (pH = 7.6), and OPA pore water (pH = 7.6) solutions after a contact time of 5 days under aerobic conditions.

Solution	**SHE Eh/mV**	**Species / %**			
		Pu(III)	**Pu(IV)**	**Pu(V)**	**Pu(VI)**
0.2 M HNO_3	800 ± 50	57 ± 3	43 ± 2	0	0
0.4 M $NaClO_4$	600 ± 50	0	0	100 ± 5	0
OPA pore water	500 ± 50	0	51 ± 3	49 ± 3	0

As can be seen from Tab. 21, at pH 7.6 the majority of Pu(III) was oxidized to Pu(V) in both $NaClO_4$ and OPA pore water solutions. Table 22 shows that Pu(V) is the dominant species in 0.4 M $NaClO_4$ solution at pH 7.6, while in OPA pore water both Pu(IV) and Pu(V) are present with about 50%. The measured Eh values of Pu(III) and Pu(IV) in all solutions agree well with data from Takeno et. al. [83].

Redox behavior of Pu(III) and Pu(IV) under anaerobic conditions [23]

To investigate the redox behavior of Pu close to environmental conditions, the redox stability of Pu(III) and Pu(IV) was studied under anaerobic conditions (Ar atmosphere). Aliquots from Pu(III) or Pu(IV) stock solutions were added to 0.2 M HNO_3 (pH = 0.9), 0.4 M $NaClO_4$ (pH = 7.6), or OPA pore water (pH = 7.6, I = 0.4 M). The Pu(III) and Pu(IV) concentrations were 30 ppb in all samples. Eh and pH values were measured immediately after addition of Pu as well

as after 5 days. The speciation of Pu was analyzed by CE-ICP-MS after 60 min, 80 min, and 5 days. Furthermore, the redox stability of a mixture of Pu(III) and Pu(IV) (each 50 ppm) was also investigated under same experimental conditions by CE-ICP-MS after a contact time of 5 days.

Figure 43 shows the distribution of the different Pu species in OPA pore water as a function of time after addition of 30 ppb Pu(III) under anaerobic conditions.

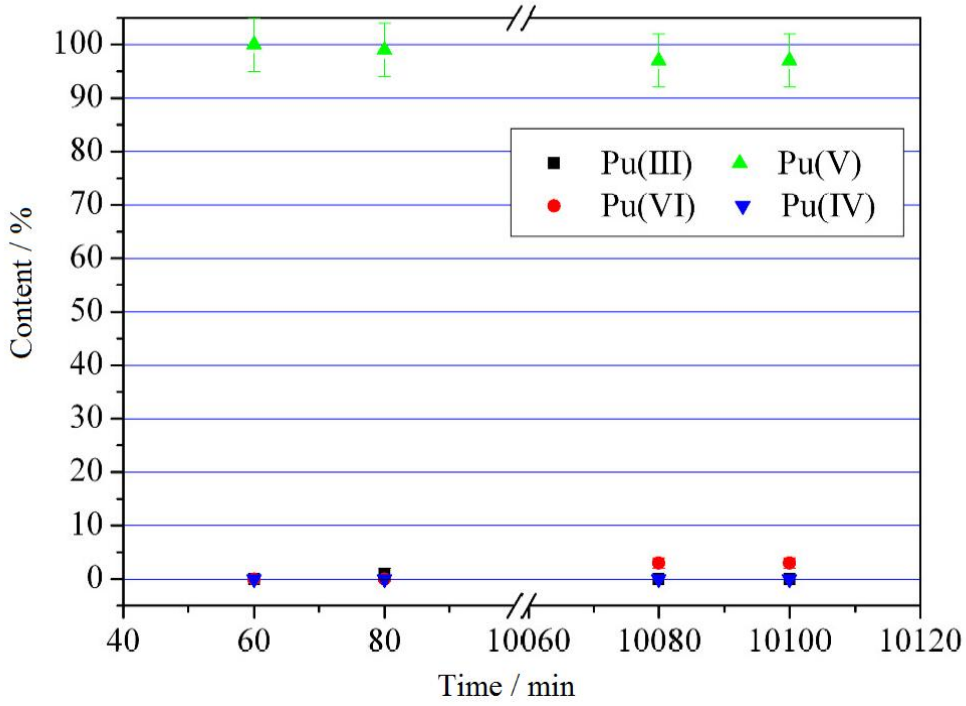

Figure 43: Pu species as a function of time after addition of 30 ppb Pu(III) to OPA pore water (pH = 7.6) under anaerobic conditions.

Figure 44 shows the distribution of the Pu species as a function of time after addition of 30 ppb Pu(IV) to OPA pore water under anaerobic conditions.

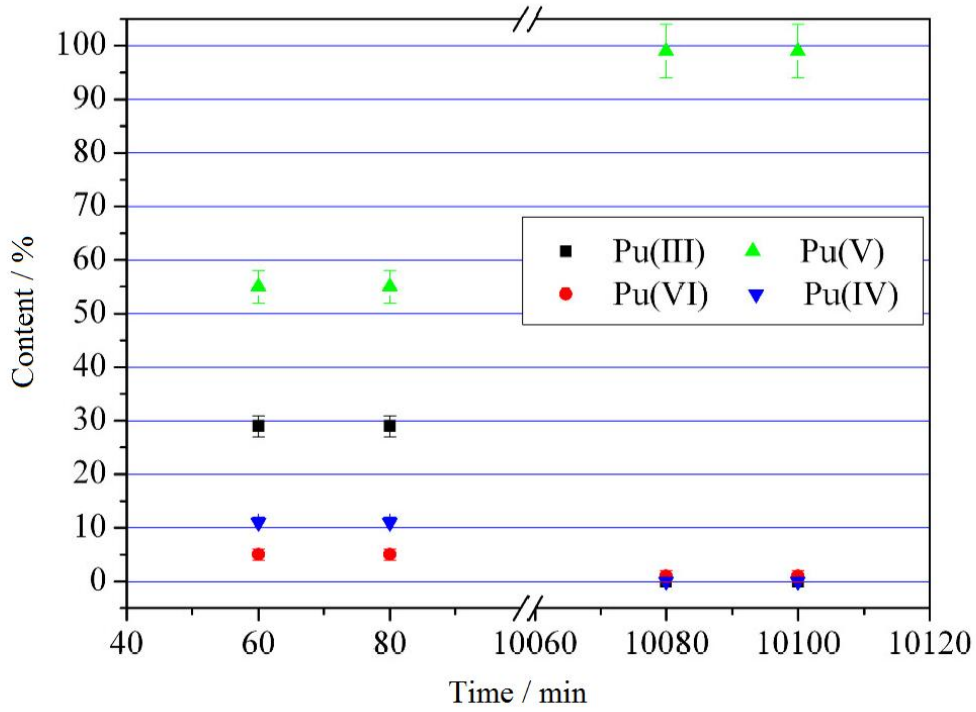

Figure 44: Pu species as a function of time after addition of 30 ppb Pu(IV) to OPA pore water (pH = 7.6) under anaerobic conditions.

As can be seen from Figs. 43 and 44, under anaerobic conditions Pu(V) is the dominating species in OPA pore water after a contact time of 7 days independent of the initial Pu oxidation state. The oxidation of Pu(III) to Pu(V) in OPA pore water under anaerobic conditions was completed within the first hour. The Pu species after addition of 30 ppb Pu(III) or Pu(IV) to 0.2 M HNO_3 (pH = 0.9), 0.4 M $NaClO_4$ (pH = 7.6), and OPA pore water (pH = 7.6) after a contact time of 7 days under anaerobic conditions are presented in Tabs. 23 and 24.

Table 23: Pu species and Eh values of 30 ppb Pu(III) in 0.2 M HNO_3 (pH = 0.9), 0.4 M $NaClO_4$ (pH = 7.6), and OPA pore water (pH = 7.6) after a contact time of 7 days under anaerobic conditions.

Solution	**SHE Eh / mV (after 5 days)**	**Species / %**			
		Pu(III)	**Pu(IV)**	**Pu(V)**	**Pu(VI)**
0.2 M HNO_3	647 ± 50	75 ± 4	4 ± 1	10 ± 1	11 ± 1
0.4 M $NaClO_4$	297 ± 50	0	0	32 ± 2	68 ± 4
OPA pore water	334 ± 50	0	0	97 ± 5	3 ± 1

Table 24: Pu species and Eh values of 30 ppb Pu(IV) in 0.2 M HNO_3 (pH = 0.9), 0.4 M $NaClO_4$ (pH = 7.6), and OPA pore water (pH = 7.6) after a contact time of 7 days under anaerobic conditions.

Solution	SHE Eh / mV (after 5 days)	Species / %			
		Pu(III)	Pu(IV)	Pu(V)	Pu(VI)
0.2 M HNO_3	611 ± 50	99 ± 5	0	1 ± 1	0
0.4 M $NaClO_4$	469 ± 50	0	0	78 ± 4	22 ± 2
OPA pore water	376 ± 50	0	0	99 ± 5	1 ± 1

As can be seen, Pu(V) is the dominating species in OPA pore water under anaerobic conditions. In 0.4 M $NaClO_4$ solutions at pH 7.6 a mixture of Pu(V) and Pu(VI) was found. In case of 30 ppb Pu(III) in 0.2 M HNO_3, all Pu oxidation states were presented in solutions after 7 days. The analogous experiment with 30 ppb Pu(IV) in HNO_3, only Pu(III) was detected after 7 days. Under anaerobic conditions, the measured Eh values in pore water solutions (for both Pu(III) and Pu(IV) experiments) were lower than for 0.4 M $NaClO_4$ (pH 7.6), 0.2 M HNO_3 and related Eh values under aerobic conditions.

4.3.3 CE-RIMS

Another aim of this work was to improve the sensitivity of speciation methods for Np and Pu. For the detection and speciation of Np and Pu at ultratrace level, offline coupling of CE and RIMS has been successfully applied. Pu samples for RIMS measurements were collected off-line with the CE technique and filaments were prepared by electrodeposition and measured [23, 26]. Furthermore, RIMS was applied for first time to detect smallest amount of ^{237}Np and to determine the oxidation states of Pu in supernatant after Pu sorption on OPA.

RIMS measurements on ^{237}Np

The detection and speciation of Np at an ultratrace level require highly sensitive and selective methods. While the short-lived isotope ^{239}Np can be detected by means of γ-ray spectrometry, only very few sensitive and selective methods exist for the detection ^{237}Np. Due to its long half-life, radiometric methods are not sensitive enough, while most mass spectrometric methods are limited by isobaric interferences.

Therefore, we have developed a RIMS method for the detection of ^{237}Np. In RIMS, sample atoms are evaporated from a heated filament and ionized by laser radiation of three different wavelengths. The laser ions are separated by a time-of-flight (TOF) mass spectrometer and finally detected by multi channel plate (MCP) detectors. The wavelengths of the laser radiation match three subsequent optical transitions of Np and are chosen to excite the atom into an autoionizing state (AI) in the last step. Since the involved optical transitions are unique to Np, this kind of ionization shows an outstanding selectivity for the element.

The samples for RIMS are prepared by electrodeposition of Np from a 20% solution of $(NH_4)_2SO_4$ onto a Ta foil at a voltage of 14 V. After electrodeposition, the foil is covered by sputtering with a ~ 1 µm layer of Ti, which serves as a reducing agent.

The laser setup consists of three tunable titanium-sapphire lasers (Ti:sa) with output powers of up to 3 W at a repetition rate of 10 kHz. The Ti:sa lasers are jointly pumped by a frequency doubled Nd:YAG laser (DM-60, Photonics Industries, Bohemia, NY, USA). Since the Ti:sa lasers in use can only generate radiation between 11500 and 14000 cm^{-1}, the light of one laser has to be frequency doubled by a β-barium borate crystal (BBO) to reach the ionization potential of Np at 50535 cm^{-1} with a three-step excitation scheme.

Because only few energy levels of Np suitable for a three step excitation/ionization scheme with Ti:sa lasers were known, resonance ionization spectroscopy (RIS) was applied to identify such levels. The setup used for RIS is similar to one used for RIMS and also consists of three Ti:sa lasers. A graphite furnace loaded with ~1 µg Np was used as an atomic beam source in these experiments. Compared to the setup described above, this leads to a much higher ionization efficiency, but makes background suppression for thermally emitted ions impossible.

In order to identify possible second excitation states (SES), frequency doubled light from a Ti:sa laser was used to excite Np atoms into different first excitation states (FES) between 24798 and 26264 cm^{-1} taken from literature [84]. A second Ti:sa was scanned across its tuning range to populate SES. The light from a third Ti:sa was introduced for nonresonant ionization of the Np atoms from the SES. In a separate experiment, two Ti:sa lasers were used to populate several SES identified previously, while the third laser was scanned in order to excite AI levels. Our experiments led to the identification of numerous previously unknown high-lying energy levels and AI states of Np [26]. Up to now, the most efficient ionization could be obtained with the excitation scheme shown in Fig. 45. Applying this scheme, an overall efficiency for the detection of ^{237}Np of 2×10^{-6} could be demonstrated, which corresponds to a limit of detection of 1×10^{7} atoms (4 fg).

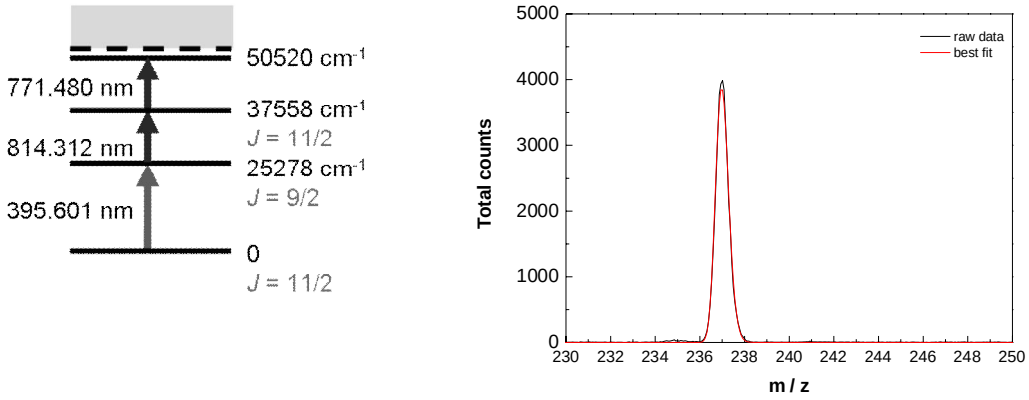

Figure 45: Scheme for resonant excitation and ionization of ^{237}Np and mass spectrum obtained with 4×10^{11} atoms ^{237}Np yielding a detection efficiency of 2×10^{-6}.

RIMS measurements on ^{239}Pu

As already mentioned, CE-RIMS was carried out for the first time with real samples from batch experiments for the determination of the K_d values of Pu(III) and Pu(IV) sorbed on OPA. At first, the coupling of CE to RIMS was tested by determining the speciation in samples which contained only Pu(III) or Pu(IV) at different concentrations of 0.05 ppt, 5.0 ppt, and 500 ppt. The samples were prepared by mixing defined aliquots from freshly prepared stock solutions of Pu(III) and Pu(IV) to 1 M CH_3COOH solution. The related fractions were separated by CE and the Pu content in each fraction was determined by RIMS. The results are shown in Tab. 25.

Table 25: RIMS results of Pu(III) and Pu(IV) samples at different concentrations.

Conc. / ppt	**0.05**	**5**	**500**
Pu(III) fraction	2.77×10^6	2.04×10^9	4.39×10^8
Pu(IV) fraction	1.88×10^7	1.88×10^9	1.91×10^9
$\sum_{theo.}$ atoms	10^7	10^9	10^{11}

As can be seen from Tab. 25, in case of the low concentrations (0.05 and 5 ppt) the number of atoms found in the Pu(III) and Pu(IV) fractions are rather close to the theoretically expected value of Pu atoms. However, for the higher concentration (500 ppt) the obtained values are too low, maybe duo to sorption effects on the wall of the capillary. The values given in Tab. 25 for 0.05 ppt Pu are close to the detection limit of this method.

RIMS application for real Pu/OPA batch samples

As shown before in Sect. 4.1, about 99% of initial Pu was removed from solution and sorbed on OPA in a short time and only 1% of Pu remained in the solution. At this very low Pu concentration, it is not possible to perform speciation studies by using conventional methods. Using CE-RIMS speciation investigation at ultratrace concentrations was possible. CE-RIMS was therefore applied for the first time to real samples from batch experiments of Pu(III) and Pu(IV) sorbed on OPA under anaerobic conditions in OPA pore water at pH 7.6. For each oxidation state, 2 samples with S/L ratios of 1.0 g/L (sample 1) and 10.0 g/L (sample 2) were chosen. After separation of the solid and liquid phases, aliquots from supernatants were taken and the Pu species were separated by CE. After preparing the filaments, RIMS analyses were carried out.

For each sample, four filaments were prepared with the fractions 1 to 4 of "Pu(III)", "Pu(V)/Pu(VI)", "Pu(IV)", and the "Pu- background/not separated species", respectively.
As an example, Figs. 46 a – d show the mass spectra of fractions 1 – 4 of the sample 1 (S/L = 1.0 g/L), where Pu(III) was added for the batch experiments.

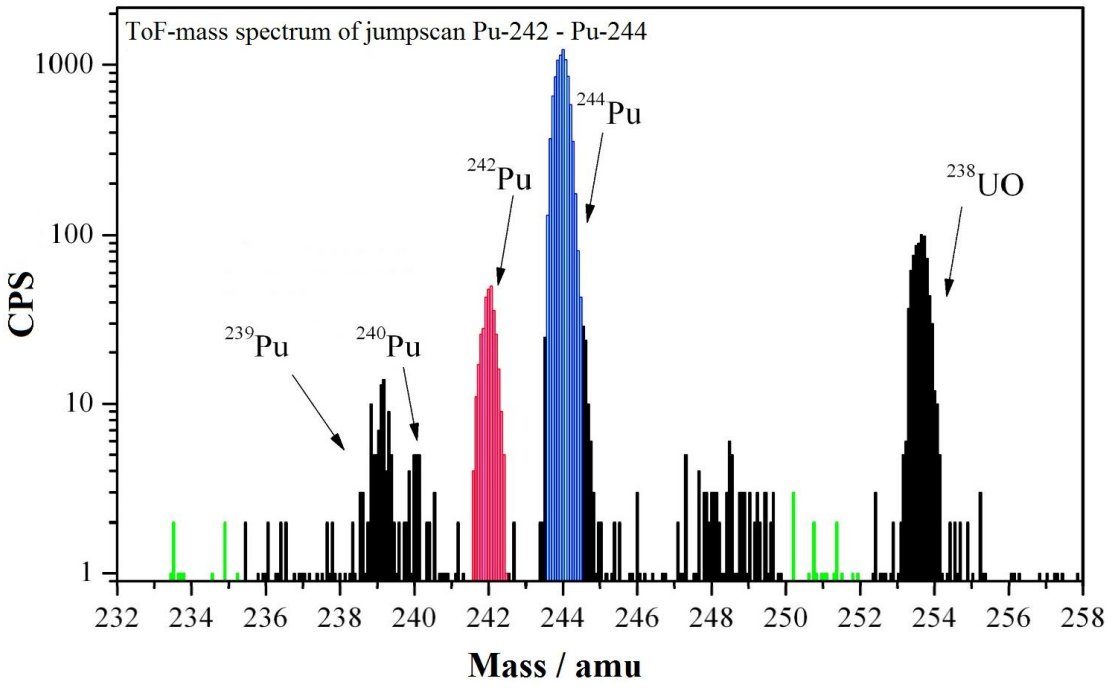

Figure 46a: CE-RIMS spectrum of fraction 1 (Pu(III)) of the sample 1.

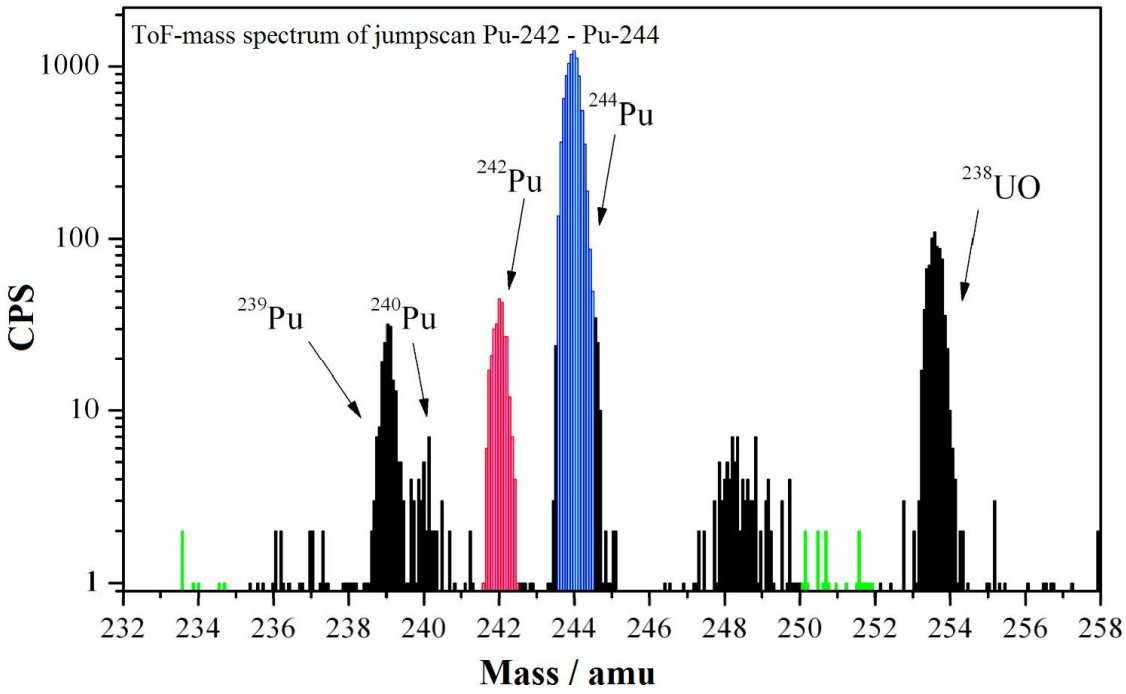

Figure 46b: CE-RIMS spectrum of fraction 2 (Pu(V)/Pu(VI)) of sample 1.

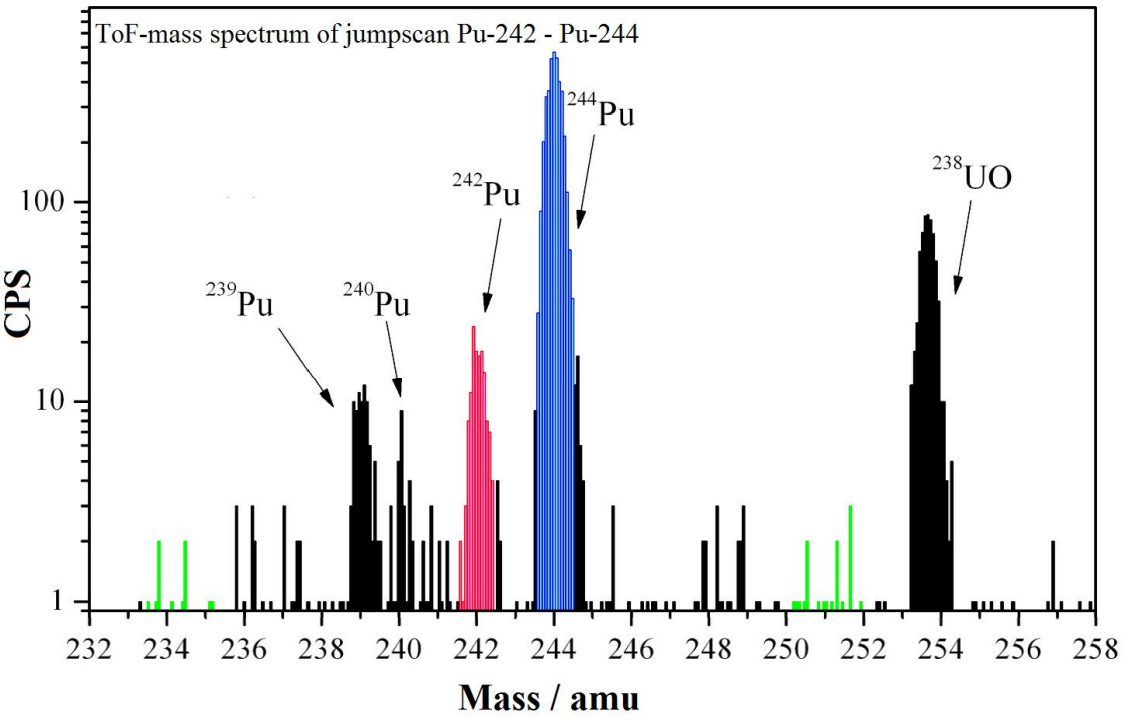

Figure 46c: CE-RIMS spectrum of fraction 3 (Pu(IV)) of sample 1.

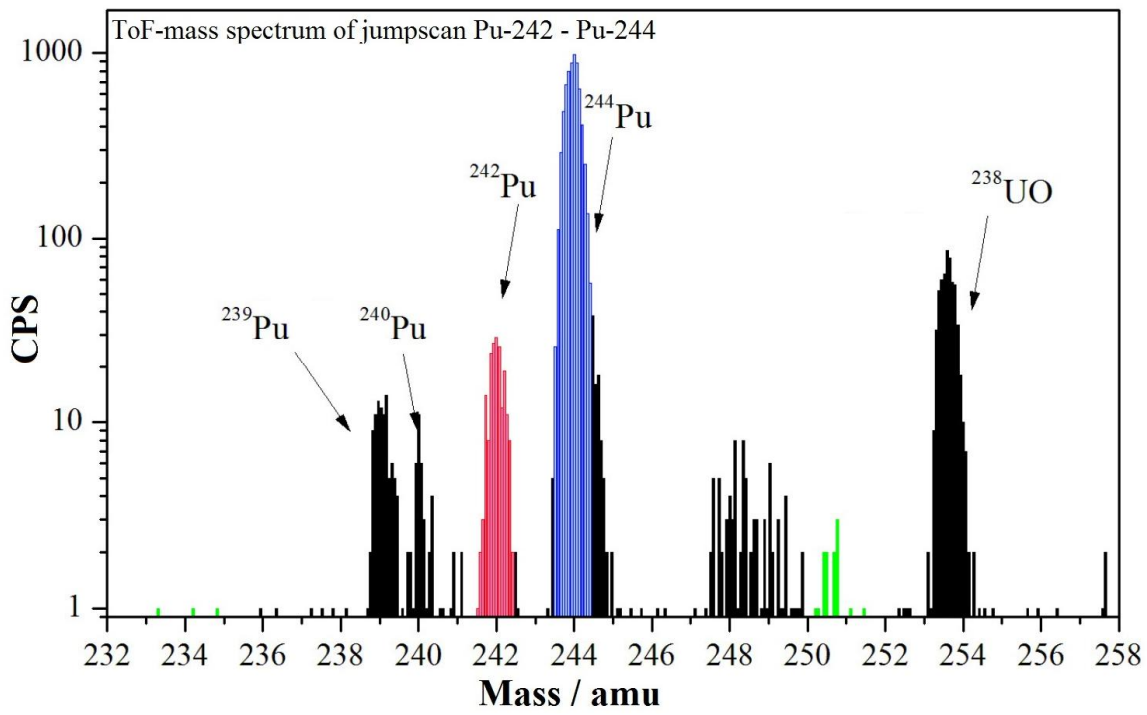

Figure 46d: CE-RIMS spectrum of fraction 4 (Pu-background/not separated species) of sample 1.

As can be seen from Figs. 46 a – d, well resolved mass spectra of the isotopes ^{239}Pu, ^{240}Pu, ^{242}Pu (as analysis isotope), ^{244}Pu (as tracer isotope), and the molecular ion ^{238}UO (as impurity in the sample) were obtained. A fluctuation in the amount of ^{239}Pu/^{240}Pu can be seen in the spectra. This is an indicator of a contamination in the samples. The ^{238}UO content remains relatively constant.

The determined atomic numbers of ^{242}Pu were converted in content percentage, based on the total amount of ^{242}Pu atoms in each of the four filaments of the samples 1 and 2. The distribution of Pu species in the samples obtained from CE-RIMS analysis is given in Tab. 26.

Table 26: Species composition in sample 1 and 2 obtained from CE-RIMS analysis.

Sample	^{242}Pu atoms			
	Pu(III)%	**Pu(V/VI)%**	**Pu(IV)%**	**Background%**
	Pu(III) batch experiment			
1	28.3 ± 4.8	23.8 ± 4.4	26.5 ± 7.0	21.3 ± 4.8
2	40.8 ± 11.9	22.2 ± 7.1	37.0 ± 14.8	-[a]
	Pu(IV) batch experiment			
1	25.9 ± 3.4	30.2 ± 3.6	16.6 ± 3.1	27.3 ± 4.5
2	95.1 ± 6.7	2.8 ± 0.4	1.2 ± 0.3	1.0 ± 0.2

[a] not analyzed filament

As can be seen from Tab. 26, after sorption of Pu on OPA from a Pu(III) solution, the pore water supernatant contained a mixture of Pu(III), Pu(V)/Pu(VI) and Pu(IV). In conclusion, the conditions (pH, Eh, ionic composition) in the pore water were oxidizing for Pu(III). A reducing effect due to the anaerobic environment and the OPA could not be observed. Analogous to the results of Pu(III), the supernatant after Pu(IV) uptake contained a mixture of Pu(III), Pu (V)/(VI), and Pu(IV).

As a conclusion, a mixture of different Pu oxidation states in supernatant solutions was obtained independent of the initial Pu oxidation state added to the suspensions. RIMS was successfully applied to real samples. It was possible to detect and determine the Pu species at ultratrace concentrations close to environmental conditions.

5 Summary

The objective of this project was to investigate the main transport and retardation processes of the actinides, mainly neptunium (Np) and plutonium (Pu), for a repository of spent nuclear fuels in an accidental scenario. The aim of this study was to deliver input parameters for the performance assessment of a future repository. The results should improve the thermodynamic databases for the immobilization of actinides by clay rocks and allow an assessment of argillaceous rocks as potential host for nuclear waste disposal.

The interaction of Np and Pu in their relevant oxidation states with natural Opalinus Clay (OPA) and the influence of humic acid (HA, M42) have been studied in detail. Furthermore, batch experiments with thorium (Th), uranium (U), and americium (Am) were performed for comparison.

The sorption of Np(V) on OPA was studied in batch experiments as a function of various parameters. The results showed that Np(V) uptake is strongly influenced by pH, aerobic/anaerobic conditions, partial pressure of CO_2, background electrolyte, ionic strength, and temperature. Stronger sorption was found under anaerobic conditions due to partial reduction of Np(V) to Np(IV). Under aerobic condition, the sorption decreases significantly at pH > 9 duo to carbonate complexation in aqueous solution. The use of $NaClO_4$ as a background electrolyte leads to an overestimation of Np(V) sorption on OPA compared to OPA pore water. It was also confirmed that Np(V) sorption on OPA is an endothermic reaction. The influence of HA on the sorption of Np(V) and Pu(IV) on OPA was investigated as a function of pH, partial pressure of CO_2 for Np, and solid-to-liquid ratio for Pu(IV). The mobilizing effect of HA on the sorption of Np on OPA (pH > 7.5) was more pronounced at higher Np(V) concentration. In case of Pu(IV), HA effects the sorption on OPA in pore water at pH 7.6 and reduces the K_d value by about one order of magnitude.

Diffusion experiments of Np(V) with intact OPA bore cores were performed as a function of temperature and presence/absence of HA (M42) by using OPA pore water (pH = 7.6) as mobile phase. From these experiments the diffusion parameters were determined for the first time.

The sorption of NpO_2^+, UO_2^{2+}, PuO_2^{2+}, Pu^{3+}, Am^{3+}, Pu^{4+}, and Th^{4+}on OPA was investigated in batch experiments and distribution coefficients were determined. It was shown that the sorption of all actinides in OPA pore water (pH = 7.6) was proportional to the solid-to-liquid ratio of OPA. The K_d value depends on the oxidation state of actinide element. The tri- and tetravalent actinides are stronger sorbed on OPA with higher K_d values compared with hexa- and pentavalent actinides (U and Np), which are weakly sorbed.

Batch and diffusion experiments were combined with microscopic X-ray synchrotron radiation techniques (X-ray absorption spectroscopy (XAS), micro XAS (µ-XAS), micro X-ray fluorescence spectroscopy (µ-XRF), and micro X-ray diffraction (µ-XRD)) to identify the sorbed Np and Pu species on the surface of OPA. XAS measurements on bulk samples of Np(V) sorbed on OPA under anaerobic conditions show that Np(V) carbonate complexes are formed on the OPA surface. Under anaerobic conditions, inner-sphere sorption of a mixture of Np(V) and Np(IV) was observed. In the case of Pu, it was confirmed that Pu(IV) is the dominating oxidation state, independent of the initial Pu oxidation state, background electrolyte, presence/absence of HA, and aerobic/anaerobic conditions. Inner-sphere sorption of Pu(IV) on OPA was also observed. Additionally, it was shown that the type of OPA (aerobic or anaerobic) has a significant influence on the speciation of Pu on OPA.

From µ-XRF measurements, the spatial distributions of Fe, Ca, Mn, and sorbed Np or Pu on OPA thin sections were determined. µ-XANES (micro X-ray absorption near-edge structure) measurements of Np and Pu hot spots showed a reduction of Np(V) to Np(IV) and of Pu(VI) to Pu(IV) in both sorption and diffusion samples. This result agrees well with EXAFS results on bulk samples. Furthermore, µ-XRD measurements performed around Np or Pu hot spots showed that pyrite and siderite are the redox-active mineral phases in OPA.

The redox behavior of Pu under environmental conditions at trace level concentrations was studied using CE-ICP-MS (capillary electrophoresis coupled to inductively coupled plasma mass spectrometry) and CE-RIMS (capillary electrophoresis coupled to resonance ionization mass spectrometry). With the CE-ICP-MS method the limit of detection for all four oxidation states of Pu in solution could be reduced down to 0.5 ppb.

6 References

[1] Gomper, K.: Zur Abtrennung langlebiger Radionuklide. In Radioaktivität und Kernenergie, Hoffmann, J.; Kuczera, B., Eds. Forschungszentrum Karlsruhe, pp. 153 - 167 (2001).

[2] Hoth, P., Wirth, H., Reinhold, K., Bräuer, V., Krull, P., Feldrappe, H.: Endlagerung radioaktiver Abfälle in tiefen geologischen Formationen Deutschlands – Untersuchung und Bewertung von Tongesteinsformationen. Bundesanstalt für Geowissenschaften und Rohstoffe BGR, Hannover/Germany (2007).

[3] NAGRA: Projekt Opalinuston – Synthese der geowissenschaftlichen Untersuchungsergebnisse, Entsorgungsnachweis für abgebrannte Brennelemente, verglaste hochaktive sowie langlebige mittelaktive Abfälle. Technical Report NTB 02-03, NAGRA Nationale Genossenschaft für die Lagerung radioaktiver Abfälle, Wettingen/Switzerland (2002).

[4] OECD: Safety of geological disposal of high-level and long-lived radioactive waste in France – An international peer review of the "Dossier 2005 Argile" concerning disposal in the Callovo-Oxfordian formation. NEA No. 6178, OECD (2006).

[5] Honty, M., De Craen, M.: Mineralogy of the Boom Clay in the Essen-1 borehole. External report SCK·CEN-ER-87; SCK·CEN Belgian Nuclear Research Centre, Mol/Belgium (2009).

[6] Gautschi, A.: Hydrogeology of a fractured shale (Opalinus Clay): Implications for deep geological disposal of radioactive wastes. Hydrogeol. J. **9**, 97 - 107 (2001).

[7] Van Loon, L. R., Soler, J. M.: Diffusion of HTO, $^{36}Cl^-$, $^{125}I^-$ and $^{22}Na^+$ in Opalinus Clay: Effect of confining pressure, sample orientation, sample depth and temperature. PSI technical report 04-03, Paul Scherrer Institut, Villigen/Switzerland (2004).

[8] Lieser, K. H., Mühlenweg, U.: Neptunium in the hydrosphere and in the geosphere. Radiochim. Acta **43**, 27 - 35 (1988).

[9] Thompson, R. C.: Neptunium: the neglected actinide. A review of the biological and environmental literature. Radiat. Res. **90**, 1 - 32 (1982).

[10] Kaszuba, J. P., Runde,W. H.: The aqueous geochemistry of neptunium: dynamic control of soluble concentrations with applications to nuclear waste disposal. Environ. Sci. Technol. **33**, 4427 - 4433 (1999).

[11] Choppin, G. R.: Humics and radionuclide migration, Radiochimica Acta **44/45**, 23 - 28 (1988).

[12] Clark, D.: The chemical complexities of plutonium. Los Alamos Sci. **26**, 364 - 381 (2000).

[13] Clark, D. L., Hecker, S. S., Jarvinen, G. D., Neu, M. P.: Plutonium. In: The Chemistry of the Actinide and Transactinide Elements. 3rd Ed. (Morss, L. R., Edelstein, N. M., Fuger, J., Katz, J. J., eds.) Springer, Dordrecht, The Netherlands, Chapt. 7, pp. 813 - 1264 (2006).

[14] Pearson, F. J.: Opalinus Clay experimental water: A1 type, Version 980318, PSI internal report TM-44-98-07. Paul Scherrer Institut, Villigen/Switzerland (1998).

[15] Joseph, C., Schmeide, K., Sachs, S., Brendler, V., Geipel, G., Bernhard, G.: Sorption of uranium(VI) onto Opalinus Clay in the absence and presence of humic acid in Opalinus Clay pore water. Chem. Geol. **284**, 240 - 250 (2011).

[16] Fröhlich, D. R., Amayri, S., Drebert, J., Reich, T.: Sorption of neptunium(V) on Opalinus Clay under aerobic/anaerobic conditions. Radiochim. Acta **99**, 71 - 77 (2011).

[17] Sachs, S., Schmeide, K., Brendler, V., Křepelová, A., Mibus, J., Geipel, G., Heise K. H., Bernhard, G.: Investigation of the complexation and the migration of actinides and non-radioactive substances with humic acids under geogenic conditions. Complexation of humic acids with actinides in the oxidation state IV Th, U, Np. Report FZR-399, Forschungszentrum Rossendorf, Dresden, Germany (2004).

[18] Sachs, S.: Kurzcharakterisierung der synthetischen Huminsäure Typ [14C]M42 (Chargen R2/06 und R2/06A) im Vergleich zur synthetischen Huminsäure Typ M42 (Charge M145), Forschungszentrum Dresden-Rossendorf, personal communication (2006).

[19] Gustafsson, J. P.: Geochemical equilibrium speciation model Visual MINTEQ V. 2.52. KTH, Department of Land and Water Resources Engineering, Stockholm/Sweden (2007), http://www.lwr.kth.se/English/OurSoftware/vminteq.

[20] Cohen, D.: Electrochemical studies of plutonium ions in perchloric acid solution. J. Inorg. Nucl. Chem. **18**, 207 - 210 (1961).

[21] Cohen, D.: The absorption spectra of plutonium ions in perchloric acid solutions. J. Inorg. Nucl. Chem. **18**, 211 - 218 (1961).

[22] Kuczewski, B., Marquardt, C. M., Seibert, A., Geckeis, H., Kratz, J. V., Trautmann, N.: Separation of plutonium and neptunium species by capillary electrophoresis-inductively coupled plasma-mass spectrometry and application to natural groundwater samples. J. Anal. Chem. **75**, 6769 - 6774 (2003).

[23] Wunderlich, T.: Anwendung der CE-ICP-MS und RIMS sowie Entwicklung und Anwendung der CE-RIMS auf Umweltproben. Johannes Gutenberg-Universität Mainz, PhD Thesis 2009.

[24] Grüning, C., Huber, G., Klopp, P., Kratz, J. V., Kunz, P., Passler, G., Trautmann, N., Waldek, A., Wendt, K.: Resonance ionization mass spectrometry for ultratrace analysis of plutonium with a new solid state laser system, Int. J. Mass Spectrom. **235**, 171 - 178 (2004).

[25] Wendt, K., Trautmann, N.: Recent developments in isotope ratio measurements by resonance ionization mass spectrometry. Int. J. Mass Spectrom. **242**, 161 - 168 (2005).

[26] Raeder, S., Stöbener, N., Gottwald, T., Passler, G., Reich, T., Trautmann, T., Wendt, K.: Determination of a three-step excitation and ionization scheme for resonance ionization and ultratrace analysis of Np-237. Spectrochim. Acta **B66**, 242 - 247 (2011).

[27] Neck, V., Runde, W., Kim, J. I., Kanellakopulos, B.: Solid-liquid equilibrium reactions of neptunium(V) in carbonate solution at different ionic-strength. Radiochim. Acta **65**, 29 - 37 (1994).

[28] Wu, T., Amayri, S., Drebert, J., Van Loon, L. R., Reich, T.: Neptunium(V) sorption and diffusion in Opalinus Clay. Environ. Sci. Technol. **43**, 6567 - 6571 (2009).

[29] Van Loon, L. R., Soler, J. M., Bradbury, M. H.: Diffusion of HTO, $^{36}Cl^-$ and $^{125}I^-$ in Opalinus Clay samples from Mont Terri: Effect of confining pressure. J. Contam. Hydrol. **61**, 73 - 83 (2003).

[30] Van Loon, L. R., Eikenberg, J.: A high-resolution abrasive method for determining diffusion profiles of sorbing radionuclides in dense argillaceous rocks. Appl. Radiat. Isot. **63**, 11 - 21 (2005).

[31] Matz, W., Schell, N., Bernhard, G., Prokert, F., Reich, T., Claußner, J., Oehme, W., Schlenk, R., Dienel, S., Funke, H., Eichhorn, F., Betzl, M., Pröhl, D., Strauch, U., Hüttig, G., Krug, H., Neumann, W., Brendler, V., Reichel, P., Denecke, M. A., Nitsche, H.: ROBL-a CRG beamline for radiochemistry and materials research at the ESRF. J. Synchrotron Rad. **6**, 1076 - 1085 (1999).

[32] Ravel, B., Newville, M.: ATHENA, ARTEMIS, HEPHAESTUS: Data analysis for X-ray absorption spectroscopy using IFEFFIT. J. Synchrotron Rad. **12**, 537 - 541 (2005).

[33] George, G. N., Pickering, I. J.: EXAFSPAK: A suite of computer programs for analysis of X-ray absorption spectra. Stanford Synchrotron Radiation Laboratory, Stanford, CA, USA (2000).

[34] Ankudinov, A. L., Bouldin, C. E., Rehr, J. J., Sims, J., Hung, H.: Parallel calculation of electron multiple scattering using Lanczos algorithms. Phys. Rev. B **65**, 104107/ 1-11 (2002).

[35] Demartin, F., Gramaccioli, C. M., Pilati, T.: The importance of accurate crystal structure determination of uranium minerals. II. Soddyite $(UO_2)_2(SiO_4)\cdot 2H_2O$. Acta Cryst. **C48**, 1 - 4 (1992).

[36] Volkov, Y. F., Visyashcheva, G. I., Tomilin, S. V., Kapshukov, I. I., Rykov, A. G.: Study of the carbonate compounds of pentavalent actinides with alkali metal cations. Radiokhim. **23**, 243 - 247 (1981).

[37] Benedict, U., Dabos, S., Dufour, C., Spirlet, J. C., Pagès, M.: Neptunium compounds under high pressure. J. Less-Common Met. **121**, 461 - 468 (1986).

[38] Chtoun E. H., Hanebali L., Garnier P.: Analyse par diffraction des rayons x, méthode de Rietveld, de la structure des solutions solides $(1-x)A_2Ti_2O_7$ - xFe_2TiO_5 A= Eu, Y. Annales de Chimie **26(3)**, 27 - 32 (2001).

[39] Borca, C. N., Grolimund, D., Willimann, M., Meyer, B., Jefimovs, K., Vila-Comamala, J., David, C.: The microXAS beamline at the Swiss Light source: towards nano-scale imaging. J. Phys. **186**, 012003, 1 - 3 (2009).

[40] Roßberg, A., Reich, T., Bernhard, G.: Complexation of uranium(VI) with protocatechuic acid - application of iterative transformation factor analysis to EXAFS spectroscopy. Anal. Bioanal. Chem. **376**, 631 - 638 (2003).

[41] Lande, J., Webb, S.: The Area Diffraction Machine. Stanford Synchrotron Radiation Laboratory, Stanford/USA (2007).
http://www.areadiffractionmachine.googlecode.com

[42] Bürger, S., Banik, N. L., Buda, R. A., Kratz, J. V., Kuczewski, B., Trautmann, N.: Speciation of the oxidation states of plutonium in aqueous solutions by UV-vis spectroscopy, CE-ICP-MS, and CE-RIMS. Radiochim. Acta **95**, 433 - 438 (2007).

[43] Amayri, S., Jermolajev A., Reich, T.: Neptunium(V) sorption on kaolinite. Radiochim. Acta **99**, 349 - 357 (2011).

[44] Wu, T., Amayri, S., Reich, T.: Neptunium(V) sorption onto gibbsite. Radiochim. Acta **97**, 99 - 103 (2009).

[45] Langmuir, D.: Aqueous Environmental Geochemistry. Prentice Hall, Upper Saddle River, pp. 353 - 364 (1997).

[46] Amayri, S., Drebert, J., Fröhlich, D. R., Kaplan, U., Reich, T.: Distribution coefficients for the sorption of actinides (Th, U, Np, Pu, Am) on Opalinus Clay in synthetic pore water (in preparation 2011).

[47] Pearson, F. J., Arcos, D., Bath, A., Boissin, J.-Y., Fern´andez, A. M., Gäbler, H.-E., Gaucher, E., Gautschi, A., Griffault, L., Hern´an, P., Waber, H. N.: Mont Terri Project - Geochemistry of water in the Opalinus Clay formation at the Mont Terri Rock Laboratory. Reports of the Federal Office for Water and Geology, Geology Series, No. 5, Bern (2003).

[48] Banik, N. L., Buda, R. A., Bürger, S., Kratz, J. V., Trautmann, N.: Sorption of tetravalent plutonium and humic substances onto kaolinite. Radiochim. Acta **95**, 569 - 575 (2007).

[49] Schmeide, K., Bernhard, G.: Sorption of Np(V) and Np(IV) onto kaolinite: Effects of pH, ionic strength, carbonate and humic acid. Appl. Geochem. **25**, 1238 - 1247 (2010).

[50] Buda, R. A., Banik, N. L., Kratz, J. V., Trautmann, N.: Studies of the ternary systems humic substances - kaolinite - Pu(III) and Pu(IV). Radiochim. Acta **96**, 657 - 665 (2008).

[51] Fröhlich, D. R.: Speziation von Neptunium bei der Migration in Tongestein. Johannes Gutenberg-Universität Mainz, PhD Thesis 2011.

[52] Fröhlich, D.R., Amayri, S., Drebert, J., Reich, T.: Influence of temperature and background electrolyte on the sorption of neptunium(V) on Opalinus Clay. Appl. Clay Sci. (submitted 2011).

[53] Brasser, T., Droste, J., Müller-Lyda, I., Neles, J., Sailer, M., Schmidt, G., Steinhoff, M.: Endlagerung wärmeentwickelnder radioaktiver Abfälle in Deutschland. GRS - 247, GRS Gesellschaft für Anlagen- und Reaktorsicherheit mbH (2008).

[54] Lu, N., Reimus, P. W., Parker, G. R., Conca, J. L., Triay, I. R.: Sorption kinetics and impact of temperature, ionic strength and colloid concentration on the adsorption of plutonium-239 by inorganic colloids. Radiochim. Acta **91**, 713 -720 (2003).

[55] Runde, W., Conradson, S. D., Efurd, D. W., Lu, N., Van Pelt, C. E., Tait, C. D.: Solubility and sorption of redox-sensitive radionuclides (Np, Pu) in J-13 water from Yucca Mountain site: comparison between experiment and theory. Appl. Geochem. **17**, 837 - 853 (2002).

[56] Bauer, A., Rabung, T., Claret, F., Schäfer, T., Buckau, G., Fanghänel, T.: Influence of temperature on sorption of europium onto smectite: The role of organic contaminants. Appl. Clay Sci. **30**, 1 - 10 (2005).

[57] Tertre, E., Berger, G., Castet, S., Loubet, M., Giffaut, E.: Experimental sorption of Ni^{2+}, Cs^{+} and Ln^{3+} onto montmorillonite up to 150 °C. Geochim. Cosmochim. Acta **69**, 4937 - 4948 (2005).

[58] Tertre, E., Berger, G., Simoni, E., Castet, S., Giffaut, E., Loubet, M., Catalette, H.: Europium retention onto clay minerals from 25 to 150 °C: Experimental measurements, spectroscopic features and sorption modelling. Geochim. Cosmochim. Acta **70**, 4563 - 4578 (2006).

[59] Angove, M. J., Johnson, B. B., Wells, J. D.: The influence of temperature on the adsorption of cadmium(II) and cobalt(II) on kaolinite. J. Col. Inter. Sci. **204**, 93 - 103 (1998).

[60] Ward D. B., Brady P. V.: Effect of Al and organic acids on the surface chemistry of kaolinite. Clays Clay Miner. **46**, 453 - 465 (1998).

[61] Machesky, M. L., Wesolowski, D. J., Palmer, D. A., Ichiro-Hayashi, K.: Potentiometric titrations of rutile suspensions to 250°C. J. Col. Inter. Sci. **200**, 298 - 309 (1998).

[62] Bradbury, M. H. and Baeyens, B.: Far field sorption data bases for performance assessment of a high-level radioactive waste repository in an undisturbed Opalinus Clay host rock. PSI report 03-08, Paul Scherrer Institut, Villigen / Switzerland (2003).

[63] Van Loon, L. R., Baeyens, B., Bradbury, M. H.: Diffusion and retention of sodium and strontium in Opalinus Clay: Comparison of sorption data from diffusion and batch sorption measurements, and geochemical calculations. Appl. Geochem. **20**, 2351 - 2363 (2005).

[64] Wang, X. K., Chen, Y. X., Wu, Y. C.: Diffusion of Eu(III) in compacted bentonite - effect of pH, solution concentration and humic acid. Appl. Radiat. Isot. **60**, 963 - 969 (2004).

[65] Wang, X. K., Chen, C. L., Zhou, X., Tan, X. L., Hu, W. P.: Diffusion and sorption of U(VI) in compacted bentonite studied by a capillary method. Radiochim. Acta **93**, 273 - 278 (2005).

[66] Tachi, Y., Shibutani, T., Sato, H., Yui, M.: Sorption and diffusion behavior of selenium in tuff. J. Contam. Hydrol. **35**, 77 - 89 (1998).

[67] Tachi, Y., Shibutani, T., Sato, H., Yui, M.: Experimental and modeling studies on sorption and diffusion of radium in bentonite. J. Contam. Hydrol. **47**, 171 - 186 (2001).

[68] Mukai, S., Kataoka, S.: Diffusion of some radionuclides in compacted Ca-bentonite under reducing condition. Radiochim. Acta **82**, 179 - 182 (1998).

[69] Bradbury, M. H., Baeyens, B. A: Comparison of apparent diffusion coefficients measured in compacted kunigel V1 bentonite with those calculated from batch sorption measurements and D_e (HTO) data: A case study for Cs(I), Ni(II), Sm(III), Am(III), Zr(IV) and Np(V). PSI technical report Nr. 03-02, Paul Scherrer Institut, Villigen / Switzerland (2003).

[70] Glaus, M. A., Rosse´, R., Van Loon, L. R., Yaroshchuk, A. E.: Tracer diffusion in sintered stainless steel filters: Measurement of effective diffusion coefficients and implications for diffusion studies with compacted clays. Clays Clay Miner. **56**, 677 - 685 (2008).

[71] Wang, J. H.: Self-diffusion and structure of liquid water. I. Measurement of self-diffusion of liquid water with deuterium as tracer. J. Am. Chem. Soc. **73**, 510 - 513 (1951).

[72] Kozai, N., Inada, K., Kozaki, T., Sato, S., Ohashi, H., Banba, T.: Apparent diffusion coefficients and chemical species of neptunium(V) in compacted Na-montmorillonite. J. Contam. Hydrol. **47**, 149 - 158, (2001).

[73] Duff, M. C., Newville, M., Hunter, D. B., Bertsch, P. M., Sutton, S. R., Triay, I. R., Vaniman, D. T., Eng, P., Rivers, M. L.: Micro-XAS studies with sorbed plutonium on tuff. J. Synchrotron Rad. **6**, 350 - 352 (1999).

[74] Duff, M. C., Hunter, D. B., Triay, I. R., Bertsch, P. M., Kitten, J., Vaniman, D. T.: Comparison of two micro-analytical methods for detecting the spatial distribution of sorbed Pu on geological materials. J. Contam. Hydrol. **47**, 211 - 218 (2001).

[75] Reich, T., Bernhard, G., Geipel, G., Funke, H., Hennig, C., Rossberg, A., Matz, W., Schell, N., Nitsche, H.: The Rossendorf Beam Line ROBL - a dedicated experimental station for XAFS measurements of actinides and other radionuclides. Radiochim. Acta **88**, 633 - 637 (2000).

[76] Clark, D. L., Conradson, S. D., Ekberg, S. A., Hess, N. J., Neu, M. P., Palmer, P. D., Runde, W. Tait, C. D.: EXAFS studies of pentevalent neptunium carbonato complexes. Structural eluclidation of the principal constituents of neptunium in groundwater environments. J. Am. Chem. Soc. **118**, 2089 - 2090 (1996).

[77] Reich, T., Reich, T. Y., Amayri, S., Drebert, J., Banik, N. L., Buda, R. A., Kratz, J. V., Trautmann, N.: Application of XAFS spectroscopy to actinide environmental science. AIP Conf. Proc. (X-Ray Absorption Fine Structure (XAFS13)) **882**, 179 - 83, (2007).

[78] Moyes, L. N., Jones, M. J., Reed, W. A., Livens, F. R., Charnock, J. M., Mosselmans, J. F. W., Hennig, C., Vaughan, D. J., Pattrick, R. A. D.: An X-ray absorption spectroscopy study of neptunium(V) reactions with mackinawite (FeS). Environ. Sci. Technol. **36**, 179 - 183 (2002).

[79] Marcus, M., XY display with mask.exe. ALS Advanced Light Source, LBNL Lawrence Berkeley National Laboratory, Berkeley/USA, http://xraysweb.lbl.gov/uxas/Beamline/Software/Documentation/Documentation.htm, (2007).

[80] Conradson, S. D., Clark, D. L., Neu, M. P., Runde, W. H., Tait, C. D.: Characterizing the plutonium aquo ions by XAFS spectroscopy. Los Alamos Sci. **26**, 418 - 421 (2000).

[81] Conradson, S. D., Al Mahamid, I., Clark, D. L., Hess, N. J., Hudson, E. A., Neu, M. P., Palmer, P. D., Runde, W. H., Tait, C. D.: Oxidation state determination of plutonium aquo ions using X-ray absorption spectroscopy. Polyhedron **7**, 599 - 602 (1998).

[82] Dardenne, K., Seibert, A., Denecke, M. A., Marquardt, Ch. M.: Plutonium(III,IV,VI) speciation in Gorleben groundwater using XAFS. Radiochim. Acta **97**, 91 - 97 (2009).

[83] Takeno N.: Atlas of Eh-pH diagrams intercomparison of thermodynamic databases; Geological survey of Japan open file report No. 419; National institute of advanced industrial science and technology research center for deep geological environments (2005).

[84] Blaise, J., and Wyart, J.-F.: Selected constants, energy levels and atomic spectra, Vol. 20, tables internationales de constantes, Université P. et M. Curie, Paris, (1992).

7 Acknowledgment

This work was financed by the Federal Ministry of Economics and Technology (BMWi) under contract No. 02E10166 and Actinet-I3 under contract No. 232631. We acknowledge the ESRF and SLS for provision of synchrotron beam time and thank A. Roßberg, A. Scheinost, C. Henning, and D. Banerjee from the Helmholtz-Zentrum Dresden-Rossendorf (HZDR) for the experimental support during the XAS measurements at ROBL. For support during the µ-XAS experiments we thank D. Grolimund and C. Borca from Paul Scherrer Institute (PSI). Further we thank N. Beiser and N. Groschopf from the Institute of Geosciences, Johannes Gutenberg-Universität Mainz for XRF analysis and Dr. Ch. Marquardt from the Institute for Nuclear Waste Disposal, Karlsruher Institut für Technologie (KIT), for providing the OPA samples. M. Biegler, J. Huth, and J. Krause from the Max-Planck-Institut für Chemie in Mainz are acknowledged for preparation and microprobe measurements of the OPA thin sections.

Daniel Fröhlich and Nils Stöbener were financially supported by the DFG Interdisciplinary Research Training Group Program 826 “Trace Analysis of Elemental Species: Development of Methods and Applications”.

We would like to thank all colleagues who contributed to the success of this work.

Berichtsblatt

1. ISBN oder ISSN geplant	2. Berichtsart (Schlussbericht oder Veröffentlichung) Schlussbericht
3. Titel Wechselwirkung und Transport von Actiniden im natürlichen Tongestein unter Berücksichtigung von Huminstoffen und Tonorganika – Wechselwirkung von Neptunium und Plutonium mit natürlichem Tongestein	
4. Autor(en) [Name(n), Vorname(n)] Amayri, Samer; Drebert, Jakob; Fröhlich, Daniel; Kaplan, Ugras; Kratz, Jens Volker; Reich, Tobias; Stöbener, Nils; Trautmann, Norbert; Wunderlich, Thomas	5. Abschlussdatum des Vorhabens Juni 2011
	6. Veröffentlichungsdatum geplant
	7. Form der Publikation KIT-Bericht
8. Durchführende Institution(en) (Name, Adresse) Institut für Kernchemie, Johannes Gutenberg-Universität Mainz, Fritz-Straßmann-Weg 2, 55128 Mainz	9. Ber. Nr. Durchführende Institution
	10. Förderkennzeichen 02E10166
	11. Seitenzahl 98
12. Fördernde Institution (Name, Adresse) Bundesministerium für Wirtschaft und Technologie (BMWi) 53107 Bonn	13. Literaturangaben 84
	14. Tabellen 26
	15. Abbildungen 46
16. Zusätzliche Angaben	
17. Vorgelegt bei (Titel, Ort, Datum)	

18. Kurzfassung

Das Ziel dieses Projektes war die Untersuchung von Transport- und Rückhalteprozessen von Actiniden, hauptsächlich von Neptunium (Np) und Plutonium (Pu), für den Fall ihrer Freisetzung aus einem Endlager für abgebrannten Kernbrennstoff. Die Wechselwirkung von Np und Pu in verschiedenen Oxidationszuständen mit dem natürlichen Opalinuston (OPA) aus Mont Terri, Schweiz, wurde detailliert studiert. Zum Vergleich wurden Experimente mit Thorium (Th), Uran (U) und Americium (Am) durchgeführt.

In Batch-Experimenten wurde die Sorption von NpO_2^+, UO_2^{2+}, Pu^{3+}, Am^{3+}, Pu^{4+} und Th^{4+} an OPA in Porenwasser bei pH 7,6 untersucht und die Verteilungskoeffizienten (K_d-Werte) bestimmt. Es konnte gezeigt werden, dass die drei- und vierwertigen Actiniden an OPA stark sorbieren und die K_d-Werte größer sind als für die fünf- und sechswertigen Actiniden, die nur schwach sorbieren.

Detaillierte Studien zur Sorption von Np(V) an OPA in Abhängigkeit von pH, aeroben/anaeroben Bedingungen, CO_2-Partialdruck, An- und Abwesenheit von Huminsäure, Hintergrundelektrolyt, Ionenstärke und Temperatur zeigten, dass diese Parameter die Sorption von Np(V) stark beeinflussen.

In Diffusionsexperimenten mit intakten OPA-Bohrkernen und OPA-Porenwasser als mobile Phase wurden die Parameter für die Diffusion von Np(V) als Funktion der Temperatur in An- und Abwesenheit von Huminsäure erstmalig bestimmt.

Die Speziation von Np und Pu an der OPA-Mineraloberfläche nach der Sorption bzw. Diffusion wurde mit verschiedenen Synchrotronstrahlungsmethoden (Röntgenabsorptionsspektroskopie (XAS), µ-XAS, Mikroröntgenfluoreszenz (µ-XRF) und Mikroröntgenbeugung (µ-XRD) ermittelt. Diese Experimente zeigten, dass Np(IV) und Pu(IV) die dominierenden Spezies bei der Sorption und Diffusion in OPA sind. Die µ-XRD Messungen bestätigten, dass Fe(II)-haltigen Mineralphasen (Pyrit und Siderit) die redoxaktiven Mineralphasen in OPA sind, die die Speziation von Np und Pu nach der Aufnahme durch OPA bestimmen.

Für die Ultraspurenbestimmung von Np- und Pu-Spezies im umweltrelevanten Konzentrationsbereich wurden die CE-RIMS und CE-ICP-MS erfolgreich eingesetzt.

Die erhaltenen Daten verbessern die thermodynamische Datenbasis für die Wechselwirkung von Actiniden mit Tongestein und dienen als Eingangsparameter für die Langzeitsicherheitsanalyse eines nuklearen Endlagers.

19. Schlagwörter

Sorption, Diffusion, Opalinuston, Np, Pu, Th, U, Am, Huminsäure, Verteilungskoeffizienten, Diffusionsparameter, Speziationsuntersuchungen, XAFS, µ-XRF, µ-XRD, CE-ICP-MS, CE-RIMS, Langzeitsicherheitsanalyse

20. Verlag Karlsruher Institut für Technologie	21. Preis

Document Control Sheet

1. ISBN or ISSN planned	2. type of document (e.g. report, publication) Final Report
3. title Migration of actinides in natural clay: Interaction of neptunium and plutonium with natural clay	
4. author(s) (family name, first name(s)) Amayri, Samer; Drebert, Jakob; Fröhlich, Daniel; Kaplan, Ugras; Kratz, Jens Volker; Reich, Tobias; Stöbener, Nils; Trautmann, Norbert; Wunderlich, Thomas	5. end of project June 2011
	6. publication date planned
	7. form of publication KIT Report
8. performing organization(s) (name, address) Institute of Nuclear Chemistry, Johannes Gutenberg-Universität Mainz, Fritz-Strassmann-Weg 2, 55128 Mainz	9. originator's report no.
	10. reference no. 02E10166
	11. no. of pages 98
12. sponsoring agency (name, address) Bundesministerium für Wirtschaft und Technologie (BMWi) 53107 Bonn	13. no. of references 84
	14. no. of tables 26
	15. no. of figures 46
16. supplementary notes	
17. presented at (title, place, date)	

18. abstract

The objective of this project was to investigate the transport and retardation processes of the actinides, mainly neptunium (Np) and plutonium (Pu), from a repository of spent nuclear fuels in an accidental scenario. The interaction of Np and Pu in their relevant oxidation states with natural Opalinus Clay (OPA) from Mont Terri, Switzerland, has been studied in detail. Furthermore, experiments with thorium (Th), uranium (U), and americium (Am) were performed for comparison.

The sorption of NpO_2^+, UO_2^{2+}, Pu^{3+}, Am^{3+}, Pu^{4+}, and Th^{4+} on OPA in pore water at pH 7.6 was investigated in batch experiments and distribution coefficients (K_d) were determined. The results showed that the tri- and tetravalent actinides are strongly sorbed on OPA with K_d values higher than those of the penta- and hexavalent actinides, which are weakly sorbed.

The sorption of Np(V) on OPA was studied as a function of pH, aerobic/anaerobic conditions, partial pressure of CO_2, presence/absence of humic acid, background electrolyte, ionic strength, and temperature. The results showed a strong influence of these parameters on Np(V) sorption.

Diffusion parameters for Np(V) were determined for the first time from diffusion experiments with intact OPA bore cores as a function of temperature and presence/absence of humic acid using OPA pore water as mobile phase.

The speciation of Np and Pu on the OPA mineral surface after sorption and diffusion processes was investigated by using different X-ray synchrotron radiation techniques (X-ray absorption spectroscopy (XAS), micro XAS (µ-XAS), micro X-ray fluorescence spectroscopy (µ-XRF), and micro X-ray diffraction (µ-XRD)). The results showed that Np(IV) and Pu(IV) are the most dominant species after sorption and diffusion processes. Furthermore, µ-XRD studies confirmed that iron-bearing mineral phases (pyrite and siderite) are the redox-active mineral phases of OPA that determine the speciation of Np and Pu after uptake on OPA.

CE-RIMS and CE-ICP-MS were successfully applied to detect the Np and Pu species at ultratrace concentrations close to environmental conditions.

The results of this study improve the thermodynamic database for the uptake of actinides by clay rocks and serve as input parameters for the performance assessment of a future nuclear waste repository.

19. keywords

Sorption, diffusion, Opalinus Clay, Np, Pu, Th, U, Am, humic acid, distribution coefficients, diffusion parameters, speciation, XAFS, µ-XRF, µ-XRD, CE-ICP-MS, CE-RIMS, long-term risk assessment

20. publisher Karlsruher Institut für Technologie	21. price